NORTHWESTERN UNIVERSITY

Strategies for the Design and Field Deployment of Cell-Free Biosensors

A DISSERTATION

SUBMITTED TO THE GRADUATE SCHOOL
IN PARTIAL FULFILLMENT OF THE REQUIREMENTS

for the degree

DOCTOR OF PHILOSOPHY

Chemical and Biological Engineering

By

Walter Thavarajah

EVANSTON, ILLINOIS

September 2022

Abstract

Three in ten people worldwide lack access to a safely managed source of drinking water, with one in ten lacking access to a drinking water service altogether. This is projected to worsen in the coming years as climate change, infrastructure degradation, and poor governance work to further increase global water insecurity. Tracking this problem and guiding public health interventions will require a means to generate accurate, high resolution water quality data, but unfortunately, existing technologies are unequipped to meet this need. Gold standard analytic methods require infrastructure that is limited in affected areas, while accurate point-of-use tests are prohibitively expensive and require training beyond the skill level of the average user.

Cell-free biosensors offer a powerful alternative to these technologies. They consist of cellular lysate or the reconstituted components necessary for gene expression, along with a genetically encoded sensor for the given target of interest. So far, these sensors have only been characterized in the lab or in non-representative field studies, leaving a dearth of information on their real-world function. My research aims to fill that void. More specifically, it follows the path from regulating gene expression *in vitro* using fluoride, a top priority water contaminant, to putting a fluoride biosensor in the hands of general users in a real-world study site. Further development of this technology could yield a suite of deployable biosensors for priority water contaminants, expanding testing capacity and reducing the impact water insecurity has in driving global disease burden, poverty, and inequity.

Acknowledgements

To Mom, Dad, and Kavina: None of this would have been possible if you hadn't put in a truly incredible amount of work to support the family and my education. Now, we've gone Walter and Kavina Thavarajah to Dr. and 2nd Lieutenant Thavarajah. How's that for making it in America?

To Phil Kyriakakis: I was done with science until you took a chance on me with iGEM and kept me on in Todd's lab. Thanks for teaching me how to be a mentor and getting me started in synthetic biology – I couldn't have made it here without your support and guidance.

To Julius Lucks: Working in this lab is what brought out my real potential as a scientist. I will always appreciate that.

To Erika Arvay, Drew Wolek, Justin Peruzzi, Katie Warfel, and Other Jardo: You ever wonder how much money we've spent drinking our way through Chicago? Because that was my favorite part of grad school. I'll miss all of you.

To Jonathan Chan and Kirsten Jung: SAD squad - hell yeah.

To Adam Silverman and Matt Verosloff: Thanks for always looking out for me, especially in my first year. I still don't understand why we can't agree on what we'd do for a Cell paper, but I can let it slide – just this once.

To Jenni Li, Laura Hertz, Edric Choi, Dylan Brown, David Bushhouse, and Charlotte Knopp: Having all of you around made wrapping up a PhD during the apocalypse almost fun. Thanks for putting up with my nonsense and being the captive audience for my daily rants. Don't worry, though, I'll be back in a minute – I'm just going to the store to get a pack of cigarettes.

To Amy Hua and Vivienne Gunadhi: UCSD wouldn't have been the same without you two. You can probably delete those photos now, though.

To Jon Falcone, Kyle Domaszcewicz, and Piyush Prakash: I was a goblin in grade school and I'm a goblin now. Thanks for sticking around, guys.

Table of Contents

List of Figures

Main Text Figures

Appendix Figures

List of Tables

Main Text Tables

Supplemental Tables

Chapter 1 - Introduction and Background

1.1 The need for low-cost, scalable testing methods

Reliable access to clean drinking water is essential for human well-being, economic development, and political stability. Impaired water quality, quantity, and accessibility, however, are projected to increase both in frequency and severity due to population increase, climate change, persistent water infrastructure degradation, and poor water governance[1–5]. As such, institutions like the World Economic Forum[6] and the US Government[7] have identified the burgeoning water crisis as a top global threat that may undermine progress in protecting human health and serve as a structural driver of poverty and inequity.

The turn of the millennium saw the creation of the United Nations (UN) Millennium Development Goals – 8 humanitarian grand challenges to be resolved by 2015[8]. These goals were monitored and refined over the next fifteen years[9], and after an extensive revision process, 2016 saw the launch of the Sustainable Development Goals (SDGs) for 2030, each of which is accompanied by targets and progress indicators. Sustainable Development Goal (SDG) 6 aspires to "the availability and sustainable management of water and sanitation for all," with SDG Target 6.1 seeking to "achieve universal and equitable access to safe and affordable drinking water for all". Progress towards SDG 6.1 is tracked by Indicator 6.1.1, "the proportion of population using safely managed drinking water services," defined as services that are located on premises, available when needed, and free from contamination[10]. The Joint Monitoring Programme (JMP), housed within the United Nations Children's Fund (UNICEF) and the World Health Organization (WHO), is the official UN mechanism that has been tasked with monitoring progress towards this goal[11].

Accurate tracking and surveillance of global drinking water sources will require significant advances in water quality monitoring technology[12,13]. Although location on premises and availability when needed can be relatively easily quantified, objectively determining drinking water safety (i.e., if a source is "safely managed") necessitates the use of technologies to detect the

presence of specific contaminants. There are countless potential contaminants that could pose health risks; JMP focuses on three that are globally prevalent and universally recognized as deleterious to human health: arsenic and fluoride (naturally abundant chemical contaminants), and *Escherichia coli* (an indicator of fecal contamination)[14,15].

Due to the ubiquity of these contaminants and resource limitations in most affected areas, ideal technologies for global water quality monitoring should be inexpensive, simple enough for an untrained individual to use, and capable of rapidly (within minutes to hours) providing results onsite. Notably, they would not necessarily need to be quantitative; the ability to determine if a contaminant is above or below a risk threshold can provide sufficient actionable information, though technologies that can provide quantitation would enhance their use and impact. However, current gold-standard methods for assessing water quality do not fulfill these criteria. Most technologies require expensive equipment and reagents, reliable electricity sources, technically skilled operators, and transportation infrastructure[16]. For example, the equipment to run qPCR (a DNA amplification technique for pathogen detection) and mass spectrometry (a molecular analysis technique for chemical detection) costs tens of thousands of dollars excluding operational expenses, must be operated by a trained technician, and cannot be brought into the field, thus necessitating sample transport for centralized analysis. As such, these methods come at a significant resource burden, which prohibits widespread deployment[15].

While there has been progress in developing more user-friendly field kits capable of rapidly detecting even trace contaminant levels in the field, there is still significant work to be done before they can be widely adopted for global monitoring or individual use[3,12]. Existing field kits frequently require sample processing steps that are beyond the skill level of an untrained user, along with expensive supplemental equipment or consumables that are often hazardous chemicals[17–20]. Collectively, these limitations preclude the scale and frequency of monitoring that is needed to effectively track progress towards SDG 6.1. There is thus an urgent unmet need for low-cost,

field-deployable water quality tests, as evidenced by the UN High Level Panel on Water's call for higher resolution data on water quality to better address the global water crisis[3].

1.2 Engineered platforms for point-of-use biosensing

Synthetic biology has the potential to address this need by harvesting naturally occurring biosensors and repurposing them to detect contaminants of interest. The use of genetically encoded biological parts facilitates rapid sensor development; unlike traditional sensing methods that must be purpose-built for their intended targets, genetically encoded biosensors enable the sensing of virtually any target on a single, modular platform. Biosensors have already been developed to detect a wide range of chemicals[21,22,31,32,23–30], as well as bacterial[33–38] and viral[39–45] pathogens. Recently reported biosensors have even been packaged in handheld, easy-to-use formats, facilitating widespread field deployment[22,23,37].

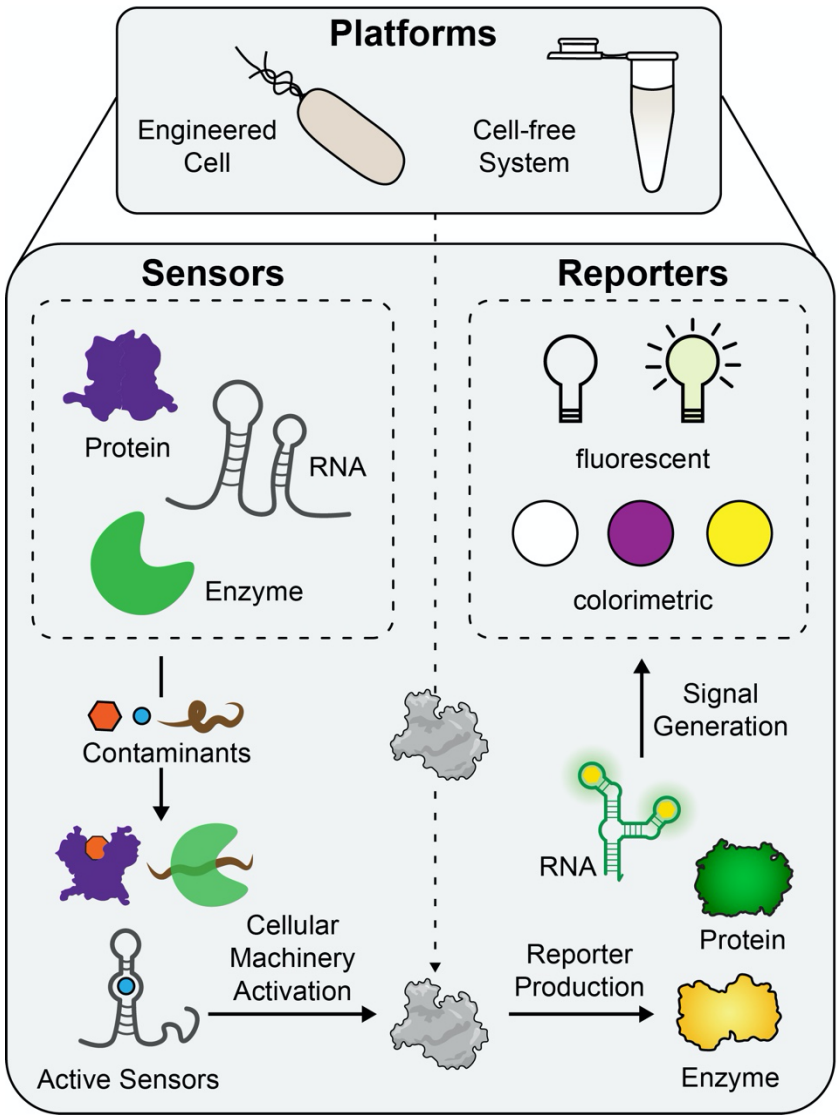

Figure 1-1. Components of a cell-free biosensor.
A sensor is a biomolecule that recognizes a specific target chemical or fragment of a pathogen's genome. This recognition event activates cellular machinery (gray), which uses gene expression to generate an output signal in the form of a reporter RNA or protein to indicate the presence of the contaminant. When engineering a biosensor, the sensor and reporter are combined in either an engineered cell or a cell-free system that supports the biological reactions necessary to generate a signal. Figure adapted from "A primer on emerging field-deployable synthetic biology tools for global water quality monitoring[46]."

Previous attempts to engineer synthetic biosensors focused on using live cells to create "whole-cell" biosensors, which have been used in the past few decades to detect several priority targets[29,30,47,48]. Use of live hosts, however, also presents several challenges[49]. For instance, whole-cell biosensors must be kept alive during use, requiring bacterial growth media and potentially a field-deployable incubator, which increases the amount of supplemental equipment

that must be brought into the field. Furthermore, whole-cell biosensors can only detect targets that are not toxic to the cell. The synthetic DNA engineered into the cell may also mutate or be lost as cells grow and divide, preventing or distorting sensor and reporter production. Furthermore, the use of live cells inherently confers biocontainment concerns, though methods to encapsulate[50] or disable[51] whole-cell sensors are being explored to mitigate this risk.

As an alternative, recent advances in of cell-free expression gene expression technologies have enabled the creation of "cell-free" biosensors[52], which are composed of either cellular lysate or the reconstituted necessary components for transcription and translation. Unlike whole-cell biosensors, they provide an *in vitro* platform for the gene expression process, eliminating the need to maintain cell health and alleviating biocontainment concerns. The open cell-free reaction environment also enables precise control of type and amount of the various cofactors and DNAs supplied to the reaction, allowing for more precise and elegant tuning and optimization strategies while simultaneously removing transport limitations. Furthermore, these systems retain their functionality after lyophilization[23,39,40], facilitating reaction transport and long-term storage. For these combined strengths, cell-free extract presents a promising platform to move forward with point-of-use biosensor development.

1.3 Noncoding RNA and its diagnostic applications

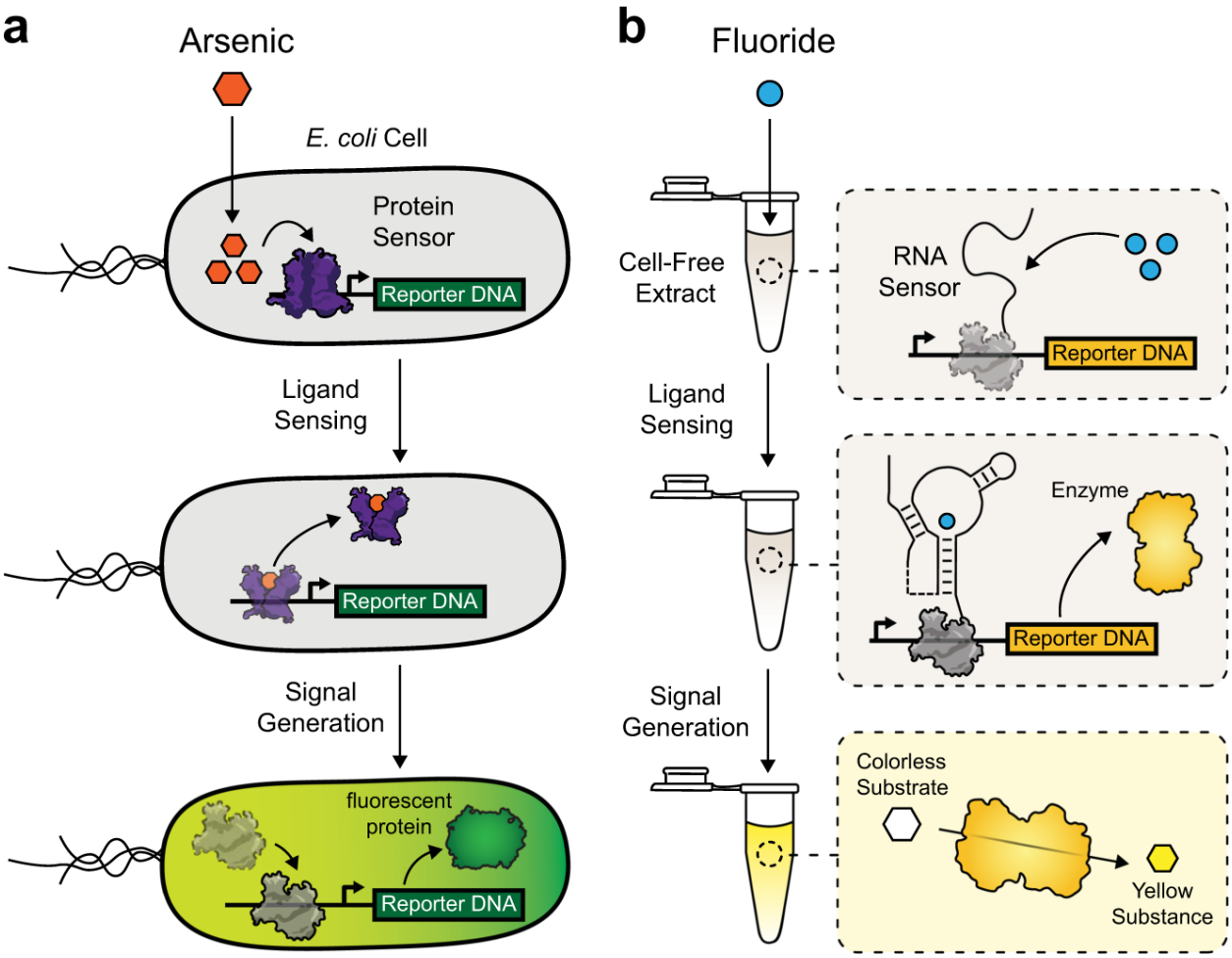

Figure 1-2. Biosensors for waterborne chemical contaminants.
(a) Detection of arsenic using a protein sensor in a whole-cell biosensor. Once the protein sensor recognizes arsenic, it releases reporter DNA and allows a reporter molecule such as a fluorescent protein to be produced. **(b)** Detection of fluoride using an RNA sensor in a cell-free biosensor. The RNA sensor recognizes fluoride and changes its shape to allow the production of a reporter molecule. The specific reporter molecule shown is an enzyme that can convert a colorless substrate into a yellow substance. Figure adapted from "A primer on emerging field-deployable synthetic biology tools for global water quality monitoring[46]."

Previously developed cell-free biosensors have shown significant promise for detecting a wide range of small-molecule contaminants[22,23,53,54]. These biosensors are typically protein-based – broadly speaking, these sensors use transcription factors responsive to the target of interest to regulate production of a reporter producing a detectable output. While this strategy is effective in many cases, it still presents several opportunities for improvement. Because transcription factors are *trans*-acting regulators, sensor tuning requires optimization over multiple parameters, which

grows increasingly difficult with increasing sensor complexity. Furthermore, while there have been substantial advances in our ability for *de novo* protein design[55], we still lack the ability to engineer allosteric ligand binding proteins. With the emergence of unnatural contaminants including industrial runoff, pharmaceutical products, and pesticides, a lack of natural transcription factors and inability to engineer synthetic ones may preclude biosensor engineering.

As an alternative to protein regulators, riboswitches present a means by which to address these needs. They are *cis*-acting functional RNAs that reside in the 5' untranslated region (UTR) of genes, gating expression by folding into different conformations based on the presence or absence of their cognate ligand[56,57]. Natural riboswitches have been characterized for a variety of small molecules and ions[58], typically regulating expression of proteins metabolizing or exporting them. Riboswitches can be broken down into two interacting parts: the aptamer, an RNA motif that binds to the riboswitch's cognate ligand, and the expression platform, which structurally rearranges to permit or forbid gene expression based on ligand binding. There are two broad categories of riboswitch, each differing on the level at which they regulate gene expression. Transcriptional riboswitches regulate gene expression by folding into an intrinsic terminator upstream of the gene of interest in their OFF state, while translational riboswitches regulate gene expression by occluding the ribosome binding site (RBS) upstream of the gene of interest in their OFF state.

Riboswitches have several important strengths when used as biosensors. Because they operate on transcriptional, rather than translational, timescales, they could enable faster-acting control of the genes they regulate if coupled to a transcriptional output. As *cis*-acting regulators, riboswitch-based sensors also have fewer components to optimize than transcription factor-based sensors. Furthermore, we have more than 30 years of validated methods to select for ligand binding RNA[59–61], enabling aptamer generation for a wide range of targets. Combined with high throughput biosensor generation methods[62] and techniques to alter riboswitch specificity[63], this

set of tools may soon allow us to generate synthetic riboswitches to detect arbitrary targets of interest.

1.4 Conclusion and overview

Despite their massive potential, cell-free biosensors are currently an academic, rather than industrial technology. Because of this, there are several substantial gaps in our knowledge of these sensors that need to be bridged before approaching the question of widespread adoption. While we can sense ligands in the lab under ideal conditions, these sensors lack in-depth characterization, tolerance to harsh environments, and accommodations for a general user base. My graduate research has focused on rectifying these shortcomings.

Broadly speaking, this thesis is a study of one specific cell-free biosensor, and the work I have done to take it from my bench into the real world. Following this section, Chapter 2 discusses methods to take a natural biosensor and adapt it to detect fluoride, an environmental contaminant of global interest. The following chapters then expand upon this project in two different ways: Chapter 3 focuses on membrane encapsulation strategies to enhance sensor function, while Chapter 4 builds on the initial field deployment efforts outlined in Chapter 2 and characterizes the non-scientific user experience with the sensors. I conclude with a discussion of outstanding needs in point-of-use biosensing, along with potential avenues to address them.

Chapter 2 - Development of a Cell-Free, Riboswitch-Based, Fluoride Biosensor

Preface

This text is adapted from the manuscript "Point-of-Use Detection of Environmental Fluoride via a Cell-Free, Riboswitch-Based Biosensor," published in ACS Synthetic Biology in 2019. I am first author of this work, which helped to establish broad strategies for future efforts in cell-free biosensor engineering and deployment. Briefly, this work involves using the *Bacillus cereus crcB* fluoride riboswitch to detect fluoride in a cell-free reaction using both fluorescent and colorimetric reporters. Our most significant finding from this project was that these reactions could be lyophilized, transported, then rehydrated onsite for point-of-use fluoride sensing. Furthermore, we established rudimentary methods to tune a sensor's limit of detection with a colorimetric reporter by tuning reaction composition. Collectively, the methods used to build and tune these cell-free fluoride biosensors went on to inform the encapsulation and field deployment studies discussed further in Chapter 3 and Chapter 4, respectively.

2.1 Introduction

Safe drinking water availability is an important contributor to public welfare[64]. However, safe water sources are not available to a large portion of the globe, with an estimated 3 billion people using water from either an unsafe source or a source with significant sanitary risks[65]. One particularly dangerous contaminant is fluoride, which leaches into groundwater from natural sources. Long-term exposure to fluoride concentrations above 2 parts per million (ppm) can cause dental and skeletal fluorosis, heavily burdening communities in resource-limited settings[66]. Though large-scale remediation strategies are available, they are resource-intensive and difficult to deploy[66,67]. This problem is compounded by the reliance of gold-standard sensing methods on expensive analytical equipment, making detection difficult in areas with the greatest need[67]. While many emerging fluorescent and colorimetric chemical fluoride sensors exist, these either require supplementary imaging equipment or utilize toxic organic solvents, hampering their use in real-

world conditions[68]. To facilitate targeted remediation and empower affected individuals, there is a pressing need for a more practical, rapid, and field-deployable solution to monitor the presence of fluoride in water.

We sought to leverage the advantages of cell-free biosensing platforms to create a new approach for monitoring for the presence of fluoride in water using a fluoride-responsive riboswitch that regulates the expression of the CrcB fluoride efflux pump in *Bacillus cereus*[69]. By configuring the *B. cereus crcB* fluoride riboswitch to control the transcription of downstream reporter genes[70], we show that a cell-free gene expression system can activate both protein and RNA reporter expression in the presence of fluoride. With an enzymatic colorimetric reporter, we demonstrate detection of fluoride concentrations at the Environmental Protection Agency (EPA) Secondary Maximum Contaminant Level of 2 ppm[71]. Notably, these cell-free biosensors showed more accurate sensing with a lower limit of detection than several tested commercially available consumer fluoride testing kits. We also demonstrate that our fluoride biosensor can be lyophilized for long-term storage and distribution, allowing us to detect fluoride in unprocessed groundwater obtained and tested onsite in Costa Rica. This work exemplifies the potential of riboswitches as practical biosensing tools and helps lay the foundation for utilizing cell-free biosensing systems in rapid and field-deployable water quality diagnostics to address pressing challenges in global health.

2.2 Fluoride riboswitch control of reporter expression in cell-free reactions

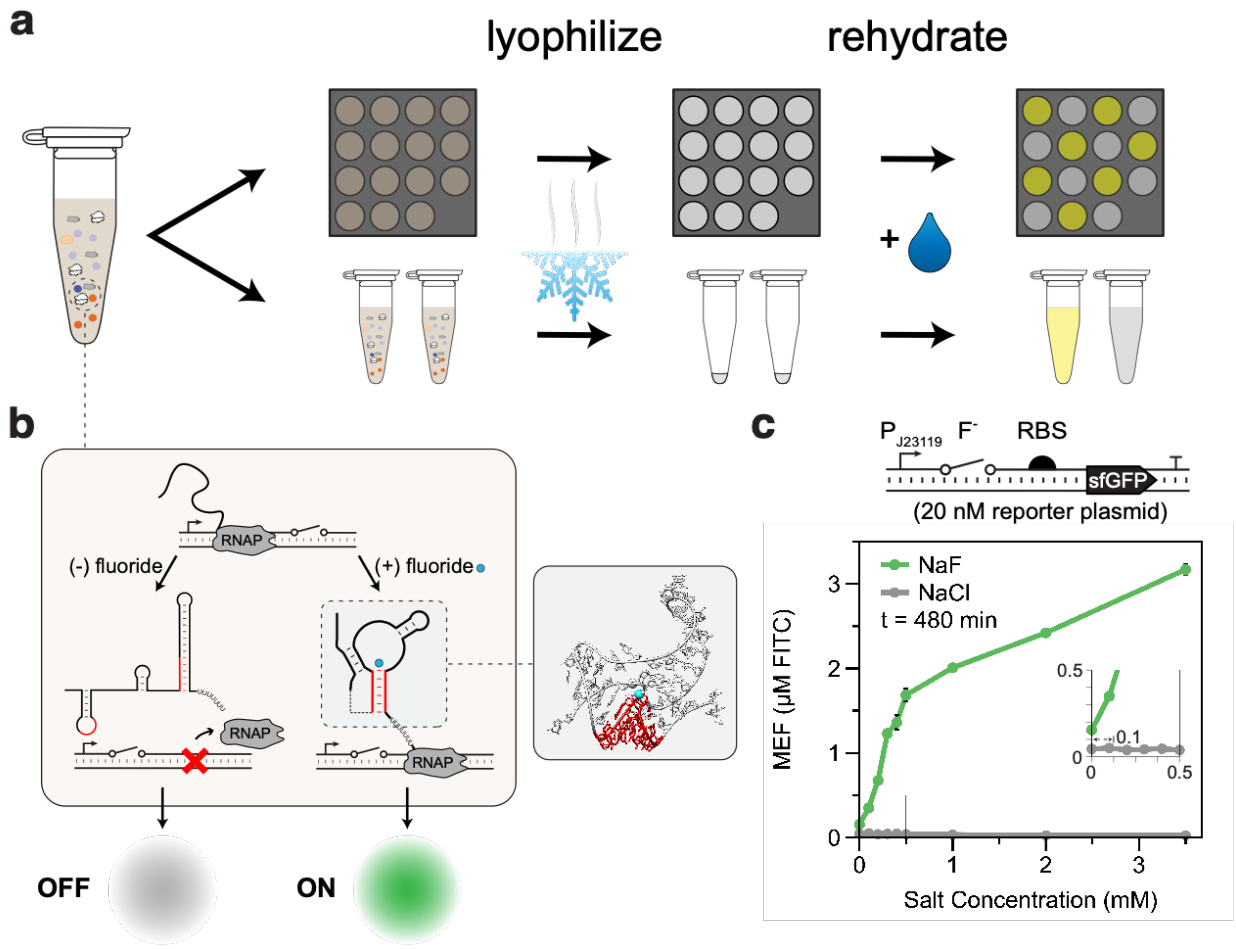

Figure 2-1. Cell-free biosensor engineering strategy.
(a) Schematic for lyophilization of a cell-free reaction in tubes or on paper disks. Rehydration with a water sample allows the designed biosensing reaction to proceed to yield a detectable signal. **(b)** Schematic for fluoride riboswitch-mediated transcriptional regulation in cell-free extract. The riboswitch folds cotranscriptionally into one of two mutually exclusive states, depending on the presence of fluoride. In the absence of fluoride, the riboswitch folds into a terminating hairpin, precluding downstream gene expression. Fluoride binding stabilizes a pseudoknot structure (red paired region, inset from PDB: 4ENC) that sequesters the terminator and enables the expression of downstream reporter genes. **(c)** Schematic of a cell-free fluoride biosensor, consisting of a DNA template encoding the fluoride riboswitch controlling the expression of sfGFP. Eight-hour endpoint fluorescence measurements for reactions containing NaF (dark green) or NaCl (gray) are shown below. Error bars represent one standard deviation from three technical replicates.

Our point-of-use diagnostic consists of a cell-free system containing a fluoride biosensor DNA template that can be lyophilized and stored. Rehydration activates the biosensor, which encodes the fluoride riboswitch and a reporter gene that produces a detectable output if fluoride

is present (**Figure 2-1a, b**). As a starting point, we sought to characterize the regulatory activity of the *B. cereus crcB* riboswitch in the cell-free reaction environment. Previous characterization of the riboswitch's cotranscriptional folding mechanism (**Figure 2-1b**) confirmed that it functions with *E. coli* RNA polymerase[70], allowing us to use it in *E. coli* cell-free extract. We therefore constructed a reporter plasmid containing the riboswitch sequence followed by a strong ribosome binding site (RBS) and the coding sequence of the reporter protein superfolder green fluorescent protein (sfGFP), all placed downstream of a constitutive *E. coli* σ^{70} promoter (all plasmid details in **Supplemental Table 1**).

After optimizing the level of Mg^{2+} within the reaction conditions for riboswitch performance (**Supplemental Figure 1**), we determined the fluoride sensor's dose-response to fluoride by titrating across a range of NaF concentrations. All tested conditions caused a measurable increase in expression over the OFF state, with activation seen at NaF concentrations as low as 0.1 mM (**Figure 2-1c**, green line and inset). This threshold is important, since 0.1 mM NaF is equivalent to the EPA's 2 ppm secondary maximum contaminant level for fluoride in drinking water, its most stringent risk threshold[71]. However, because the signal-to-noise ratio at 0.1 mM NaF is below 3, we estimated the reliable lower limit of detection to be 0.2 mM NaF. Importantly, the system also has low leak – we observed minimal activation of gene expression in the absence of NaF. Titration of identical concentrations of NaCl showed no increase in expression at any condition, demonstrating that the riboswitch is highly specific for fluoride (**Figure 2-1c**, grey line). This result corroborates a previous and more extensive characterization in *E. coli* of the switch's specificity for fluoride[69]. Thus, without any optimization of riboswitch structure or function, the sensor can discriminate health-relevant concentrations of fluoride dosed into laboratory water samples.

2.3 Changing reporters to tune sensor speed and detection threshold

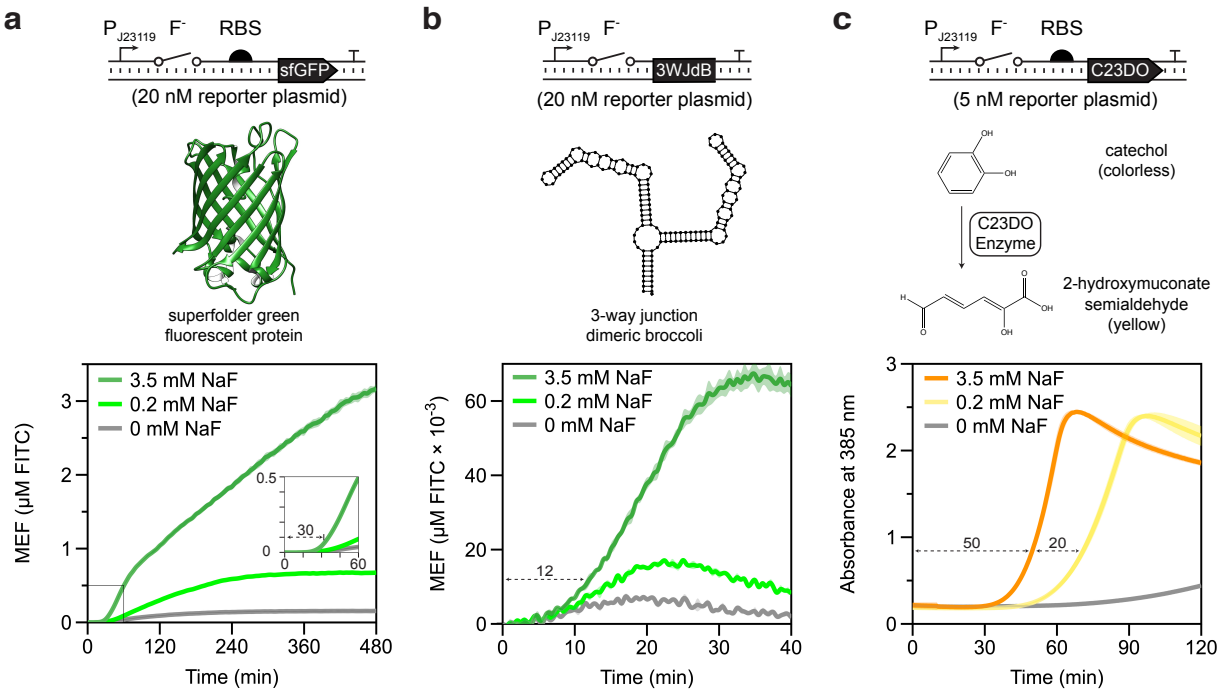

Figure 2-2. Riboswitch modularity allows fluorescent protein, RNA aptamer and enzymatic colorimetric reporter outputs.
Biosensor DNA template layouts and concentrations shown above reporter information and characterization data for that reporter. **(a)** Superfolder GFP (sfGFP) reporter (structure from PDB: 2B3P). Time course of fluorescence in the presence of 3.5 mM NaF (dark green), 0.2 mM NaF (light green), or 0 mM NaF (gray). **(b)** 3-way junction dimeric Broccoli reporter (structure predicted from NUPACK [72]). Time course of fluorescence in the presence of 3.5 mM NaF (dark green), 0.2 mM NaF (light green) and 0 mM NaF (gray). **(c)** Catechol (2,3)-dioxygenase (C23DO) reporter. Reaction scheme shows the cleavage of the colorless catechol molecule into the yellow 2-hydroxymuconate semialdehyde. Time course of absorbance at 385 nm in the presence of 3.5 mM NaF (orange), 0.2 mM NaF (yellow), and 0 mM NaF (gray). For each plot, trajectories represent average and error shading represents one standard deviation from three technical replicates. (a) and (b) are reported in mean equivalent fluorescence (MEF).

Biosensor field deployment requires an output that can be quickly read with minimal supplemental equipment[73]. Using the maximally activating fluoride concentration (3.5 mM), reactions achieved measurable signal above the no-fluoride OFF state in 30 minutes at 30°C, with overall 20-fold activation relative to the no-fluoride condition at the end of the 8-hour experiment (**Figure 2-2a**). Despite this, the sensor's ON state was not distinguishable by eye for several hours even after excitation with a blue LED, presenting the need for a faster reporter.

We hypothesized that we could accelerate the sensor's response with a 3-way junction dimeric Broccoli (3WJdB)[74] reporter, an RNA aptamer that activates fluorescence of its DFHBI-1T ligand upon transcription, eliminating delays caused by translation. At all tested NaF concentrations, 3WJdB produced a signal detectable over background within 12 minutes at 30°C (**Figure 2-2b**), more than twice as fast as could be achieved with sfGFP (**Figure 2-2a**). Interestingly, this result also confirms that the fluoride riboswitch is compatible with RNA reporters, despite the potential for misfolding with the upstream riboswitch sequence. However, despite the improvement in speed, exchanging sfGFP for 3WJdB resulted in a 50-fold reduction in the sensor's fluorescent output at the maximally activating tested condition. Thus, although the RNA-level output is preferable for its speed relative to the sfGFP output if a plate reader is accessible, it is not bright enough to use for field deployment.

As an alternative to a fluorescent output, we used the colorimetric enzyme catechol (2,3)-dioxygenase (C23DO) as a reporter. C23DO has previously been used in genetically-encoded biosensors for plant viruses[41] and produces a visible reporter output by oxidizing its colorless catechol substrate to the yellow-colored 2-hydroxymuconate semialdehyde[75]. This color change allows gene expression to be read out either by light absorbance at 385 nanometers on a plate reader or by the appearance of a yellow color, visible to the naked eye. All tested fluoride concentrations produced a visible output within 70 minutes at 30°C, which we empirically defined as an absorbance of 0.8 based on our previous observations (**Figure 2-2c)**[41]. Notably, there was only a 20-minute time separation between the minimally and maximally activating conditions, highlighting the ability of enzymatic reporters to quickly amplify weak signals. Consistent with previous uses of C23DO as a reporter in a cell-free reaction[75], we observed a decay in the absorbance signal after it reached peak activation, possibly due to 2-hydroxymuconate semialdehyde degradation. This effect does not compromise sensor robustness because differences in activation for an enzymatic reporter are determined by differences in time to observable signal rather than final signal magnitude, which is determined by the amount of

substrate supplied. One disadvantage of this strategy is that activation time does not linearly correlate with fluoride concentration, limiting the sensor to only supplying a binary presence/absence result within a specified time window[73]. Despite this, the sensor's sensitivity and low leak make this presence/absence result diagnostically informative, which combined with the advantages of an easily visualized output and reasonable time to detection made C23DO our reporter of choice for a field-deployable diagnostic.

2.4 Reaction tuning and lyophilization towards biosensor field deployment

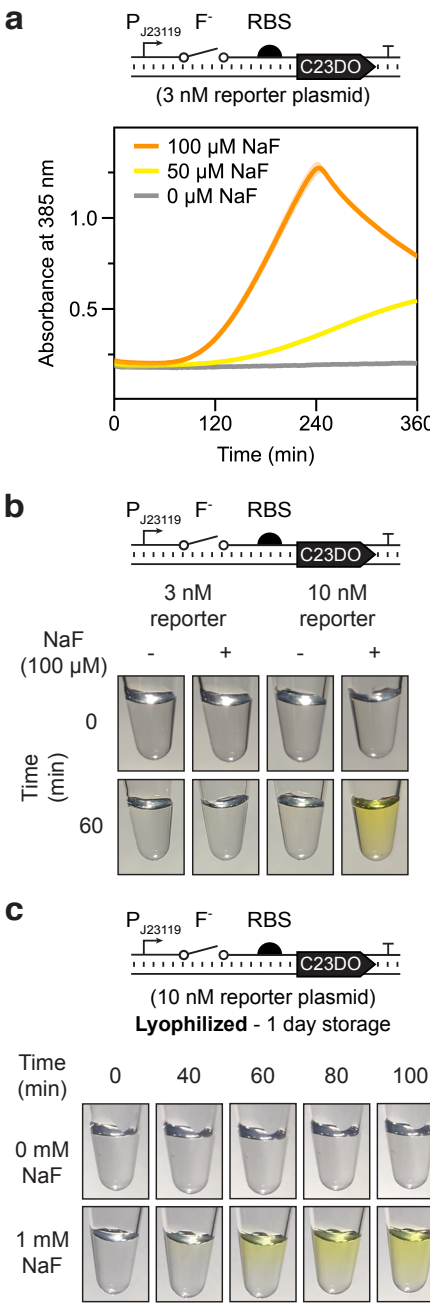

Figure 2-3. Colorimetric reporters enable fluoride sensing at environmentally relevant concentrations.
(a) Time course of 385 nm absorbance as measured by plate reader in the presence of 100 µM NaF (orange), 50 µM NaF (yellow), and 0 µM NaF (grey) using C23DO as a reporter and incubated at 30°C. Trajectories represent average and error shading represents one standard deviation from three technical replicates. **(b)** Color change observed after 1-hour for two different reporter template concentrations with and without 100 µM NaF. Tubes were mixed by pipetting and incubated at 37°C before image capture at 60 minutes. **(c)** Time lapse of rehydrated lyophilized reactions incubated at 37°C in the absence (top) and presence (bottom) of 1mM NaF.

We next took steps to optimize our sensor to detect fluoride near the EPA's secondary maximum contaminant limit of 2 ppm (100 μM). We obtained a robust ON signal with our original design, but the sensor began to leak without fluoride after 90 minutes (**Figure 2-2c**, gray line), complicating detection for trace amounts of fluoride. We attempted to mitigate this problem by reducing the amount of reporter DNA supplied to the reaction from 5 nM to 3 nM to diminish the sensor's output. In doing so, we completely suppressed leak while detecting 100 μM NaF over background (**Figure 2-3a**), but at the cost of significantly delaying activation. We could detect as low as 50 μM NaF over background in this leakless sensor, but only during an extended incubation that did not reach a visually detectable threshold within six hours.

To solve this dilemma and maintain a practical incubation time, we sought a strategy whereby tests could be interpreted as "ON" only if the yellow color appeared within some externally specified time window. Under these constraints, sensor leak is not a problem as long as the difference in timescale between the ON and OFF state is suitably longer than the test time. To implement this strategy, we increased biosensor DNA concentration to 10 nM and also increased the temperature of the CFE reaction to 37°C. Under these conditions, activation by 100 μM NaF resulted in a clear color change in sixty minutes with no visible leak in the OFF condition (**Figure 2-3b, Supplemental Figure 2**). The same conditions using 3 nM DNA template resulted in no color change within 60 minutes. This result highlights an appreciable advantage afforded by the open reaction environment of cell-free systems: the sensor's limit of detection can be tuned simply by manipulating the reaction time and the DNA concentration of the biosensor.

Recent work demonstrates that CFE reactions can be lyophilized and rehydrated when needed for on-demand biomanufacturing, nucleic acid detection, and educational activities[39,40,76,77]. To expand these applications to point-of-use small molecule detection, we next aimed to demonstrate that fluoride biosensor reactions maintain functionality after being lyophilized. We measured the impact of lyophilization on fluoride detection by lyophilizing reactions containing 10 nM C23DO reporter plasmid overnight. The reactions were then

rehydrated with laboratory grade Milli-Q water (**Figure 2-3c**, top) or water containing 1 mM NaF (**Figure 2-3c**, bottom) and incubated at 37°C. Time-lapse photography shows visible activation within 60 minutes in the 1 mM NaF condition with no leak observed within 100 minutes in the no-fluoride condition (see online publication of this manuscript). This finding, consistent with other recent reports from lyophilized cell-free systems[39,40,76,77], indicates that sensing by the fluoride riboswitch in CFE reactions is not disrupted by the lyophilization process.

We also tested the viability of lyophilized reactions stored over longer periods of time. After lyophilization, reaction tubes were wrapped in Parafilm and stored in Drierite for 3 months in darkness at room temperature and atmospheric pressure before being removed and rehydrated with laboratory grade Milli-Q water or water containing 1 mM NaF. The sample rehydrated with 1 mM NaF showed strong activation within one hour, with no leak observed in the no-fluoride condition (**Supplemental Figure 3)**. Interestingly, lyophilization appeared to suppress leak in the no-fluoride condition without impacting the ability to activate expression with fluoride. The maintained viability of reactions after three months indicates that storage in desiccant and light shielding to prevent catechol oxidation are the only requirements for long-term storage of lyophilized cell-free reactions, a crucial step towards field-deployment.

2.4 Point-of-use detection of environmental fluoride with a lyophilized biosensor

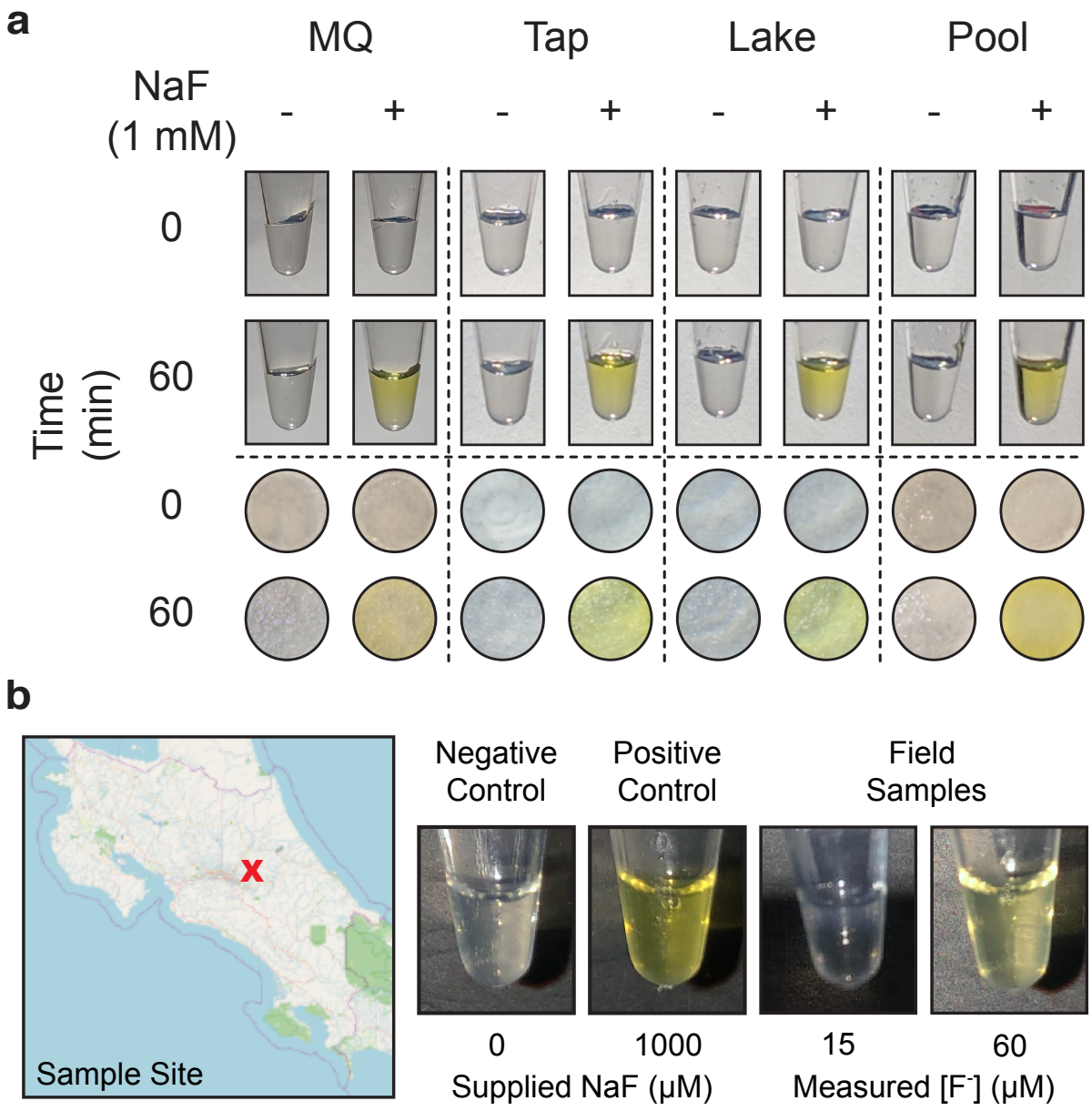

Figure 2-4. The cell-free fluoride riboswitch biosensor functions with real-world water samples and is not impacted by long-term storage and distribution.
(a) Cell-free reactions rehydrated with water samples with or without 1 mM NaF added. Lyophilized reactions in tubes are shown above lyophilized reactions on chromatography paper before and after one-hour incubation at 37°C. MQ = Milli-Q water; Tap = tap water; Lake = unfiltered Lake Michigan water; Pool = unfiltered outdoor pool water. Uncropped photos of chromatography paper experiments are available in **Supplemental Figure 2-8**. **(b)** Field testing of lyophilized cell-free reactions rehydrated with water sampled in Cartago, Costa Rica. Geographical map from OpenStreetMap[78]. The positive control contained 1 mM NaF in the reaction before lyophilization. The negative control was rehydrated with Milli-Q water, and the positive control and each test were rehydrated with 20 μL of unprocessed field sample followed by body-heat incubation for five hours. Measured fluoride concentrations obtained using a fluoride sensing electrode. Field samples are from sites B and E in **Supplementary Table 2-2**.

Components of environmental water samples, particularly natural ions like sodium, magnesium, or potassium, could poison cell-free reactions upon rehydration. These “matrix effects” would then impede the translation of a sensor from lab experiments to field testing and must be accounted for in a field-deployable diagnostic. To test the robustness of our system against matrix effects, we created mock fluoride-containing field samples by sampling water from a municipal tap, Lake Michigan, and an outdoor swimming pool, with Milli-Q water used as a control. NaF was then added to each sample to a final concentration of 1 mM. The biosensing reactions were prepared as before and pipetted into PCR tubes (**Figure 2-4a**, top) or spotted on BSA-treated chromatography paper (**Figure 2-4a**, bottom) before being lyophilized overnight. After lyophilization, reactions were immediately rehydrated with either unaltered mock field sample (- condition) or mock field sample containing 1 mM NaF (+ condition) and incubated at 37°C for one hour. For all fluoride-containing samples both in tubes and on paper, a color change was observed within one hour, with no color development in any of the no-fluoride conditions. These results confirm that the fluoride biosensor is robust against the unfiltered environmental samples tested and can be used in real-world conditions.

As the culmination of our optimization process, we tested our sensor’s ability to accurately classify fluoride-containing samples in the field. We specifically sought to follow a previously published environmental fluoride study that used conventional methods to sample and test publicly available natural and municipal water sources near the Irazu volcano in Cartago, Costa Rica, an area shown to have elevated fluoride levels (**Supplemental Figure 4**)[79]. To do this, we manufactured lyophilized fluoride biosensor reactions and transported them to Costa Rica using our simplified desiccant packaging (**Supplemental Figure 5a**) for field testing. Sampling regions identified in the previous study[79], we collected samples in 50 mL conical tubes and tested for fluoride in batch by adding unprocessed water to lyophilized reactions in PCR tubes via single-use exact volume transfer pipettes (**Supplemental Figure 2b**).

All field-testing was done onsite in Costa Rica without access to laboratory resources or equipment. Reactions were incubated at approximately 37°C by being held in the armpit, with reaction time increased to 5 hours to control for delayed activation caused by the imprecision of body heat incubation and low environmental fluoride concentrations[41]. A strong yellow color developed in every positive control reaction within an hour, confirming robustness to reaction poisoning by potential sample matrix effects (**Supplemental Table 2**). No activation was observed within 5 hours in any samples with fluoride concentrations less than 50 μM (~1 ppm) as measured in cross-validation with a commercial fluoride-sensing electrode. However, a visible color change was observed after 3.5 hours in a water sample collected from a roadside ditch measured to have a fluoride concentration of 60 μM (**Figure 2-4b**). This delayed activation aligns with our previous characterization in detecting trace concentrations of fluoride below 100 μM (**Figure 2-3a**). For all samples, the commercial electrode measurement confirmed the conclusions drawn from the cell-free sensors, with no false positives or false negatives observed under any conditions (n = 9) (**Supplemental Table 2**). By accurately detecting levels of fluoride relevant to public health concern thresholds in a real-world water source with minimal supplementary equipment, we have shown that lyophilized fluoride biosensor CFE reactions can be effectively used as low-cost, point-of-use diagnostics, demonstrating the potential of engineered biosensor elements for small molecule detection in the field.

2.5 Discussion

In this work, we have demonstrated that a fluoride riboswitch can be implemented in a CFE system to act as a field-deployable diagnostic for environmental water samples. To the best of our knowledge, this is the first demonstration of a cell-free riboswitch-based biosensor that can detect health-relevant small molecules at regulatory levels within the field. Importantly, this work represents a significant improvement in efficacy over commercially available consumer kits

(**Supplemental Figure 6)** and provides significant simplification and cost savings over gold standard electrochemical methods of fluoride detection, which cost hundreds to thousands of dollars and are cumbersome to use even for scientifically skilled operators. In contrast, our biosensors can currently be made for $0.40/reaction[76], only require a drop of water, and are robust to temperature variation, enabling incubation with body heat.

A key strength of cell-free biosensing is that biochemical parameters such as cofactor and DNA concentration can be easily tuned to reduce leak and improve dynamic range, which has been a historically difficult challenge for riboswitch engineering in cells. Furthermore, since riboswitches are *cis*-acting, only one DNA template concentration needs to be tuned per sensor, simplifying the optimization space relative to *trans*-acting RNA or protein regulators. When optimizing these reactions for the field, we found that reactions lyophilized in PCR tubes had advantages over paper-based reactions, which rapidly dried out even when incubated in sealed, humidified containers. This effect was exacerbated by the longer incubation times required for low analyte concentrations, variabilities in ambient temperature, and the practical difficulty of equipment-free incubation of paper sensors using body heat, making the tube format much more amenable to the challenges of field deployment.

This work also highlights the feasibility of using transcriptional riboswitch-mediated gene expression to convert weak-binding RNA aptamers into functional biosensors. We were surprised to find that the *B. cereus crcB* riboswitch activated so well in an *E. coli* cell-free lysate system, given the sophisticated nature of its folding mechanism and transcriptional readthrough observed both *in vitro* and *in vivo*[70,80] Transcriptional riboswitches often show weak activation due to the short timescales of their regulatory decision-making, resulting in sensitivities that are kinetically, rather than thermodynamically limited[81]. Coupling transcriptional riboswitches to enzymatic outputs like C23DO can amplify weak signals, since each reporter enzyme turns over multiple molecules of substrate[82]. The combined kinetic mechanism of switching and the signal amplification afforded by a colorimetric reporter resulted in our sensor achieving a limit of

detection of 50 μM, less than half of the lowest previously measured K_D for any fluoride aptamer[83]. Thus, this work is a powerful example of why considering only thermodynamic binding affinities during aptamer selection can exclude promising, diagnostically relevant sensors.

The strategies we present here could be applied to optimize the performance of a large number of natural riboswitches for the detection of metabolites and ions relevant to environmental and human health monitoring[58]. Additionally, the compatibility of CFE reactions for high-throughput screening[84] and the simple format of our DNA expression construct could be used to characterize the thousands of "orphan" riboswitches that have been bioinformatically identified but bind to unknown ligands[85]. We imagine that these strategies could even be used to re-engineer riboswitches to have novel function[61,86,87]. As the rules of riboswitch mechanisms are deciphered at deeper levels[70,88–90], we hope to reach a sufficient understanding to design their functional properties to meet the global needs for field-deployable environmental and health diagnostics.

2.6 Materials and Methods

Plasmid Construction

Plasmids were assembled using Gibson assembly (New England Biolabs, Cat#E2611S) and purified using a Qiagen QIAfilter Midiprep Kit (QIAGEN, Cat#12143). pJBL7025 and pJBL7026 were assembled from pJBL3752. A table of all plasmid sequences can be found in Supplemental Table 1.

Extract Preparation

Extracts were prepared according to published protocols using sonication and postlysis processing in the Rosetta2 (DE3) pLysS strain[91]. Briefly, cells are plated on a chloramphenicol-selective agar plate and incubated overnight then used to inoculate a 20 mL overnight starter culture for a 1 L final culture. This culture is grown to an optical density (OD600) of 3.0 ± 0.2 then

pelleted and lysed by sonication before centrifugation for 10 minutes at 4°C and 12,000*g*. After lysis, extracts were incubated with shaking for 80 minutes at 37°C and 200 rpm then recentrifuged under the same conditions. The supernatant was injected into a 10K MWCO dialysis cassette (ThermoFisher, 66380) and dialyzed at 4°C for three hours before a final centrifugation under the same conditions and snap-freezing in liquid nitrogen.

CFE Experiment

CFE reactions were prepared according to established protocols[91]. Briefly, reactions are composed of cell extract, a reaction buffer containing NTPs, amino acids, buffering salts, crowding agents, and an energy source, and a mix of template DNA and inducers in an approximately 30/30/40 ratio. Between reactions, the only conditions varied are DNA template and concentration, inducer concentration, and buffering magnesium glutamate concentration, the last of which is optimized by extract. Optimal magnesium glutamate concentration was 20 mM for shelf stability and field deployment experiments and 12 mM for all other data. Little variability was seen in extract performance between batches using the appropriate optimal magnesium concentrations (**Supplemental Figure 7**).

For an example reaction setup, refer to the Supplemental Experimental Design Spreadsheet. All kinetic CFE reactions were prepared on ice in triplicate at the 10 µL scale. 33 µL of a mixture containing the desired reaction components was prepared and then 10 µL was pipetted into three wells of a 384-well plate (Corning, 3712), taking care to avoid bubbles. Plates were sealed (ThermoScientific, 232701) and kinetic data was monitored on a BioTek Synergy H1m plate reader for sfGFP (20 nM reporter plasmid, emission/excitation: 485/520 nm every five minutes for 8 hours at 30°C), C23DO (variable reporter plasmid concentration, 385 nm absorbance every 30 seconds for 4-6 hours at 30°C), and 3WJdB (20 nM reporter plasmid, emission/excitation 472/507 nm every 30 seconds for 2 hours at 30°C). C23DO reactions were supplemented with 1mM catechol and 3WJdB reactions were supplemented with 20 µM DFHBI-

1T. For all fluorescence experiments, a no-DNA negative control was prepared in triplicate for every extract being tested. All reported fluorescence values have been baseline-subtracted by the average of three samples from the no-DNA condition. Baseline subtraction was not performed for catechol reactions because reaction progress is determined from time to activation rather than maximal absorbance value. For the data depicted in Figure 1C, NaF and NaCl titrations were performed in separate experiments.

Mean Equivalent Fluorescence Calibration

Fluorescence measurements were calibrated to a standard curve of fluorescein isothiocyanate (FITC) fluorescence to give standardized fluorescence units of μM equivalent FITC following a previously established procedure[22]. Briefly, serial dilutions were performed from a 50 μM stock and prepared in a pH 9.5, 100 mM sodium borate buffer. Fluorescence values for these samples were read at an excitation wavelength of 485 nm and emission wavelength of 515 nm for sfGFP and an excitation wavelength of 472 nm and emission wavelength of 507 nm for 3WJdB. These values were then used to calculate a linear conversion factor relating the plate reader's output in arbitrary units to the FITC standard curve.

Lyophilization

All lyophilization was performed in a Labconco FreeZone 2.5 Liter -84°C Benchtop Freeze Dryer (Cat# 710201000). A CFE reaction master mix was prepared and split into 20 μL aliquots in PCR strip tubes. Tube caps were then pierced with a pin and strips were wrapped in aluminum foil before being flash frozen in liquid nitrogen and lyophilized overnight at 0.04 mbar. After lyophilization, pierced PCR strip tube caps were replaced. Tubes were then sealed with parafilm and placed directly into Drierite (Cat#11001) for storage at room temperature (**Supplemental Figure 5a)**.

Paper Sensors

Individual sensors were punched out of Whatman 1 CHR chromatography paper (3001-861) using a Swingline Commercial Desktop Punch (A7074020). Tickets were then placed in a petri dish and immersed in 4% BSA for one hour before being transferred to a new dish and left to air dry overnight. After drying, tickets were spotted with 20 µL of CFE reaction and placed in plastic jars (QOSMEDIX 29258), which were loosely capped and wrapped in aluminum foil before being flash frozen in liquid nitrogen and lyophilized overnight at 0.04 mbar. For testing, tickets were transferred to new jars and rehydrated with 20 µL of sample solution. Jars were then closed and sealed with parafilm before incubation for one hour at 37°C.

Field Deployment

20 µL lyophilized reactions were prepared with 10 nM pJBL7025 and 1 mM catechol. As a positive control, additional reactions were lyophilized after being pre-enriched with 1 mM NaF. Supplemental Table 2 contains a complete list of sample site locations and water sources tested. 50 mL water samples were collected and stored in Falcon tubes (Fisher Scientific, Cat# 14-432-22) without any processing or filtration. Reactions were rehydrated by using 20 µL exact volume transfer pipettes (Thomas Scientific, 1207F80) to pull from collected samples. Three reactions were run at each sample site: (1) a positive control rehydrated with the sample, (2) a blank reaction rehydrated with the sample, and (3) a negative control reaction rehydrated with purified water to test for any reaction leak. Reactions were placed in a plastic bag and incubated at body temperature in the armpit for five hours using established protocols and marked as activated if a visible yellow color was observed[41]. Quantitative measurements of fluoride concentration of the same sample were taken with an Extech ExStik Waterproof Fluoride Meter (Cat# FL700).

Image Capture

All images were captured with via cell phone camera, with no specialized photography setup and no post-capture editing done aside from cropping image borders. Tubes were illuminated from below via desk lamp to highlight reaction color change. Paper sensors were illuminated from above via desk lamp and photographed without removal from the plastic jars used for incubation.

Acknowledgements

We would like to thank Professor Ana Gabriela Calderón Cornejo (Universidad de Costa Rica) and Eduardo Quirós Morales for assistance with biosensor field-testing. We also thank Ashty Karim (Northwestern University) and Professor Robert Batey (University of Colorado, Boulder) for helpful comments in preparing the manuscript, along with Khalid Alam (Stemloop, Inc.) for editing the supplemental video, Jaeyoung Jung (Northwestern University) for assistance with designing the graphical abstract, and Thomas Shahady (University of Lynchburg) for helpful comments about water sampling in Costa Rica. This work was supported by the Air Force Research Laboratory Center of Excellence for Advanced Bioprogrammable Nanomaterials (C-ABN) Grant FA8650-15-2-5518 (to M.C.J. and J.B.L), the David and Lucile Packard Foundation (to M.C.J.), an NSF CAREER Award (1452441 to J.B.L.), and the Camille Dreyfus Teacher-Scholar Program (to M.C.J. and J.B.L.). A.D.S. was supported in part by the National Institutes of Health Training Grant (T32GM008449) through Northwestern University's Biotechnology Training Program. The views and conclusions contained herein are those of the authors and should not be interpreted as necessarily representing the official policies or endorsements, either expressed or implied, of the Air Force Research Laboratory, Air Force Office of Scientific Research, or US Government.

Author Contributions

Conceptualization, W.T., A.D.S., M.C.J., & J.B.L.; Data Curation, W.T., A.D.S., & M.S.V.; Formal Analysis, W.T & A.D.S.; Investigation, W.T., A.D.S, & M.S.V.; Methodology, W.T., A.D.S., M.S.V., & J.B.L.; Project administration, W.T. & J.B.L.; Validation, W.T., A.D.S., & M.S.V.; Funding acquisition, N.K., M.C.J., & J.B.L.; Writing – original draft, W.T., A.D.S., & J.B.L.; Writing – review & editing, W.T., A.D.S., M.S.V., M.C.J., & J.B.L.

Competing Interests Statement

The authors have submitted one provisional patent application (U.S. Patent Application Serial No. 62/813,368) for the technologically important developments included in this work. J.B.L is a cofounder of Stemloop, Inc. J.B.L.'s interests are reviewed and managed by Northwestern University in accordance with their conflict-of-interest policies.

Data Availability

All source data for main and SI figures was deposited open access in Northwestern's Arch database (https://arch.library.northwestern.edu). Data can be accessed via https://doi.org/10.21985/N2RJ64.

Chapter 3 - Encapsulating Cell-Free Biosensors to Mitigate Matrix Effects

Preface

This text is adapted from the manuscript "Robust and Tunable Performance of a Cell-Free Biosensor Encapsulated in Lipid Vesicles," currently available on *bioRxiv*. I am second author of this work, which was conducted in collaboration with Margrethe Boyd from the Kamat Lab in the Northwestern University Biomedical Engineering Department. My contribution to this work was primarily in high-level project direction, experimental design, reagent sourcing, and manuscript editing. This work addresses one of the key concerns regarding the deployment of cell-free biosensors – sample matrix effects. By encapsulating reactions in a bilayer membrane with tunable properties, we can control transport into and out of the reaction and therefore protect reaction components from degradation. Here, we use this technique to protect the fluoride biosensor described in Chapter 2 from extravesicular RNAses. Moving forward, refinement of this technique could enable sensing in environments with extreme pH or salt concentration, facilitating future studies like the field deployment efforts described in Chapter 4.

3.1 Introduction

Cell-free systems have emerged as a powerful technology to detect a wide variety of molecular signals, including chemical contaminants relevant to the environment and human health[23,25,26,54,92–96] and markers of disease and infection[21,33,34,40–42,97,98]. By reconstituting purified cellular machinery in vitro, these systems enable use of natural microbial sensing mechanisms in a low-cost, distributable, and easily tunable platform. Despite these key advantages, removal from the cell also eliminates certain features of the cell's native membrane barrier - such as reaction containment, protection from reaction inhibitors, and selective gating - all of which can add important functionality to cell-free biosensors[99].

Efforts to deploy sensors highlight these limitations caused by the absence of cellular membranes. For example, without a barrier between the sensor and the sample, detecting targets

in complex matrices like polluted water or biological samples requires additional modifications to the reaction or preparation protocols[73,94,100]. Cell-free sensors are also sensitive to dilution, and therefore require a controlled reaction environment[101]. One strategy to mitigate these limitations is to recapitulate some of the lost features of the cell membrane by encapsulating cell-free sensors inside of synthetic membranes. Encapsulation enables tuning of the reaction environment on a molecular scale, enabling control of molecular interactions and addition of active membrane features to advance sensing capabilities, all while maintaining many of the tunable, advantageous features of cell-free systems[99].

There are two major considerations in designing encapsulated cell-free sensors: determining the impacts of a confined reaction environment on sensor function and choosing an appropriate target molecule and application. In terms of reaction confinement, the small scale of the encapsulated environment can impact reactant loading, reaction time, and limit of detection[102–104]. These effects have been shown to impact the basic processes of gene expression[105], which in turn affects cell-free biosensors that regulate reporter gene expression at the level of transcription or translation[52]. Of the wide range of genetic regulatory networks used for biosensing, RNA-based biosensors that regulate transcription require the fewest components and operate on a faster timescale[23,106], which may reduce the impacts of confinement on sensor function. Riboswitches — noncoding RNA elements upstream of protein coding genes that change their structure in response to specific ligands to regulate gene expression — could offer an opportunity to address these constraints due to reaction confinement.

Previous proof-of-concept studies have focused on encapsulation of two synthetic, translationally regulated riboswitches that respond to membrane-permeable signals: theophylline[101,107,108] and histamine[109]. Both riboswitches have been successfully encapsulated in bilayer vesicles, generating either a fluorescent protein readout or a protein-mediated response upon analyte entry into the vesicle interior[101,107–109]. Encapsulation of transcriptionally regulated riboswitches has proven difficult to date, however; efforts to encapsulate a transcriptionally

regulated adenine riboswitch showed poor switching activity and were subsequently abandoned[108]. This could be due to specific features of the adenine riboswitch or due to a general property of transcriptional riboswitches, which require dynamic conformational changes during transcription to enact their mechanism – a process which could be impacted by general features of confinement or electrostatic interactions with the lipid bilayers[110,111]. Despite these potential challenges, the mechanisms underlying transcriptionally regulated riboswitches are being further uncovered[90]. These sensors have demonstrated the feasibility of detecting environmentally important analytes in cell-free systems and can function with RNA-level outputs[23] - a key feature which may mitigate resource constraints - motivating further efforts for their encapsulation and deployment.

A second major consideration in encapsulated sensor development is the selection of an appropriate target and application. Of the many potential uses of encapsulated biosensors, water quality monitoring is one of the most compelling from a global perspective. One in three people globally lack access to safe drinking water[112], and the ability to identify contaminated water sources is essential for their quarantine or remediation[12]. Fluoride is among the most concerning of these contaminants; chronic exposure to fluoride binds it to the calcium in teeth and bones, weakening them and causing lifelong health consequences[113]. From both environmental and anthropogenic sources, fluoride exposure is especially problematic in parts of China, Africa, South America, and India[113,114], with high fluoride concentrations also found in groundwater across the United States[114]. This diversity of sample sources comes with a corresponding increase in potential reaction inhibitors, presenting the need for a robust sensor that retains function in complex matrices. Encapsulated fluoride biosensing reactions would address this need, delivering far-reaching global health benefits and establishing a framework to address future water quality challenges.

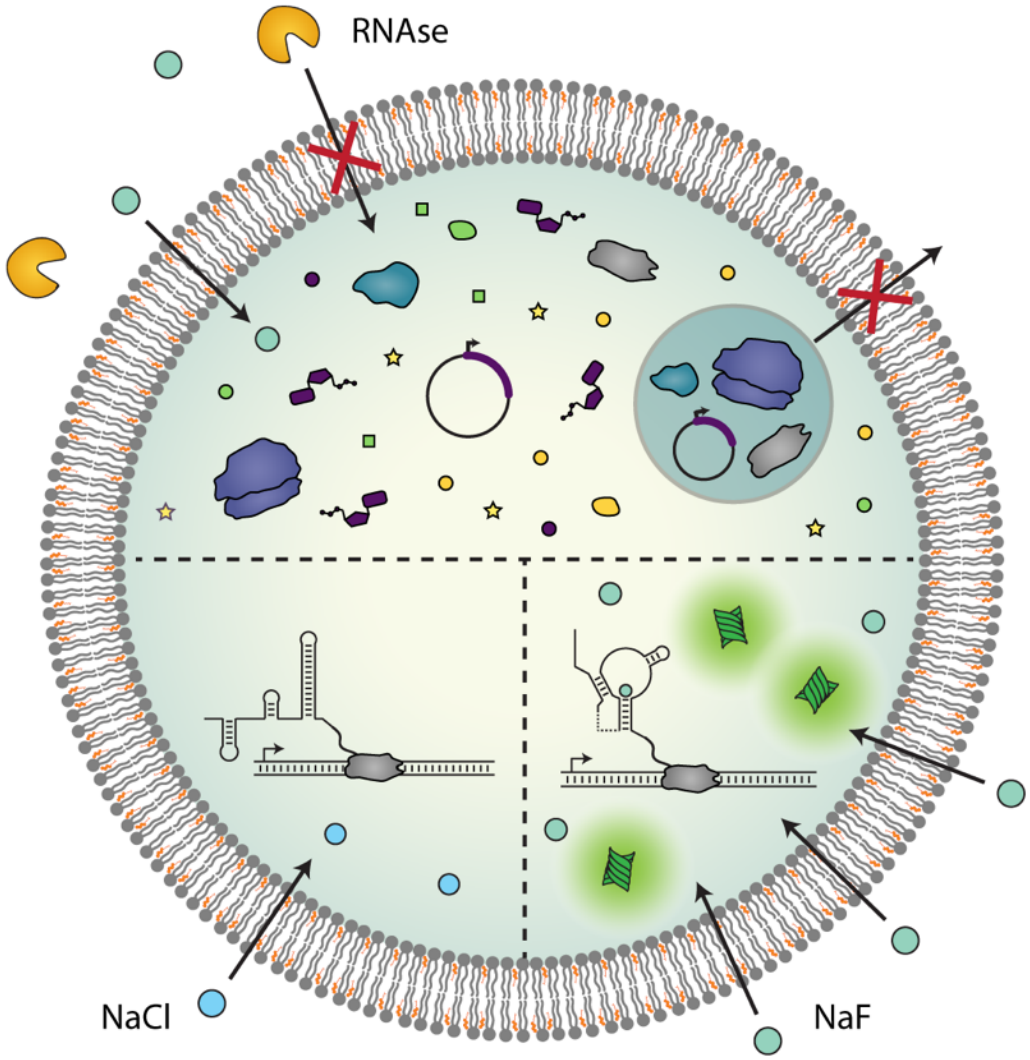

Figure 3-1. Encapsulated cell-free sensors.
Encapsulation of cell-free systems creates a semipermeable barrier between sensor components and the environment, which modulates their molecular interactions. Reactants are contained within the vesicle interior, while proteins and other large molecules in the external sample are excluded from vesicle entry (top). Small, membrane-permeable molecules can diffuse into the vesicle interior, initiating a riboswitch-mediated response that is specific to an analyte of interest (bottom right). The riboswitch folds into a terminating conformation in the absence of sufficient concentrations of target analyte (bottom left).

In this study, we sought to develop vesicle-based sensors for fluoride by encapsulating a transcriptionally regulated, fluoride-responsive riboswitch within bilayer membranes (**Figure 3-1**). We first encapsulate the riboswitch, then demonstrate its ability to detect externally added fluoride and show that membrane composition can be modified to tune sensitivity to exogenous ions. We also demonstrate that encapsulation protects cell-free reactions from sample degradation,

particularly from extravesicular degradative enzymes. Finally, we couple riboswitch output to both fluorescent and colorimetric reporters and show that vesicle-based sensors can detect fluoride in real-world water samples. This work demonstrates the potential of encapsulated, riboswitch-based sensors for biosensing applications, complimenting existing cell-free sensor engineering strategies and enabling sensing in otherwise inhospitable environments.

3.2 A transcriptionally regulated fluoride riboswitch can function inside lipid vesicles

We first sought to confirm that a transcriptional riboswitch can function when encapsulated inside lipid vesicles. For the riboswitch, we chose the fluoride responsive riboswitch from Bacillus cereus, which we previously showed can be used to control the expression of several different reporter proteins and fluorescent RNA aptamers in bulk E. coli extract-based cell-free systems[23]. In this system, the fluoride riboswitch is encoded within a single DNA template, downstream of a consensus E. coli promoter sequence, and upstream of a reporter coding sequence. In the absence of fluoride, E. coli polymerase transcribes the riboswitch sequence, causing it to fold into a conformation that exposes a transcriptional terminator hairpin and subsequently causes RNA polymerase to stop transcription[70]. In the presence of fluoride, fluoride binding to the riboswitch aptamer domain prevents the terminator from folding, allowing transcriptional elongation of the reporter coding sequence.

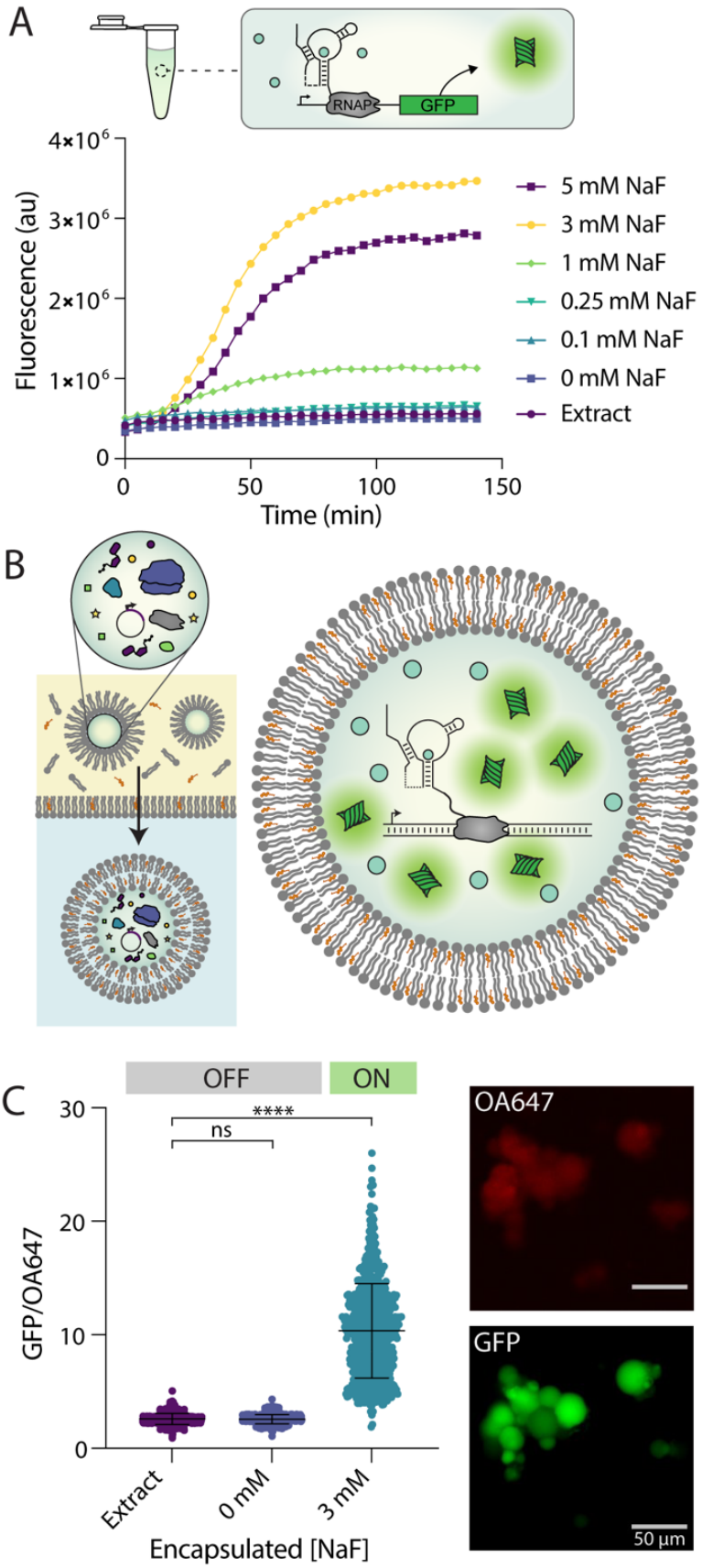
A
RNAP
GFP
4×10^6
3×10^6
2×10^6
1×10^6
0
Fluorescence (au)
0
50
100
150
Time (min)
5 mM NaF
3 mM NaF
1 mM NaF
0.25 mM NaF
0.1 mM NaF
0 mM NaF
Extract
B
C
OFF
ON
****
ns
30
20
10
0
GFP/OA647
Extract
0 mM
3 mM
Encapsulated [NaF]
OA647
GFP
50 µm

Figure 3-2. A fluoride riboswitch can function within bilayer vesicles.
(a) Riboswitch-regulated GFP expression in bulk conditions in response to increasing fluoride concentrations. In the presence of NaF the riboswitch folds into an "ON" state, which allows expression of a GFP reporter molecule. **(b)** Double emulsion assembly allows the encapsulation of functional cell-free reactions. Assembled reactions are vortexed into a lipid/oil mixture, then centrifuged into an aqueous solution (left). The resulting vesicles contain cell-free reactions which can respond to co-encapsulated fluoride by expressing GFP (right). **(c)**. GFP/OA647 fluorescence, which indicates GFP concentration relative to the OA647 volume marker inside each liposome. GFP/OA647 fluorescence increases inside of vesicles when 3 mM NaF is co-encapsulated compared to no DNA (Extract) or no fluoride (0 mM NaF) controls. Micrographs show variations in GFP fluorescence between vesicles from the same population, which results in a distribution of fluorescence values. Scale = 50 μm. Black lines indicate mean fluorescence and standard deviation. **** $p \leq 0.0001$, nonsignificant (ns) $p > 0.1234$; p-values generated using a One-Way ANOVA and Tukey's Multiple Comparisons Test.

In this study, we first chose to use a super folder green fluorescent protein (GFP) reporter, as it allows convenient measurement of riboswitch activity. For the cell-free system, we used an E. coli S30 lysate prepared with runoff and dialysis, which has been shown to allow the function of biosensors that require bacterial polymerases[91]. Embedding the riboswitch DNA template into the extract system alongside varying concentrations of sodium fluoride (NaF) showed, as expected[23], an increase in GFP fluorescence as fluoride concentrations increased up to 3 mM, followed by a decrease in fluorescence at higher concentrations (**Figure 3-2a**). This decrease is likely caused by fluoride inhibition of the gene expression machinery[115] and is consistent with previous studies[23]. Accordingly, we used 3 mM NaF for the remainder of this study to obtain the expected maximum fluorescent output of the system.

We then set out to assess whether the fluoride riboswitch could retain functionality when encapsulated within lipid vesicles. Vesicles were synthesized using a water-in-oil emulsion transfer method[116] (**Figure 3-2b**). In this method, various membrane amphiphiles (e.g. lipids, cholesterol, fatty acids, diblock copolymers) are dissolved into an oil phase and an emulsion is formed by vortexing the aqueous cell-free reaction into this mixture. The emulsion is then layered onto a second aqueous layer, and emulsified droplets are centrifuged through the oil-water interface to generate unilamellar vesicles. Vesicle synthesis using this approach yields a distribution of different vesicle sizes on the 5-50 μm scale, which could impact our quantification of fluorescence[117]. To control for this, we also incorporated a protein-conjugated dye, ovalbumin-

conjugated Alexafluor 647 (OA647), which served as a volume marker and allowed us to detect the vesicle interior regardless of GFP expression level[109,118]. After synthesis, vesicles were incubated under varying conditions at 37°C, and protein expression was assessed using epifluorescent microscopy. Vesicles were imaged using GFP and Cy5.5 channels, and images were analyzed using the NIS-elements AR software program[119], which allowed us to automatically select vesicle interiors using the OA647 marker and report GFP fluorescence in those regions. This protocol allowed us to analyze hundreds of vesicles per sample, maintain the same selection parameters between samples, and minimize the impact of user selection bias in the analysis. Additionally, the encapsulated volume marker allowed us to report GFP expression relative to OA647 fluorescence to control for possible variability in vesicle size or loading. Using this method, we were able to ensure that our measurements were isolated to intact (non-lysed) vesicles which retained their protein cargo (**Supplemental Figure 9**).

Using the above approach, we encapsulated cell-free reactions with and without fluoride present in the bulk reaction mixture. We chose to use a 2:1 ratio of cholesterol and POPC phospholipid as membrane amphiphiles due to their previous use in similar encapsulated expression studies[101,107–109,117]. Upon co-encapsulation of the riboswitch with 3 mM NaF we observed GFP expression inside vesicles, indicating the riboswitch was in the “ON” state (**Figure 3-2c**). In contrast, in the absence of DNA (extract only) or in the absence of fluoride (0 mM NaF) we observed minimal GFP expression, indicating an “OFF” state (**Figure 3-2c**). This high level of GFP induction inside vesicles by fluoride indicates that membrane encapsulation does not eliminate the ability of the riboswitch to fold properly and does not cause significant nonspecific expression.

We observed that populations of vesicles exhibited variations in GFP fluorescence between individual liposomes after 6 hours of incubation (**Figure 3-2c**), a phenomenon which has been observed in similar studies across multiple encapsulation protocols[101,104,109,116,120–122]. It has been hypothesized that these variations in gene expression may be caused by variability in

vesicle loading and/or varied levels of molecular exchange with the surrounding buffer for vesicles of different sizes[104,120,121,123]. To report this variability across vesicle populations we have included metrics of skew for each population result (**Supplemental Tables 3-5**). Even after taking this variability into account, however, induction of GFP expression is clearly observable across the vesicle population, indicating proper riboswitch sensor activity and a robust response to fluoride in encapsulated sensors.

3.3 External fluoride can be detected by an encapsulated riboswitch

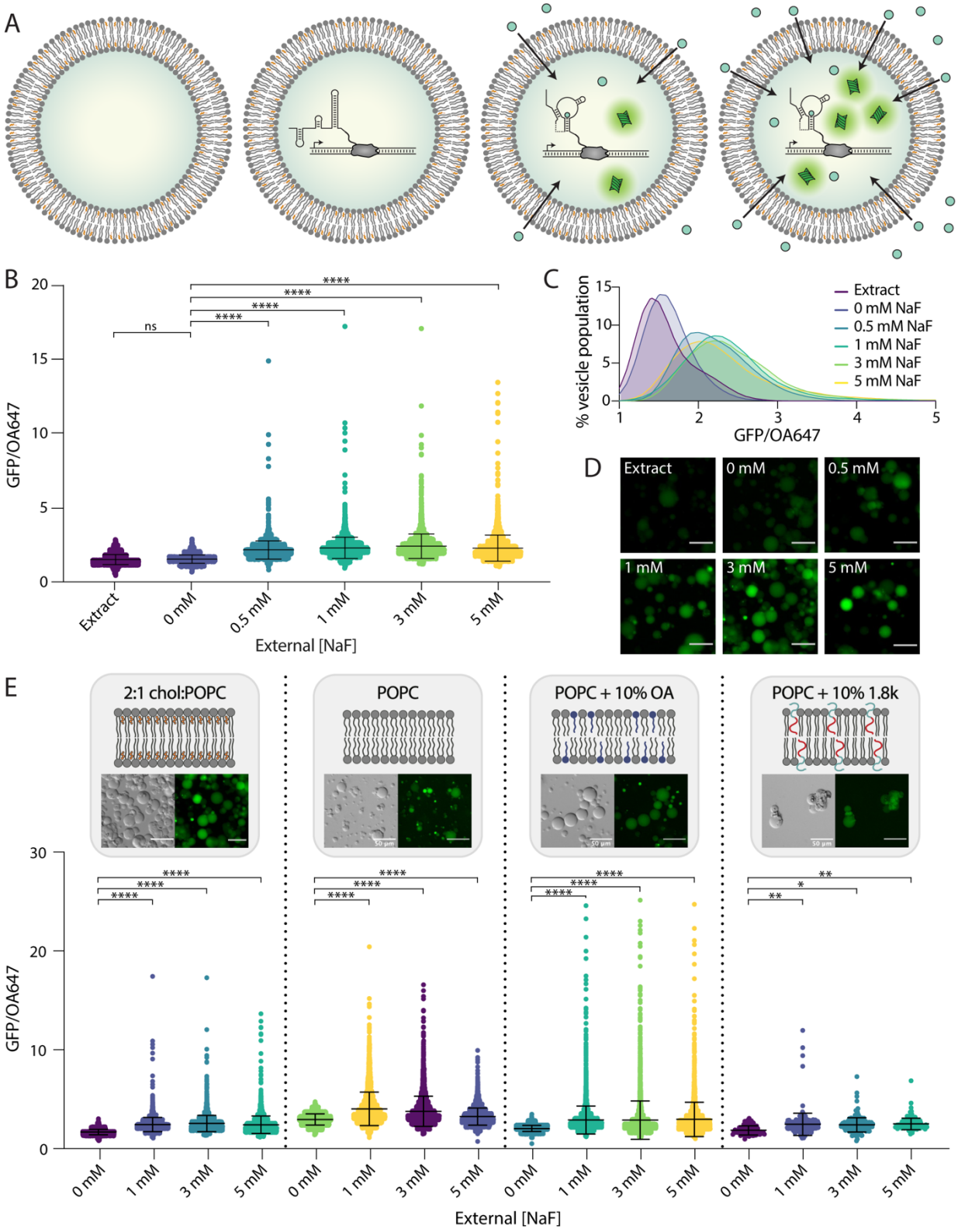

Figure 3-3. Detection of external fluoride by encapsulated sensors.
(a) Schematic of conditions. Vesicles were prepared encapsulating extract only (left), or fully assembled reactions without NaF. Upon addition of increasing fluoride in the external solution, expression of GFP inside vesicles increases (right). **(b)** GFP/OA647 fluorescence as a result of riboswitch activity in 2:1 cholesterol:POPC vesicles in response to increasing NaF added externally. Black lines indicate mean fluorescence ratio and standard deviation. **(c)** Histogram of vesicle populations shown in (b). Data plotted with lowless curve fitting. **(d)** GFP fluorescence in micrographs of vesicles with increasing external concentrations of NaF. Scale = 50 μm. **(e)** GFP/OA647 fluorescence in response to increasing fluoride shown from left to right: 2:1 cholesterol:POPC membranes (data from B); pure POPC lipid membranes; POPC + 10% oleic acid membranes; POPC + 10% 1.8k PEO-b-PBD membranes. Composition and morphology of each membrane composition indicated by schematics and micrographs, respectively. **** $p \leq 0.0001$, ** $p \leq 0.0021$, * $p \leq 0.0332$, nonsignificant (ns) $p > 0.1234$; p-values generated using a One-Way ANOVA and Tukey's Multiple Comparisons Test.

We next sought to determine whether the encapsulated riboswitch could detect fluoride added to the external solution of pre-assembled sensor vesicles. To assess this, we prepared vesicles containing cell-free reactions without NaF present in the reaction mixture. We then titrated in NaF into the solution surrounding vesicles (**Figure 3-3a**) and imaged vesicles following incubation for 6 hours at 37°C. We observed increasing GFP expression with increasing concentrations of NaF up to 3 mM and a slight decrease in average fluorescence at 5 mM, consistent with bulk studies (**Figure 3-3**). Vesicle populations exhibited increases in both mean GFP/OA647 fluorescence and population skew in response to increasing fluoride, either of which could serve as a metric of fluoride detection (**Supplemental Table 3**). All fluoride-containing conditions exhibited a significant increase in fluorescence compared to no-DNA and no-fluoride controls (**Figure 3-3b & c, Supplemental Table 3**). When incubated with chloride, a similarly monovalent anion, a slight response to increasing ion concentration was observed, however these responses were significantly lower than any response to fluoride and did not exhibit any of the highly active vesicles that were observed in all fluoride-containing conditions (**Supplemental Figure 10**). These responses were easily distinguishable between fluoride and chloride, indicating sufficient specificity to fluoride, as has been observed previously[23]. Taken together, these results indicate that increasing concentrations of fluoride added to the extravesicular environment can be detected by the encapsulated riboswitch.

This result was somewhat unexpected, as we anticipated that the membrane would be relatively impermeable to charged fluoride ions. The observed magnitude of fluoride permeability may be explained in part by the transient formation of hydrofluoric acid (HF). HF has been shown to exhibit a permeability coefficient that is seven orders of magnitude greater than fluoride anions through lipid/cholesterol bilayers, indicating that HF travels through the membrane much more readily than its anionic F- counterpart[115,124]. We confirmed this effect by encapsulating a pH sensitive dye, HPTS, which reported a slight decrease in pH in the vesicle interior upon the addition of fluoride to the external buffer (**Supplemental Figure 11**). This result indicates an increase in proton concentration inside the vesicle as fluoride concentration increases, consistent with cross-membrane transport of HF.

Since we observed fluoride could pass through the membrane to interact with the encapsulated riboswitch, we wondered if we could alter the composition of vesicle membranes to modulate membrane permeability and thereby modulate sensitivity of these sensors to external fluoride. Membrane permeability to small molecules depends significantly on membrane composition, as various lipid chain chemistries and contributions from other amphiphilic components can impart an effect on membrane physical properties. Cholesterol, a major component of our original 2:1 cholesterol:POPC lipid composition, is known to decrease membrane permeability by increasing lipid packing and altering membrane fluidity and rigidity (50). PEO-b-PBD diblock copolymers are similarly known to reduce membrane permeability by increasing membrane viscosity, introducing steric barriers from the polyethylene glycol groups that assemble at the membrane interface, and increasing thickness and chain entanglements within the hydrophobic portions of the membrane[125,126]. In contrast, fatty acids such as oleic acid have been shown to increase membrane permeability to ionic solutes by incorporating single hydrocarbon chains that have a different shape and amphiphathicity than diacyl chains, reducing lipid chain packing and enhancing fluidity of the bilayer[127,128]. Using this series of amphiphilic

molecules, we set out to assess the capacity of membrane amphiphiles and the resulting membrane permeability to modulate the performance of an encapsulated cell-free sensor.

To explore the effect of these amphiphiles on membrane permeability to fluoride, we prepared vesicles with either 1) pure POPC lipid, 2) POPC lipid + 10% oleic acid (OA), or 3) POPC lipid + 10% PEO14-b-PBD22 polymer (MW = 1.8kDa, hereafter referred to as 1.8k) components in the lipid/oil mixture, encapsulating cell-free reactions as normal (Figure 3E). We observed an increase in overall GFP expression in both pure POPC lipid and POPC + 10% OA conditions compared to our original 2:1 cholesterol:POPC lipid composition. These results are consistent with the removal of cholesterol and the addition of oleic acid, respectively, both of which should increase membrane permeability (**Figure 3-3d**). In addition, the inclusion of oleic acid in vesicle membranes led to a reduction of sensor sensitivity, measured via a reduced concentration dependence of GFP expression on NaF concentration, indicating high permeability to any amount of external fluoride. In contrast, vesicles containing 10% 1.8k diblock copolymer exhibited very little GFP expression, indicating reduced membrane permeability. Mean POPC vesicle fluorescence peaked at 1 mM NaF, while 10% OA and 10% 1.8k diblock copolymer responses were maximum at 5 mM NaF (**Supplemental Table 4**). Taken together, these results indicate that exchanging membrane components to control membrane permeability provides a handle to tune the sensitivity of an encapsulated riboswitch to an analyte of interest. Further, the selection of highly permeable amphiphiles does not necessarily improve sensor performance and may instead increase overall signal but limit sensor resolution. A balance between analyte access and desired sensing behavior is likely an important consideration for engineering encapsulated biosensing systems depending on the desired application.

3.4 Encapsulation protects sensor components from degradation

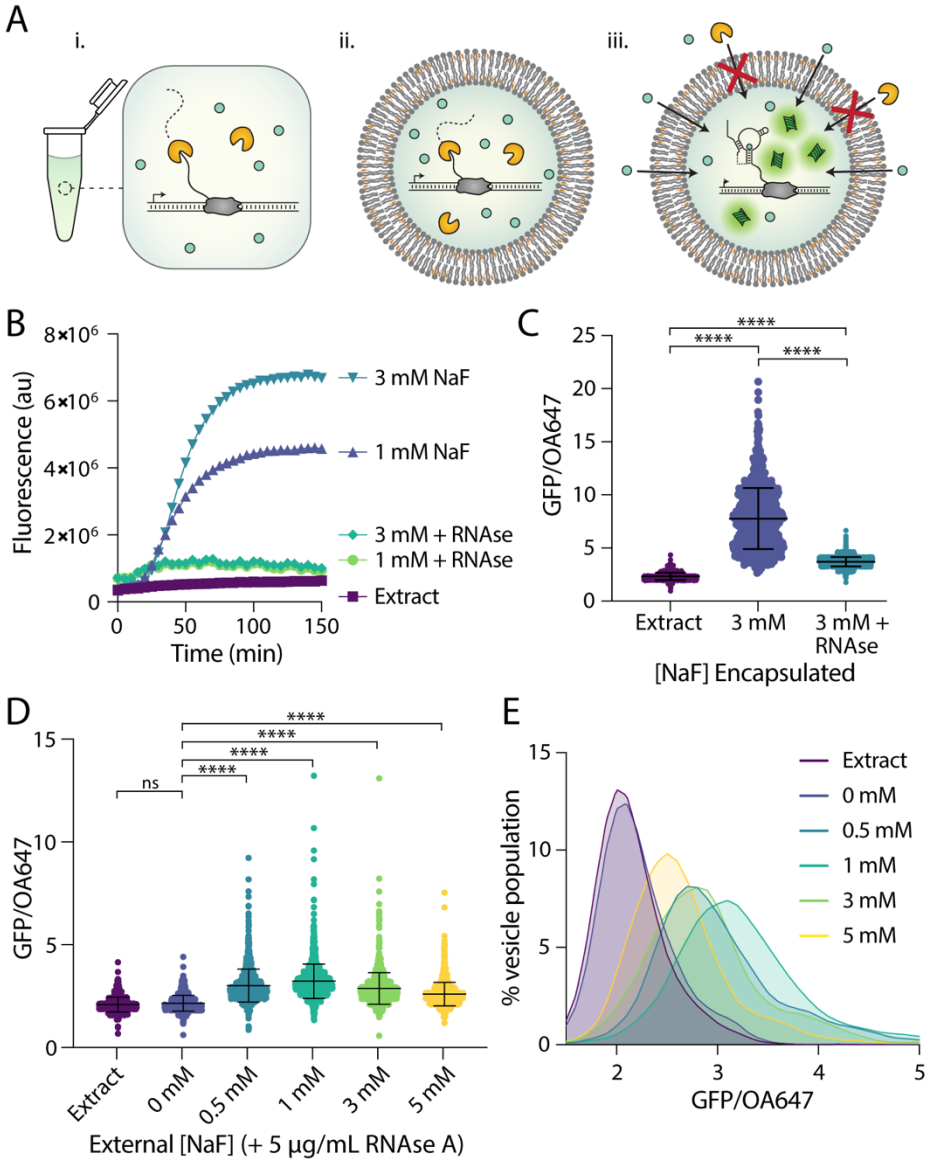

Figure 3-4. Encapsulation protects from degradation by RNAse A.
(a) Schematic of RNAse-containing conditions. RNAse A degrades the riboswitch (i) in bulk conditions and (ii) when co-encapsulated with reactants but is unable to reach reactants contained within vesicles (iii). **(b)** Riboswitch response to NaF in bulk conditions with and without RNAse A added to reaction. **(c)** Riboswitch activity as indicated by GFP/OA647 fluorescence when encapsulated with 3 mM NaF compared to the co-encapsulation of both 3 mM NaF and RNAse A. **(d)** Response of encapsulated riboswitch to externally added NaF with RNAse A present in external solution. Black lines indicate mean and standard deviation. **(e)** Histogram of data in (d). Data plotted with lowless curve fitting. **** $p \leq 0.0001$, nonsignificant (ns) $p > 0.1234$; p-values generated using a One-Way ANOVA and Tukey's Multiple Comparisons Test.

Having established that these vesicle sensors can detect external fluoride, we next wanted to explore how they might function in complex samples. One of the major benefits of membrane

encapsulation is the ability to leverage the semipermeable barrier formed by the membrane to contain and protect encapsulated components. Cell-free reactions, particularly those using riboswitches, are highly sensitive to the presence of nucleases and proteases which can degrade sensor components before a target analyte is encountered[100]. Due to their large size, however, enzymes are unable to pass through the vesicle membrane to access encapsulated reactants.

To determine whether the vesicle membrane can sufficiently protect encapsulated reactions from external degradation, we tested various vesicle assemblies in the presence of RNAse A (**Figure 3-4a**). We observed that RNAse completely eliminated the riboswitch response to NaF both in bulk conditions and when RNAse was co-encapsulated with the cell-free reaction in vesicles (**Figure 3-4b, Figure 3-4c**). In contrast, encapsulated sensors maintained the ability to respond to externally added NaF when RNAse was present in the external sample (**Figure 3-4d, Supplemental Table 5**). Interestingly, we noticed a decrease in mean GFP fluorescence at higher external NaF concentrations compared to sensors without RNAse present, which we hypothesized was due to slightly higher degrees of vesicle instability or membrane permeability from the addition of small amounts of glycerol in the RNAse buffer (**Supplemental Figure 12**). Instability could lead to higher rates of vesicle lysis and therefore lower overall GFP fluorescence, while increased permeability could cause increased reaction poisoning with high fluoride concentrations. Nevertheless, all vesicle populations exhibited increased GFP expression in the presence of fluoride, demonstrating simultaneous permeation of fluoride into the vesicle interior and exclusion of RNAse A from the cell-free reaction. These results indicate that encapsulation in bilayer membranes can sufficiently exclude RNAse from the reaction environment, thereby protecting the cell-free sensor within a semipermeable compartment. The external addition of RNAse A, demonstrated here, serves as a proof-of-concept step towards cell-free detection in complex environments, such as biological samples or highly contaminated environmental samples.

3.5 Sensors can detect fluoride in real-world samples

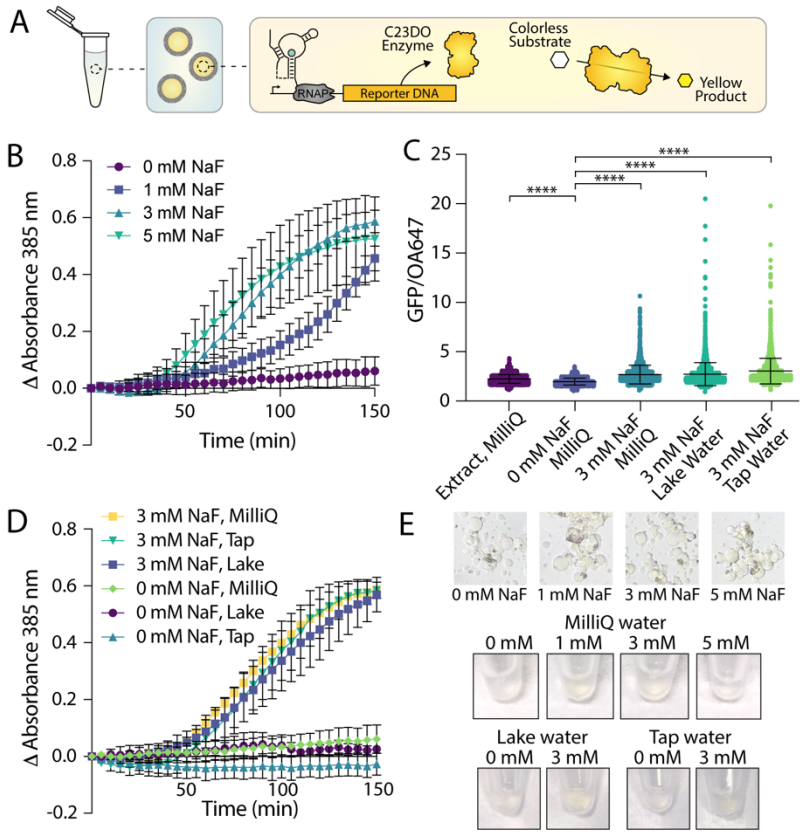

Figure 3-5. Enzymatic readout and detection of fluoride in real-world samples.
(a) Schematic of encapsulated enzymatic readout. Riboswitch activation inside vesicles leads to the expression of C23DO, resulting in the production of a yellow product that is localized to the vesicle interior. **(b)** Absorbance over time inside of vesicles encapsulating a catecholase-based readout in response to external NaF. Output is reported as a change in absorbance to account for variations in final vesicle concentration between different vesicle preparations. N=3 independent vesicle preparations. **(c)** GFP/OA647 fluorescence ratios observed in vesicles containing a GFP-based readout after incubation in outer solutions from laboratory grade water (MilliQ), tap water, and lake water supplemented with NaF. **(d)** Absorbance over time inside of vesicles incubated in samples derived from MilliQ water, tap water and lake water supplemented with either 0 mM NaF or 3 mM NaF. N=2 independent vesicle preparations. **(e)** Colorimetric changes in vesicles as viewed through a microscope eyepiece and by eye in Eppendorf tubes. **** $p \leq 0.0001$, nonsignificant (ns) $p > 0.1234$; p-values generated using a One-Way ANOVA and Tukey's Multiple Comparisons Test.

Finally, we wondered if we could extend these results to conditions that would be more relevant for real-world environmental sensing. Although fluorescence is a common readout for many biological assays, GPF fluorescence inside vesicles is difficult to monitor with common equipment, particularly in non-laboratory settings. In addition, with our vesicle-based construct, GFP fluorescence was too low to measure in vesicle populations in bulk, necessitating more

sensitive microscopy analysis methods. To address this limitation, we coupled fluoride detection to an alternative reporter enzyme, catechol (2,3)-dioxygenase (C23DO)[23]. In this system, the riboswitch "ON" state leads to the expression of C23DO, which catalyzes the conversion of its colorless substrate, catechol, to the yellow-colored 2-hydroxymuconate semialdehyde to generate a colorimetric response (**Figure 3-5a**). In bulk conditions this construct exhibits a fast and robust response to fluoride, and the colorimetric output generated is clearly distinguishable by eye for both laboratory and field-collected water samples[23].

To investigate whether this enzymatic reporter could function within our sensor vesicles, we encapsulated cell-free reactions with DNA coding for the riboswitch-C23DO construct and supplemented them with 1 mM catechol (**Figure 3-5a**). We then titrated NaF into the outer solution and monitored color changes in each population of vesicles via changes in absorbance at 385 nm. In contrast to our GFP-based readout, signal amplification from the enzyme-regulated construct allowed us to assess absorbance changes in an entire population of vesicles rather than on a vesicle-by-vesicle basis. RNAse A was also added to the outer vesicle solution to control for any unencapsulated reactions caused by vesicle lysis. The response was significantly lower than that observed in bulk (**Supplemental Figure 13**) but increases in absorption in response to increasing NaF concentrations were observed across multiple sample preparations (**Figure 3-5b**). Readout time plays a key role in sensor response[23], particularly for the 1 mM NaF condition, where amplified responses followed by signal decay make quantification difficult (**Figure 3-5b, Supplemental Figure 13**). Little expression was observed in 0 mM NaF samples in this time frame, however, which indicates potential for these sensors to serve as binary classifiers even in the presence of low fluoride concentrations. Importantly, responses to fluoride could be detected within 2 hours of incubation compared to 6 hours for the GFP-based readout.

Having demonstrated the compatibility of our encapsulated sensors with multiple reporters and their ability to detect extravesicular fluoride, we set out to test whether these sensors could be used to monitor fluoride concentrations in real-world samples. We collected water samples

from Lake Michigan and the Evanston, IL municipal tap water supply and used each sample to prepare the vesicle outer solution. We supplemented these outer solutions with either 0 mM NaF or 3 mM NaF and added vesicles with either the GFP-coupled riboswitch construct or the colorimetric construct. We observed increased GFP expression in all populations of vesicles incubated with 3 mM NaF outside compared to no-fluoride controls, with a slightly higher level of GFP expression in both lake and tap water samples compared to those incubated with laboratory-grade Milli Q water (**Figure 3-5c**). Similarly, vesicles encapsulating the enzymatic construct showed increasing absorption over time in the presence of 3 mM NaF, while all no-fluoride controls exhibited no significant changes in absorption (**Figure 3-5d**). Slight color changes were visible by eye in tubes containing vesicles, and changes in color inside of vesicles could be observed on the microscope as imaged through the eyepiece (**Figure 3-5e**). These results were consistent with those observed in bulk assays, which showed a slightly higher response to both tap and lake water and a significant difference between all 0 mM and 3 mM conditions (**Supplemental Figure 13**). The results observed here highlight the feasibility of these vesicle-based sensors to detect environmentally relevant small molecules in real-world samples, a step toward encapsulation to generate deployable cell-free sensors.

3.6 Discussion

To our knowledge, this work represents the first demonstrated function of a transcriptionally regulated riboswitch encapsulated in bilayer vesicles. We have demonstrated that this encapsulated riboswitch can detect exogenous fluoride through permeability-based sensing, generating both fluorescent and colorimetric outputs. Additionally, we have shown that responses to fluoride can be modulated by changing membrane composition, which provides a useful handle to control sensor stability and sensitivity. Looking ahead toward sensor deployment, this work establishes that encapsulation can protect cell-free sensors from degradative sample components while allowing analyte detection in real-world samples. While cell-free sensors have

been previously used for the detection of environmental molecules of interest[23,25,26,54,92–96], encapsulation of these systems may ultimately diversify the contexts within which cell-free sensors can operate.

Although encapsulation can provide powerful advantages to cell-free sensing, it also brings some limitations. The concentrations of fluoride assessed here are high compared to the Maximum Contaminant Limits set by the Environmental Protection Agency (0.5 mM vs 0.22 mM), which were chosen based on the spread of responses observed in liposomes. The variability observed in the responses of individual liposomes within a vesicle population would likely serve as a hurdle for technological use of these sensors in future applications, which may necessitate alternative vesicle assembly techniques, such as microfluidics[117], and a better understanding of the underlying biophysics of cell-free reactions inside membranes. While we explored protein-based outputs here, riboswitch expression could also be coupled to transcription-based reporting, such as aptamer-dye outputs[23], to build a transcription-only sensor that would require encapsulation of fewer components and should operate on quicker timescales. Finally, the reintroduction of a barrier between sample and sensor also requires strategies to transport specific analytes into the vesicle. Membrane compositional changes can enable permeability-based import for certain small analytes, with many natural and synthetic amphiphiles to choose from. Moving forward, we can gain even finer control of membrane permeability by incorporating transmembrane proteins to enhance sensing capabilities and introduce more advanced sensing or responsive functions. These strategies could ultimately allow new functions for these types of sensors, including conjugation-based capture methods, deployment and transport of cell-free reactions, controlled sensor degradation, or enhanced sensor biocompatibility[99].

The diversity of existing cell-free sensors could ultimately lead to a new generation of encapsulated biosensors for a wide array of analytes. With the modularity of components in these systems, vesicle-based sensors could be engineered which use various membrane components, genetic circuits, and triggered responses to detect small molecules of interest[109,129,130]. As focus

shifts toward sensor application, these platforms could offer additional handles with which to tune sensor characteristics to advance the types of contexts in which cell-free sensing can operate, allowing for detection in environments like soil, ground water, or biological samples. Finally, the incorporation of additional transcription-based cell-free systems, particularly those using riboswitch-based sensing, may ultimately allow the development of a family of encapsulated sensors that are fast, specific, and deployable.

3.7 Materials and Methods

Chemicals

POPC (1-palmitoyl-2-oleoyl-glycero-3-phosphocholine) and cholesterol were purchased from Avanti Polar Lipids Inc. Oleic acid (OA), glycerol, sucrose, glucose, HPTS (8-Hydroxypyrene-1,3,6-trisulfonic acid trisodium salt), BioUltra Mineral Oil, phosphate-buffered saline (PBS), bovine serum albumin (BSA), and NaF were purchased from Millipore Sigma. 1.8k PEO-b-PBD polymer was purchased from Polymer Source. Ovalbumin-conjugated AlexaFluor 647 (OA647), calcein dye and HEPES buffer were purchased from Thermo Fisher. RNAse A was purchased from New England Biolabs.

Plasmid construction

Plasmids were assembled using Gibson assembly (New England Biolabs, Cat#E2611S) and purified using a Qiagen QIAfilter Midiprep Kit (QIAGEN, Cat#12143). Coding sequences of the plasmids consist of the crcB fluoride riboswitch from Bacillus cereus regulating either superfolder GFP (pJBL3752) or catechol 2,3-dioxygenase (pJBL7025), all expressed under constitutive Anderson promoter J23119. Plasmid sequences available on Addgene with accession numbers 128809 (pJBL3752) and 128810 (pJBL7025).

Cell-free reaction assembly

Cell-free extract and reactions were prepared according to established protocols[23,91]. Briefly, cell-free reactions were assembled by mixing cell extract, a reaction buffer containing the small molecules required for transcription and translation (NTPs, amino acids, buffering salts, crowding agents, and an energy source), and DNA templates and inducers at a ratio of approximately 30/30/40. Sucrose was added to a final concentration of 200 mM to facilitate encapsulation. Each reaction was prepared on ice to 16.5 µL final volume in batches of 7. Reactions were prepared with 10 nM pJBL3752 (riboswitch-GFP plasmid) or pJBL7025 (riboswitch-enzyme plasmid) + 1 mM catechol. Reaction master mix was assembled, then added to DNA, inducers, sucrose, and water to a final volume of 16.5 µL per reaction aliquot. For reactions containing volume marker, reaction mix was supplemented with 1.4 µL OA647. Preparation conditions were kept consistent between reactions, only varying NaF concentration or omitting DNA for extract-only controls.

Encapsulation of cell-free reactions

Encapsulated sensors were prepared via water-in-oil double emulsion methods. Lipid films were prepared by mixing amphiphiles (lipid, cholesterol, fatty acid or polymers) in chloroform to a final amphiphile concentration of 25 mM at a volume of 200 µL. Films were dried onto the side of a glass vial under nitrogen gas, then placed in a vacuum oven overnight. 200 µL of BioUltra mineral oil was added to lipid films and heated at 80°C for 30 minutes, followed by 10 seconds of vortexing to incorporate amphiphiles into the oil. Lipid/oil mixtures were cooled on to room temperature, then placed on ice during cell-free reaction assembly. Cell-free reactions were prepared on ice as described above. Reactions were layered on top of lipid/oil mixture, then vortexed for 30 seconds to form an emulsion. Emulsions were incubated at 4°C for 5 minutes, then layered onto outer solution containing all small molecules required for transcription and translation, 100 mM HEPES buffer (pH 8), and 200 mM glucose. Samples were again incubated

at 4°C for 5 minutes, then centrifuged for 15 minutes at 18,000 rcf at 4°C. Vesicle pellets were collected by pipette and placed into fresh Eppendorf tubes. Prepared vesicles were then added in 10 µL aliquots to 20 µL fresh outer solution supplemented with NaF, certain water samples and/or RNAse A (5 µg/mL final concentration). Osmolarity of NaF stock solution was adjusted to match that of the outer solution by adding glucose to minimize osmotic effects on vesicles.

Cell-free protein expression

For bulk assays, unencapsulated reactions were prepared as described above and added to 384-well plates. Protein expression was monitored at 37°C in a SpectraMax i3x plate reader (Molecular Devices). GFP was monitored at ex: 485 nm, em: 510 nm. Catechol absorbance was monitored at 385 nm.

Encapsulated sensors with a colorimetric readout were monitored at an absorbance of 385 nm using a SpectraMax i3x plate reader at 37°C until expression reached a plateau, about 2.5 hours, after which samples were removed from plates and placed into Eppendorf tubes or microscopy chambers for imaging. Images of tubes and through the microscope eyepiece were taken using an iPhone 8. Absorbance measurements in the plate reader are reported relative to initial absorbance to control for slight differences in vesicle concentration between vesicle preparations.

Encapsulated sensors expressing GFP were incubated in outer solution for 6 hours at 37°C, then imaged on a Nikon Ti2 inverted microscope. Imaging chambers were blocked with BSA for 20 minutes, then triple rinsed with 766 mOsm PBS. Vesicles were added to equiosmolar PBS and allowed to settle for 5 minutes before imaging. Images were taken using DIC, GFP (ex: 470, em: 525) and Cy 5.5 (ex: 650, em: 720) filters under 10x magnification, 20% laser intensity, and 1 second exposure. Images were analyzed using Nikon NIS-elements AR software Advanced Analysis tool[119]: vesicles were selected using the OA647 channel. General analysis protocol was set with the following settings. Preprocessing: Local contrast, size 105, power 50%. Threshold

minimum: 393. Smooth 1x, clean 1x. Size minimum: 2 μm. Return Mean GFP, Mean OA647, Max GFP.

Encapsulated dye assays

HPTS assay: vesicles were prepared via thin film hydration with 33% Cholesterol and 66% POPC. Lipid and cholesterol in chloroform were dried onto the side of a glass vial under nitrogen gas to form a lipid film. Vesicle films were hydrated with HEPES + 0.5 mM HPTS dye overnight at 60°C. Vesicles were extruded to 400 nm, purified via Size Exclusion Chromatography (SEC), and added to a 384-well plate with equiosmolar HEPES buffer + varying concentrations of NaCl and NaF. HPTS fluorescence was monitored with excitation at 405 and 450 nm and emission at 510 nm, as characterized by Hilburger et al.[131]. HPTS fluorescence is reported as the ratio of emission intensities when excited at 450 nm/405 nm.

Calcein assay: vesicles were prepared via thin film hydration with 33% Cholesterol and 66% POPC. Lipid and cholesterol in chloroform were dried onto the side of a glass vial under nitrogen gas to form a lipid film. Vesicle films were hydrated with HEPES + 20 mM calcein dye overnight at 60°C. Vesicles were extruded to 400 nm, purified via SEC, and added to a 384-well plate with equiosmolar HEPES buffer and increasing volumes of 0.02% glycerol solution or RNAse prepared in buffer to the same final glycerol concentration (1.25 μL corresponds to the concentration used for manuscript studies). Vesicles were incubated for 4 hours at 37°C and calcein fluorescence was measured (ex: 495 nm, em: 515 nm). Vesicles were lysed with 1 μL 10% TritonX and total calcein fluorescence was measured to determine fraction release.

Statistical Analysis

All graphing and statistical analysis was conducted in Graphpad Prism. Populations of vesicles were analyzed using One-Way ANOVA analysis with Tukey's Multiple Comparisons Test

and descriptive statistics. Significance is reported as follows: **** $p \leq 0.0001$, ** $p \leq 0.0021$, * $p \leq 0.0332$, nonsignificant (ns) $p > 0.1234$.

Vesicle Analysis

Vesicles were selected using the OA647 channel. General analysis protocol was set with the following settings. Preprocessing: Local contrast, size 105, power 50%. Threshold minimum: 393. Smooth 1x, clean 1x. Size minimum: 2 mm. Return Mean GFP, Mean OA647, Max GFP.

HPTS Assay

Vesicles were prepared via thin film hydration with 33% Cholesterol and 66% POPC. Lipid and cholesterol in chloroform were dried onto the side of a glass vial under nitrogen gas to form a lipid film. Vesicle films were hydrated with HEPES + 0.5 mM HPTS dye overnight at 60°C. Vesicles were extruded to 400 nm, purified via Size Exclusion Chromatography (SEC), and added to a 384-well plate with equiosmolar HEPES buffer + varying concentrations of NaCl and NaF. HPTS fluorescence was monitored with excitation at 405 and 450 nm and emission at 510 nm, as characterized by Hilburger *et al.* (*59*). HPTS fluorescence is reported as the ratio of emission intensities when excited at 450 nm/405 nm.

Calcein Assay

Vesicles were prepared via thin film hydration with 33% Cholesterol and 66% POPC. Lipid and cholesterol in chloroform were dried onto the side of a glass vial under nitrogen gas to form a lipid film. Vesicle films were hydrated with HEPES + 20 mM calcein dye overnight at 60°C. Vesicles were extruded to 400 nm, purified via SEC, and added to a 384-well plate with equiosmolar HEPES buffer and increasing volumes of 0.02% glycerol solution or RNAse prepared in buffer to the same final glycerol concentration. Vesicles were incubated for 4 hours at 37°C and

calcein fluorescence was measured (ex: 495 nm, em: 515 nm). Vesicles were lysed with 1 mL 10% TritonX and total calcein fluorescence was measured to determine fraction release.

Funding

This work was supported by a Northwestern University Chemistry of Life Processes Institute Cornew Innovation Award (NPK, JBL), National Science Foundation grants 1844219 (NPK), 1844336 (NPK, JBL), and 2145050 (NPK), and the U.S. Department of Defense National Science & Engineering Graduate Fellowship (MAB)

Author contributions

Conceptualization: MAB, WT, JBL, NPK; Methodology: MAB, WT, JBL, NPK; Investigation: MAB, WT; Data Analysis: MAB, WT, JBL, NPK; Visualization: MAB; Writing—original draft: MAB, NPK; Writing—review & editing: MAB, WT, NPK, JBL

Competing interests

Authors declare that they have no competing interests.

Data and materials availability

Plasmid sequences available on Addgene with accession numbers 128809 (pJBL3752) and 128810 (pJBL7025).

Acknowledgments

We thank Zoila Jurado and the Murray Lab as well as the Build a Cell community for providing a water-in-oil vesicle formation protocol which we adapted for these studies. We would also like to thank Adam Silverman and Dylan Brown for preparing cell extract and reaction materials.

Chapter 4 - Field Deployment of a Cell-Free Biosensor in Nakuru County, Kenya

Preface

This text is adapted from the manuscript "The accuracy and usability of point-of-use fluoride biosensors: a field study in Nakuru County, Kenya," currently in preparation. I am co-first author of this work, alongside Patrick Mbullo Owuor from the Young Lab in the Northwestern University Anthropology Department. Put succinctly, this project is the culmination of my previous work on point-of-use biosensing. Here, we take expand upon and formalize the limited testing we did in Costa Rica in Chapter 2 by field testing our sensors in Nakuru County, Kenya, another region known to have water contamination issues from geogenic fluoride. This work distinguishes itself from contemporary biosensing studies in two ways: (1) the tests are operated by their intended end user, rather than trained scientific staff and (2) we contextualize the use of the tests with anthropological analysis of user knowledge, attitudes, and behavior. This level of real-world application is unprecedented for synthetic biology, and the accurate, onsite detection of fluoride by general users is a key validation of the cell-free biosensing in general moving forward.

4.1 Introduction

Water contamination and its resultant health and economic burdens are a pressing global health concern[132]. Sustainable Development Goal (SDG) 6 tracks progress towards the "availability and sustainable management of water and sanitation for all". Progress towards SDG target 6.1, the proportion of humans with "universal and equitable access to safe and affordable drinking water" is tracked primarily using data on drinking water infrastructure access reported by national statistics offices to UNICEF and WHO's Joint Monitoring Programme (JMP)[133].

Current estimates based on JMP data indicate that two billion people worldwide lack access to safely managed drinking water service[133], such that we are not on track to meet target 6.1 by 2030[134]. Even this estimate may be overly optimistic as current data on water quality are limited[12]. Specifically, less than half of the United Nations' member states have the resources to

generate water quality data robust enough to drive governance[134]. As such, there is an acknowledged need for more widely usable data collection technologies that can be used to track the presence of water contaminants identified as priority[135], specifically *E. Coli*, arsenic, nitrites, and fluoride[15].

Dangerous levels of fluoride are found in water sources used by tens of millions of people worldwide[17,136]. Exposure to fluoride concentrations above 1.5 ppm (or 1.5 mg/L) typically occurs when naturally occurring fluoridated salts leach into underground aquifers. Elevated levels of fluoride in groundwater occurs globally, and is of particular concern in northern and eastern Africa, the Middle East, and parts of North and South America[137,138]. Although there are health benefits to fluoride exposure below 1 ppm, including prevention of dental caries[139] and treatment of osteoporosis symptoms[140], chronic exposure to high levels of fluoride has a number of adverse effects, most notably, dental and skeletal fluorosis[141]. Fluorosis embrittles teeth and bones by binding to the calcium within them, and can cause debilitating lifelong health complications[142,143]. There is thus a pressing need to prevent or reduce exposure to fluoride concentration $\geq$1.5 ppm, the cut-off established by the WHO[15].

One of the biggest obstacles to mitigating exposure to harmful geogenic fluoride is the difficulty in identifying its presence: fluoride in water is colorless, odorless, and undetectable by taste below 2.4 ppm[144]. While it is straightforward to accurately quantify fluoride levels in laboratory settings using techniques such as ion chromatography or ion sensing electrodes[17], these require infrastructure and expertise to operate, necessitating a centralized approach to their use. A centralized approach, in turn, requires samples to be collected in the field and shipped to the laboratory, creating additional costs and logistical constraints in testing and communicating results in potentially affected areas.

Accurate point-of-use technologies currently exist to circumvent some of these limitations, but are of limited value to non-experts because of their cost, complexity, and/or accuracy[15]. For example, portable fluoride sensing electrodes and photometers can quantitatively measure

fluoride levels in water onsite, but cost hundreds to thousands of dollars and require calibration procedures and maintenance for their use. Point-of-use chemical strips offer another field-friendly alternative at less than 1 USD per test, but are prone to false negatives and frequently fail to identify even extremely high levels of fluoride[23]. As such, there is a need for accurate, simple, and affordable methods that can be used by non-experts to accurately identify water sources with fluoride levels above 1.5 ppm at the water source. Such tests can both help people make decisions about the water they consume and track global progress towards SDG 6.

Cell-free biosensing technologies offer a promising strategy for the development of accurate, simple, and affordable water quality diagnostics[46]. Biosensors are naturally occurring RNA or protein systems in cells that sense compounds relevant to cell health. These natural systems work through binding interactions to the RNAs or proteins that then trigger the expression of genes that can in turn metabolize or export the compound. Synthetic biosensors can be created by extracting these natural systems out of the cell, and reconfiguring them to express genetically encoded reporter gene that lead to a visually detectable signal to indicate the target compound's presence (i.e. color change). A key strength of these systems is that they operate as an *in vitro* reaction, outside of a living cell, and are therefore not genetically modified organisms. In addition, they can be freeze-dried and stored, facilitating manufacturing and transport to where they are needed. Rehydration of the tests with water samples thus allows them to be used as point-of-use water quality diagnostics. Furthermore biosensing reagents cost on the order of cents per test to produce[52], even in a laboratory (i.e. not at production scale). As such, they are less expensive per sample than gold-standard field-deployable technologies (**Supplemental Table 6**).

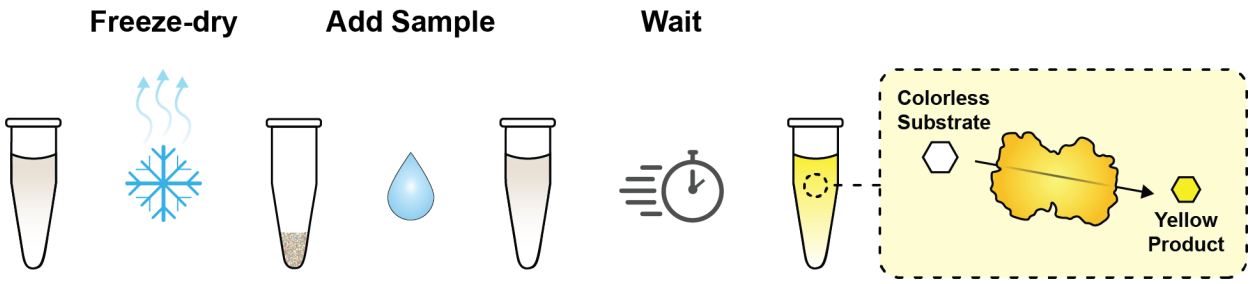

Figure 4-1. Schematic representation of a fluoride biosensor.
A sensing reaction is prepared, freeze-dried, then rehydrated with a sample of interest. An enzymatic reaction occurs in the presence of fluoride, which converts a colorless substrate in the reaction to a yellow product.

For the detection of fluoride, a naturally occurring fluoride sensing mechanism from *Bacillus cereus* has been successfully engineered into a biosensor and incorporated into a point-of-use fluoride test[23]. This test consists of a freeze-dried biosensing reaction that, when rehydrated with a water sample of interest, produces a visible yellow color in the presence of fluoride within hours (**Figure 4-1**). This cell-free fluoride biosensor test was initially field-tested in a study in Cartago, Costa Rica[23], a region with elevated levels of geogenic fluoride due to its proximity to the Irazu volcano, a known source of fluoridated salts[79]. In this previous study, tests were manufactured in Illinois and carried on board a commercial aircraft to the field site. Testing of nine different ground and surface water sources by a doctoral student revealed that the positive controls functioned in all cases, confirming that the basic biochemistry of the tests were robust to manufacturing, transportation, and field use. In addition, two samples were found to have detectable levels of fluoride. While promising, this study was limited by the small number of field samples tested, and more importantly, by the fact that tests were conducted by a single user with expertise in laboratory techniques and test operation. To determine the accuracy and usability of point-of-use fluoride test by non-experts, tests must be used by non-expert users, and sensitivity and specificity calculated.

We therefore explored the accuracy and usability of bioengineered point-of-use fluoride tests in Nakuru County, Kenya, a region with known geogenic fluoride contamination[145,146].

Specifically, we sought to evaluate test accuracy, assessed by the ability to correctly sense harmful levels of fluoride (established by the WHO as $\geq$1.5 ppm[15]) compared to photometry, a gold-standard method (Aim 1); and test usability, assessed by reported user experience with rehydrating and interpreting the tests (Aim 2). We found that the tests were highly accurate under field conditions, correctly classifying 84.2% of the 57 samples. In terms of usability, all users were able to rehydrate the biosensor, and only 1 of the 57 was misclassified by the participant. Collectively, these results suggest the utility of biosensors for point-of-use water quality testing is high, and suggest their potential for low-cost, large-scale testing.

4.2 Study design and samples

We surveyed one member of each participating household to gather information about socio-demographics; drinking water sources; knowledge, attitudes, and behaviors about fluoride and fluorosis; and experiences with household water insecurity. We then characterized biosensor test accuracy by asking each participant to provide up to three household water sources and test them with the point-of-use biosensor. A second survey was conducted on the same day with the same participant to assess their experiences with using and interpreting the output of the biosensor test and to ascertain and share fluoride concentrations using a gold standard method, i.e., fluoride photometer.

A total of 90 water samples were collected from 52 participants. Socio-demographics and knowledge, attitudes, and behaviors pertaining to fluoride and experiences with water insecurity were available for all 52 participants. The sample size available for evaluating test accuracy (Aim 1) and interpretation (Aim 2) was 57 water samples. The number of samples was reduced from 90 to 57 because shipping conditions for the first batch of tests caused test degradation, making them unsuitable to evaluate accuracy and usability (see “Characterization of biosensor accuracy with household water samples”).

4.3 Socio-demographics of study participants concerning fluoride

Sociodemographic Characteristics		**Total Households (n=52)**
Gender, n (%)		
	Female	38 (73.1%)
	Male	14 (26.9%)
Age (years)		
	Median (IQR)	41 (32, 50)
	Range	18-80
Education, n (%)		
	None	3 (5.8%)
	Some Primary	11 (21.2%)
	Completed Primary	10 (19.2%)
	Some Secondary	8 (15.4%)
	Completed Secondary	8 (15.4%)
	College/University	12 (23.1%)
Employment, n (%)		
	Agriculture	15 (28.9%)
	Small Business	12 (23.1%)
	Employee	9 (17.3%)
	Unemployed	8 (15.4%)
	Unable to Work	4 (7.7%)
	Student	2 (3.9%)
	Other	2 (3.9%)
Monthly household income		
	Mean	KES 1830 (USD 15.73)
	Median	KES 1000 (USD 8.60)
Total household size		
	Mean (SD)	4.9 (1.8)
	Median (IQR)	5 (4.6)
	Range	0-5
Number of children (≤15 y) in household		
	Mean (SD)	2 (1.43)
	Median (IQR)	2 (1,3)
Household Water Insecurity Experiences Score (0-36)		
	Mean (SD)	5.9 (8.9)
	Prevalence of water insecurity (≥12) n, (%)	14 (26.9%)

Table 4-1. Sociodemographic characteristics of participants in the geogenic fluoride drinking water study in Nakuru, Kenya (n=52).

The study included participants from a range of education and employment backgrounds, household sizes, and levels of water insecurity (**Table 4-1**). The majority of the 52 participants were women (73.1%), with a median age of 41 years. Roughly half of the participants had completed at least some secondary education. Participant occupations largely fell into three broad categories: agriculture, small businesses e.g. market stands, or unemployed. Monthly household income ranged from KES 0-9500 (median USD 8.60). The median household size was 5 people; almost half of the households had children under five years old. Approximately one quarter of households were water insecure, i.e., they struggled with reliably accessing water to meet basic domestic needs.

Most participants (73.1%) were knowledgeable about fluoride; they generally referred to it as a “salt” or “mineral” found in water. In addition, 7 participants added that fluoride impairs dental and skeletal health unprompted. When asked, most (90.4%) participants correctly identified some or all of the symptoms of fluorosis and the causal relationship between health problems and fluoride exposure. The majority of participants knew at least one person who had been affected by fluorosis 71.2%.

This knowledge is contrasted by a comparative lack of understanding of how to take measures against fluoride exposure, with 42.3% of participants reporting that they didn’t know how to prevent fluorosis, and 34.6% reporting that they didn’t know how to treat it. Notably, while approximately half (48.1%) of participants correctly identified using alternative sources of water and water treatment as methods to prevent fluorosis, fewer participants (26.9%) understood that fluorosis can only be treated with medical and dental care. The most commonly provided incorrect answer about fluorosis prevention and treatment was brushing teeth.

Although efforts were made to avoid fluoride, fluorosis was not a major concern; 71.2% of participants reported that they never or rarely worried about fluorosis. Of the 33 participants (63.5%) who reported taking precautions against fluorosis, most reported using methods that were generally effective (n = 27), including using water sources that were not known to be

contaminated, diluting borehole water with rainwater, or treating their drinking water. However, 5 participants (9.6%) reported boiling their drinking water, which does not reduce fluoride content. Complete survey responses can be found under Data Availability.

4.4 Characterization of biosensor accuracy

A first shipment of biosensor tests was used to assess 33 water samples from the first 16 households surveyed. All of these tests resulted in a faint yellow color, regardless of water source or fluoride concentration established via fluorimeter. This test failure was likely caused by thermal degradation of the tests during shipment with the commercial shipping agency. Commercial shipment routes from Illinois, USA to Nairobi, Kenya pass through hot global regions, including Dubai for this particular shipment. These conditions were much different from those in the previous study usability study in Costa Rica in which tests were transported by commercial air, with gentler shipping and storage conditions[23]. A laboratory investigation of test temperature stability indicated that elevated storage temperatures can indeed cause test components to degrade, resulting in a faint yellow color upon rehydration consistent with field observations (**Supplemental Figure 14)**.

Characteristic		
Water sample source[1]		
	Borehole/tube well	28 (49.1%)
	Rainwater	11 (19.3%)
	Protected dug well	10 (17.5%)
	Rainwater combined with borehole water	5 (8.7%)
	Surface water	1 (1.8%)
	Bottled water	1 (1.8%)
	Tap water	1 (1.8%)
Time needed for collection (roundtrip, in min)		
	Mean (SD)	5.4 (13.0)
Is sample used for cooking or drinking?		
	Yes	48 (84.2%)
	No	9 (15.8%)
Was sample treated?[2]		
	Yes	4 (7.0%)
	No	53 (93.0%)
Is respondent concerned about fluoride from this source?		
	Yes	10 (17.5%)
	No	47 (82.4%)
Fluoride concentration		
	≥1.5 ppm	45 (78.9%)
	<1.5 ppm	13 (22.8%)

[1]The first 33 of the 90 water samples were not usable for assessment of accuracy because of biosensor test degradation due to shipment conditions.
[2]Treatment methods included chlorine tablets, distillation, and/or filtration.

Table 4-2. Characteristics of water samples available for assessment of accuracy of at-home biosensor fluoride tests (n=57)

Because this discoloration could confound the intended yellow result of the test in the presence of fluoride, leading to false positives, we only used tests that had been refrigerated during shipping and transport to participants' houses to assess accuracy. The 33 water samples from the first 16 households were there excluded from analysis of accuracy, leaving a total of 57 samples from 36 households (**Table 4-2**). The majority of these water samples came from boreholes (49.1%), rainwater collection (19.3%), or protected dug wells (17.5%). The majority of

provided samples (84.2%) were used for cooking, drinking, or both, but very few (7.0%) were treated to reduce fluoride. The water points were not located far from households; mean time to collect water was approximately 5 minutes, roundtrip.

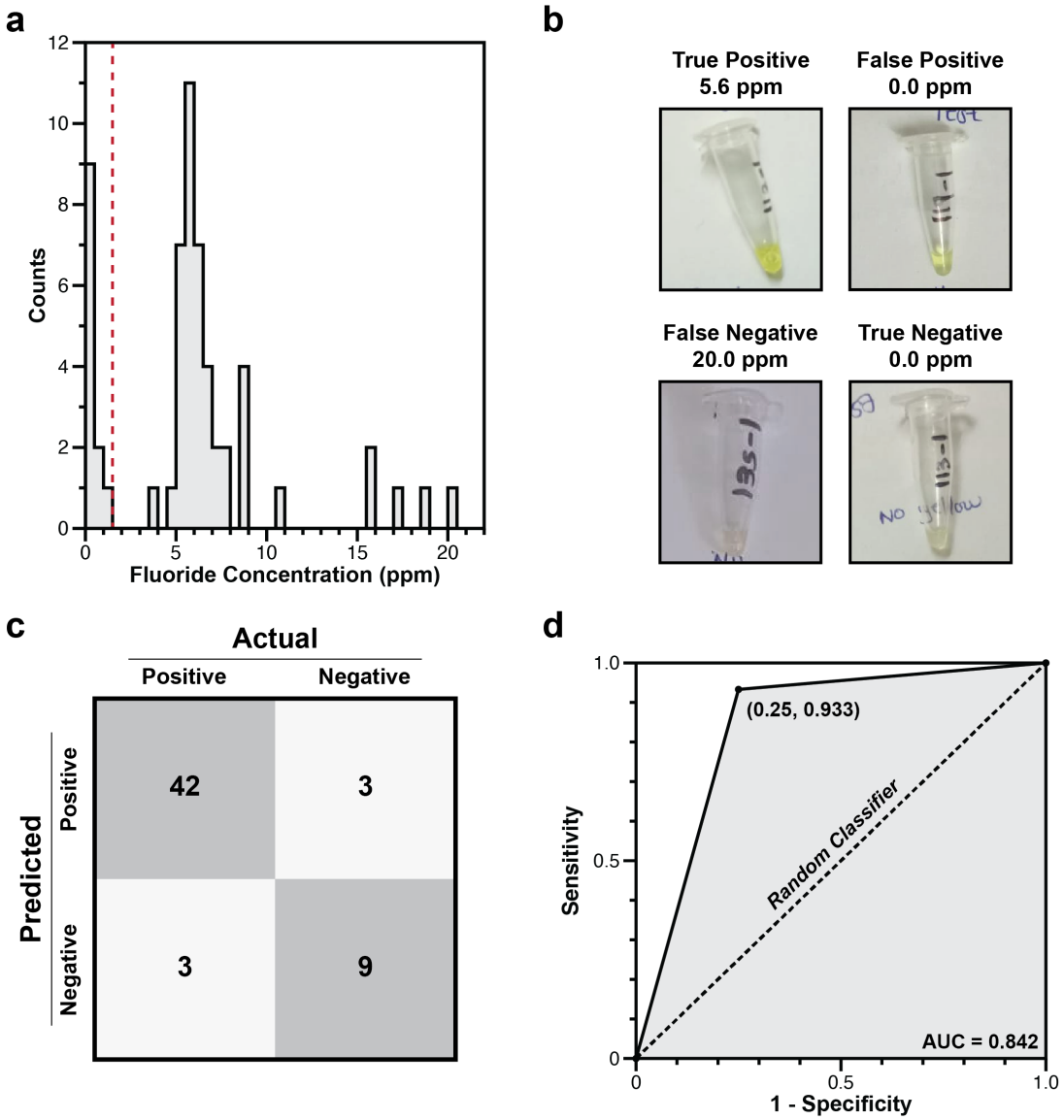

Figure 4-2. Fluoride content in 57 samples from 32 households, based on output from the point-of-use biosensor tests and the fluorimeter.
(a) Distribution of fluoride concentrations in 57 water samples, as measured by fluorimeter. The red dashed line indicates the WHO guideline for elevated levels, ≥ 1.5 ppm. **(b)** Representative images of true positive, false positive, true negative, and false negative test results. Photographs are annotated with fluoride concentrations measured by fluorimeter. **(c)** A confusion matrix of test results. “Actual” refers to classification by fluorimeter as being positive (≥1.5 ppm fluoride) or negative (<1.5 ppm fluoride). "Predicted” refers to biosensor test performance. “Negative” means no color change was observed, and “Positive” means a yellow color was visible. True positives and true negatives are shaded in grey, while false positives and false negatives are in white. **(d)** Receiver operating characteristic curve derived from classifications in panel (c). Sensitivity is calculated as (true positive)/(true positive + false negative) and specificity is calculated as (true negative)/(true negative + false positive).

Fluorimeter analysis of the water samples by field staff indicated that 45 of the 57 samples had fluoride levels above 1.5 ppm, indicating a high prevalence of geogenic fluoride in drinking water (**Table 4-2**, **Figure 4-2a**). The measured fluoride levels were also high, with mean and median fluoride concentrations of 6.0 and 5.8 ppm, respectively. Most of the 12 uncontaminated samples were rainwater (83.3%), while most of the 45 contaminated sources were from boreholes (53.3%), protected dug wells (22.2%), or rainwater mixed with borehole water (11.1%) (**Supplemental Table 7**).

Six hours after the biosensor tests were rehydrated by study participants, field staff classified the output as positive for fluoride if a yellow color was observed, and negative for fluoride if no color change was observed. Comparison of these observations to the fluorimeter results allowed tests to be classified as true positive (yellow, with measured fluoride ≥ 1.5 ppm), false positive (yellow, measured fluoride < 1.5 ppm), true negative (colorless, measured fluoride < 1.5 ppm), false negative (colorless, measured fluoride ≥ 1.5 ppm) (**Figure 4-2b**). Tabulating these results in a confusion matrix revealed that the biosensor tests correctly classified 51 samples (89.5%), and incorrectly classified 6 samples (10.5%) (**Figure 4-2c**). The test sensitivity was therefore 93.3% (95% CI 81.7% to 98.6%) and specificity was 75.0% (95% CI 42.8% to 95.5%). Plotting these data on a receiver-operating curve revealed an area under the curve of 0.842 (**Figure 4-2d**).

We identified no patterns among the incorrectly classified water samples in terms of water source or treatment. Furthermore, we observed that almost a fifth (n = 10, 17.5%) of the positive control reactions failed to activate (**Supplemental Table 7**). Despite this, we did not observe any shared characteristics between the samples with failed positive controls. Furthermore, some true positive tests had failed controls, indicating that the failure of the positive control for a given sample did not necessarily correlate to an incorrect classification by the test.

4.5 Characterization of test usability

Figure 4-3. Representative testing photographs.
The two key user activities to operate point-of-use fluoride biosensor tests are test rehydration, in which a micropipette is used to transfer water sample into a microtubule (left) and result interpretation, in which the user ascertains if a yellow color has appeared (right).

We asked the 36 participants who provided water samples for accuracy analyses about their experiences with two aspects of usability: test rehydration and test interpretation. All participants were able to successfully transfer water into the PCR tube with a micropipette (**Figure 4-3**, left), though two users (5.6%) experienced some difficulty dispensing the water. Due to field constraints, especially the distance of participants' houses from where field staff were staying, not all users were able to read the test results after 6 hours, such that some participants were asked to assess if there was a color change before the reaction was complete (**Figure 4-3**, right). At the time of readout, however, we observed agreement between participants and field staff in their

assessments of the presence or absence of a yellow color in all but one of the 57 samples used for test interpretation assessment (98.2%) (**Data Availability**).

4.6 Discussion

In what is, to our knowledge, the first description of field deployment and operation of any biosensor test by non-expert users, we found that a point-of-use fluoride biosensor test demonstrated a number of positive characteristics. For one, it was accurate at detecting fluoride. Sensitivity was 93.3%, specificity was 75.0%, such that the area under the receiver operating characteristic curve was .842, meaning that there is an 84.2% chance that the test will correctly predict fluoride contamination above the WHO limit of $\geq$1.5 ppm[147].

To our second aim, these tests were highly usable. All participants were able to hydrate the tests, and there was only one discrepancy between study staff and participant interpretation amongst the 57 samples used to assess test interpretation. In sum, participants were able to correctly identify public-health relevant concentrations of fluoride in their own household water sources, suggesting that the tests were eminently usable.

The degradation of the first batch of tests clearly highlighted that the accuracy of point-of-use biosensors are susceptible to issues from exposure to harsh temperature conditions. In this regard, mass deployment will require achieving true cold chain independence by increasing the sensor's temperature stability. This is particularly important because many regions with endemic groundwater contamination concerns – for example, Kenya[146], India[148], Pakistan[149], Bangladesh[150], and others – are in places with relatively high temperatures. As such, biosensors need to be capable of tolerating brief and extended hot periods. One of the most promising avenues for this is the addition of compounds called lyoprotectants that stabilize the system upon freeze-drying; some *in vitro* gene expression reactions can maintain integrity at 50°C for up to a month when supplemented with appropriate lyoprotectants, though similar studies have not been performed in biosensing reactions[151]. Optimizing the lyophilization process for temperature

stability and shelf life therefore stands to substantially improve the sensor's robustness, ensuring accurate water quality data in the areas where it is most needed. In addition, the inclusion of appropriate control reactions to indicate test failure will continue to be important for test accuracy.

There are several promising avenues to improve the usability of these tests. For example, issues with the ambiguity of color change could be resolved by using alternative colorimetric reporters and substrates[152] to generate more vibrant outputs. Additionally, the development of purpose-built tools to rehydrate the freeze-dried tests and facilitate the interpretation of their results stands to substantially improve user experience. For example, the tests could be embodied in a lateral flow assay,[153] such as those used in at-home pregnancy tests, for greater clarity of interpretation. In addition, shorter time to result could help with test interpretation. Future testing should also include test characterization in a wider variety of water sources, particularly acidic, alkaline, or mineral-rich samples, that may inhibit the biological processes needed for sensor activation.

These tests fill a large unmet need for establishing the fluoride content of drinking water outside of a laboratory setting. They may be useful in large-scale surveys of human health, well-being, and/or water security, such as those conducted by the World Bank, Gallup, and USAID, and of interest to people living in areas potentially affected by geogenic fluoride. They could also be valuable in areas where the presence of fluoride is well-established, because of their ability to gauge water safety after measures are taken to remove fluoride. For example, our sensors identified dangerous fluoride levels in five samples of borehole water that had been diluted with rainwater to reduce fluoride content.

In sum, the ability for a biosensor test to correctly identify water contaminated with fluoride at $\geq$1.5 ppm indicates enormous potential for a new approach to water quality diagnostics, one that requires far less equipment, expertise, infrastructure, and cost to operate. Indeed, the recent characterization of biological mechanisms to sense other priority contaminants including lead[154], copper[155], nitrites[156], and arsenic[157] suggest the possibility of analogous point-of-use tests[158] for

all of these analytes. The accuracy, simplicity, rapidity, relatively low cost, and field-friendliness of these tests would facilitate broad implementation, thereby democratizing knowledge about water safety for all.

4.7 Materials and methods

Test Manufacture

The DNA plasmid encoding the fluoride biosensor used in this study was assembled using Gibson assembly (New England Biolabs, Cat#E2611S) and purified using a Qiagen QIAfilter Midiprep Kit (QIAGEN, Cat#12143). Its coding sequence consists of the *crcB* fluoride riboswitch from Bacillus cereus regulating the production of the enzyme catechol 2,3-dioxygenase, all expressed under the constitutive *E. coli* sigma 70 consensus promoter J23119[159]. A complete sequence of the plasmid used is available on Addgene with accession number 128810 (pJBL7025).

Cell-free biosensing reactions used in the tests were set up according to previously established protocols[23,91]. Briefly, reactions consist of cleared cellular extract, a reagent mix containing amino acids, buffering salts, crowding agents, enzymatic substrate, and an energy source, and a reaction-specific mix of template DNA and sodium fluoride in an approximately 30/30/40 ratio. Test reactions contained no sodium fluoride, while positive control reactions were supplemented with 1 mM sodium fluoride to induce gene expression. Template DNA concentration for both sets of reactions was 5 nM, determined by the maximal template concentration at which no color change was observed in the absence of fluoride.

During reaction setup, master mixes of cellular extract, reagent mix, and template mix were prepared for both test and positive control reactions in 1.7 mL microcentrifuge tubes. Individual reactions were then aliquoted into 20 µL volumes in PCR tube strips for lyophilization. After aliquoting on ice, PCR tube caps were pierced with a pin, strips were wrapped in aluminum foil, then the wrapped strips were immersed in liquid nitrogen for freeze-drying for approximately

3 minutes. Reactions were immediately transferred to a Labconco FreeZone 2.5 Liter −84°C Benchtop Freeze-Dryer (Cat# 710201000) with a condenser temperature of -84°C and pressure of 0.04 mbar and freeze-dried overnight (≥16 hours).

After freeze-drying, tests were vacuum sealed (KOIOS Vacuum Sealer Machine, Amazon, Amazon Standard Identification Number (ASIN) B07FM3J6JF) in a food saver bag (KOIS Vacuum Sealer Bag, Amazon, ASIN B075KKWFYN), along with a desiccant (Dri-Card Desiccants, Uline, Cat# S-19582). Vacuum sealed reactions were then paced in a light-protective outer bag (Mylar open-ended food bags, Uline, Cat# S-11661) and impulse heat-sealed (Metronic 8-inch Impulse Bag Sealer, Amazon, ASIN B06XC76JVZ) before shipping (**Supplemental Figure 15**). Tests were also shipped with single-use 20 µL micropipettes (MICROSAFE® 20 µL, Safe-Tec LLC, Cat# 1020) for field operation.

Test Kit Shipment to Nakuru County, Kenya

A first batch of tests were shipped unrefrigerated in an uninsulated cardboard box using a standard commercial shipping service on July 22nd, 2021. Upon arrival in Kenya on July 27th, 2021, they were stored at ambient temperature they were used for testing from November 16th to November 23rd, 2021. These tests showed signs of thermal degradation on use (**Supplemental Figure 14**), indicating a need for shipment and storage below ambient temperature. The next batch of tests were therefore shipped refrigerated on January 25th, 2022. After the tests were made and packaged, they were placed in a polystyrene foam-lined container before being covered with a NanoCool refrigeration system (Peli BioThermal). The container was then sealed shut and shipped using a standard commercial shipping service. This batch of tests was held refrigerated in customs until release on February 28th, 2022 and was used from March 5th to March 14th, 2022 to generate the data on test accuracy reported in this manuscript.

Participant Recruitment

Participants were recruited from five sub-locations (Kelelwet, Kipsimbol, Kigonor, Parkview, Lalwet, and Mwariki) in Barut Ward a subdivision of Nakuru County (**Supplemental Figure 16**, geographic information adapted from OpenStreetMap[78]). This location was chosen because of high fluoride levels and familiarity with the communities.

Before any data were collected, community meetings were held in each sub-location to discuss study goals and objectives. After obtaining permission from the community and village assistant chiefs to conduct research, local community mobilizers were engaged to assist with identifying households eligible for participation. Individuals who were 18 years or older, had lived in Nakuru country for more than three months, relied on local water sources, had a child in the household, were willing to discuss their household water situation, and provide a sample of each source of water in the household for fluoride testing were eligible. We sought to recruit 10-12 participants from each of the five sublocations to ensure a range of socio-demographic characteristics and drinking water sources. Having a child resident was a criterion in order to elucidate community understandings about fluorosis in children.

Data Collection

After obtaining informed written consent, participants were asked survey questions (**Supplemental Table 8**); this took approximately 30 minutes. Topics included household sociodemographic information, knowledge, attitudes, and behaviors about fluoride and fluorosis, and household water insecurity using the validated Household Water Insecurity Experiences (HWISE) scale[160]. The 12 HWISE items query the frequency of experiences with water insecurity in the prior month; “never” is scored 0, “often/always” scored 3, for a range of 0-36. These data were collected to be able to investigate if user experiences or attitudes about testing varied by experiences with fluorosis or water insecurity. Participants were also asked about the number of sources of their water and willingness to provide and test water samples. Survey responses were recorded on tablets using Open Data Kit (ODK)[161].

After completion of the survey, participants provided 1-3 samples of water from different household sources. They then received a brief (5 minute) explanation of the testing process, and then tested their own household samples using the fluoride biosensor tests. Each test consisted of a microtube that was a positive control, and a second microtube in which the sample of interest was tested. To test their samples, participants first removed the tests from the light-protective foil pouch and vacuum sealed pouch containing desiccant, both of which were then discarded (**Supplemental Figure 15**). A micropipette was then filled with 20µL water by slowly immersing it to the fill line. To dispense the water, the thumb and index finger were used to cover the holes in the micropipette while the bulb was then squeezed with the other hand. The reactions were then incubated at ambient temperature for up to six hours, shorter if there was a visible color change. During this incubation time, participants were asked to check hourly for yellow color change and note the time taken for it to occur. Tests were expected to turn yellow if fluoride levels were $\geq$1.5 ppm, with no color change for tests of water below this level. All positive controls were expected to turn yellow. Color change was read after placing reactions on a sheet of white paper for visual contrast.

The study team returned to conduct a second survey on user experiences with the testing process and to test the water samples using the gold standard photometer. Participants were asked about their experiences with the testing procedure as well as their interpretation of the color of the results of the sample and control tests. Photographs of the completed reactions were also taken at this time. Finally, quantitative fluoride measurements were taken by the field team with a Hanna Instruments Fluoride High Range Photometer Kit (Cat# HI97739C), a gold standard method used to assess the accuracy of the bioengineered tests.

Photometry results on actual measured fluoride concentrations of water samples were shared with and explained to participants. At the conclusion of the second survey, each participant was given KES 500 (USD 4.30) as remuneration for the time and effort spent participating in the research. Each participating household was also given a ceramic drinking water filter.

During surveying and water testing, participants and research assistants maintained COVID-19 protocols as per the local area guidelines. Study staff were vaccinated, maintained appropriate social distancing, sanitized hands, and cleaned field tools after each household visit.

Data Analysis

Data were exported from ODK into Microsoft Excel for analysis. Basic descriptive statistics were performed to describe participant socio-demographics and experiences with usability, including if participants' interpretation of color change matched that of study staff. Open-ended items about fluoride and fluorosis knowledge, attitudes, and behavior were grouped thematically and coded independently by two authors. Knowledge-related responses were characterized as "correct" if consistent with conventional biomedical understanding, "incorrect", or unfamiliar.

Tests were classified as 'ON' by the Kenya-based field team if they were visibly yellow after six hours, and 'OFF' if there was no observable color change by eye. These assessments were independently validated by US-based team from photographs of the completed tests. Tests classified as 'ON' were marked true positive if they corresponded to a photometer measured fluoride concentration $\geq$ 1.5 ppm, and false positive if they corresponded to a photometer measured fluoride concentration <1.5 ppm. Tests classified as 'OFF' were marked as true negative if they corresponded to a photometer measured fluoride concentrations < 1.5 ppm, and false positive if they corresponded to a photometer measured fluoride concentrations $\geq$1.5 ppm. Sensitivity was determined by the ratio of true positive results to total positive measurements (combined true and false positives), while specificity was determined by the ratio of true negative results to total negative measurements (combined true and false negatives). Confidence intervals for sensitivity and specificity were calculated using the diagt module in Stata[162] using counts of true positives, true negatives, false positives, and false negatives.

Human Subjects Approval

We obtained ethical approval for this study from Northwestern University's (IRB STU00215306) and Amref Health's (AMREF-ESRC P1003/2021) Institutional Review Boards. We also received authorization from the Ministry of Planning and Development, Nakuru County, which is responsible for coordinating research activities in the county and relevant Ministries. All participants provided written consent to participate in the study activities, including consent to take pictures of the at-home testing.

Acknowledgments

We would like to thank Charlotte Knopp (Northwestern University) for managing reaction shipment from the United States to Kenya. We also thank Dylan Brown (Northwestern University) for helpful insights on sensor temperature stability and for providing some reagents used in this study, along with Hilary Bethancourt (Northwestern University) for advice on statistical analysis. For their assistance with data collection, we thank Janet Barsolai Chepchirchir and Maxwell Otieno Aduogo, along with James Yegon (SOAR-Kenya Academy) for assistance with community mobilization. Finally, we thank our study participants for giving us access to their homes and sharing their experiences. This work was supported by the Carnegie Corporation; the Crown Family Center for Jewish and Israel Studies; the support of the American people provided to the Feed the Future Sustainable Intensification Innovation Lab through the United States Agency for International Development Cooperative Agreement AID-OAA-L-14-00006; the United States Army Contracting Command W52P1J-21-9-3023.

Author Contributions

Conceptualization, W.T., P.M.O, J.B.L, & S.L.Y.; Data Curation, P.M.O, D.A., K.K., & R.A.; Formal Analysis, W.T. & R.A.; Investigation, P.M.O, D.A., & K.K.; Methodology, W.T., P.M.O, D.A., K.K., J.B.L., S.L.Y.; Project administration, W.T., P.M.O., J.B.L., & S.L.Y.; Funding

acquisition J.B.L. & S.L.Y.; Writing – original draft, W.T., P.M.O. , R.A., J.B.L, S.L.Y; Writing – review & editing, W.T., P.M.O., D.A., K.K., R.A., J.B.L., & S.L.Y.

Competing Interests

The authors declare the following competing financial interest(s): W.T. and J.B.L. hold a patent (International Publication Number WO 2020/185451 A3) for the technologically important developments included in this work. J.B.L is a cofounder of Stemloop, Inc. J.B.L.'s interests are reviewed and managed by Northwestern University in accordance with their conflict-of-interest policies.

Data Availability

All source data for the main and SI figures were deposited open access in Northwestern's Arch database (https://arch.library.northwestern.edu). Data can be accessed via DOI: 10.21985/n2-zyy5-cp15.

Materials and Correspondence

Materials requests and correspondence should be directed to Julius B. Lucks (jblucks@northwestern.edu) and Sera L. Young (sera.young@northwestern.edu).

Chapter 5 - Concluding Remarks

5.1 On the development of new sensors and sensing systems

From an academic perspective, we are rapidly approaching – or have already reached – the end of the period where making a new sensor is in and of itself considered novel. While this is an encouraging sign of the field's maturation, it poses questions about how to move forward from here. One possible avenue is the pursuit of projects that enhance or add new functions to sensors. As an illustrative example, previously published work detecting atrazine via its metabolic conversion to cyanuric acid[54] is a new sensor, but the novelty lies in the conversion process, which can be applied to biosensors in general. Listed here are several outstanding needs in cell-free biosensing, along with comments on the state of the field in that regard.

Improving sensitivity and specificity for natural biosensors

The fluoride riboswitch used in this thesis responds to diagnostically relevant levels of fluoride without optimization. However, this is not the case for all natural sensors. Indeed, many characterized sensors for high impact contaminants including lead and copper can only detect their intended targets far above real-world levels[158]. Furthermore, some characterized sensors also exhibit cross-reactivity, activating in the presence of non-cognate ligands. Moving forward, developing strategies to tune sensitivity and specificity will allow us to use riboswitches or transcription factors that we cannot currently implement in a biosensor, expanding our library of available tools.

Directed evolution is one particularly promising avenue to accomplish this. For example, evolutionary methods have allowed us to engineer transcription factors and riboswitches to change their specificity and enable the precise sensing of non-native ligands[163–165]. Additionally, using nucleic acid computation in concert with a natural biosensor can enable sensitization or desensitization[158,166]. While an alternative to both of these methods would be to simply perform high throughout sensor characterization until a suitable candidate is found, these tools would

allow us to work with established, well-defined systems instead of searching for hypothetical superior ones. Furthermore, the ability to precisely and predictably alter biosensor behavior would enable their fine-tuning for specific intended applications.

Engineering synthetic proteins and RNAs for biosensing

Beyond the need to tune the sensitivity of specificity of natural sensors, there is also a need for methods to rapidly engineer bespoke proteins and RNAs to detect targets of interest. Drawing from nature is an effective strategy when a microbial population has both an evolved response to a given target and an available genome sequence. However, with the rise of unnatural contaminants such as synthetic antibiotics, pesticides, and other harmful industrial compounds, we may lack the tools to detect some emerging targets.

Thankfully, we already have a well-tread suite of methods to generate ligand binding RNA against virtually any target[60,167–170]. This is counterbalanced by a lack of reliable methods to translate aptamers derived from these selections into functional riboswitches. This stems from a feature of the selection method; aptamer selection enriches for sequences that bind strongly to their intended target, while a synthetic riboswitch would require a sequence that enables bistability based on ligand presence when fused to an expression platform. Furthermore, strategies are emerging to select for aptamers in a context that facilitates their implementation in a riboswitch[61,63,171,172], along with strategies for pairing these selected aptamers to modular expression platforms[89]. While the field of synthetic riboswitch engineering[62,172–176] suffers from a lack of investment compared to its amino acid-based counterpart, building on our existing knowledge could enable the application of our powerful ability to generate ligand binding RNAs to the creation of RNA-based genetic regulators.

Compared to the engineering of synthetic riboswitches, the process of engineering synthetic regulatory proteins faces a separate list of equally daunting challenges. Designing new transcription factors would require the ability to generate novel DNA and ligand binding domains,

along with the allosteric behaviors that govern gene activation or repression. While we have not yet developed protein engineering strategies to the point where we can design allosteric mechanisms from scratch, there has been substantial process in tuning allostery by modifying existing systems[177–180]. Furthermore, we have seen significant advances in our ability to computationally predict a protein's structure from its sequence[55,181–184]. Moving forward, combining high throughput protein engineering, expression, and characterization with computational tools to aid *de novo* structure design could enable the creation of allosteric regulators binding any number of diagnostically relevant targets.

Developing methods for sample quantification

While it is possible to extrapolate inducer concentration from final gene expression in a biosensor, this process offers a rough estimate at best. For example, while strong activation generally indicates high inducer levels, but it is difficult to translate these observations into quantitative measurements. Though presence/absence measurements with respect to a threshold are often enough to provide actionable information, quantitative or semi-quantitative readouts would allow for more nuanced decision making and are therefore more desirable.

There already exists wide variety of semi-quantitative colorimetric assays. For example, a pH strip indicates acidity or alkalinity based on final color change, while a Bradford assay estimates protein concentration based on color intensity. For measuring gene expression, the parameter of interest is instead time to activation, with shorter times indicating higher levels of gene expression and therefore higher initial analyte concentration. Utilizing this, previous work has yielded a strategy for semi-quantitative measurement of analyte concentrations by comparing time to result against a set of colorimetric standards[73]. More recent work has also shown that low-cost supplementary equipment can be used to measure change in color[185], potentially enabling automated, objective analyses of colorimetric readouts.

As an alternative, we could also devise means to quantify analyte concentrations by engineering genetic circuitry within the biosensing reaction. Recent work has yielded a set of design principles for applying logic to biosensing reactions[158,166,186], enabling the creation of rudimentary computational systems using genetic circuits. As our ability to design these circuits from orthogonal parts improves, we will be able to design progressively more complicated biological signal processing architectures. By devising genetically encoded means to interpolate initial inducer concentration from final generated signal, these architectures could remove some of the ambiguity inherent in interpreting sensor results.

5.2 On transitioning cell-free biosensors from academic to general use

While cell-free systems are a very promising platform for field deployable biosensing, there are still obstacles to overcome before they are ready for the transition out of the lab. The research presented in this thesis demonstrates that this transition is possible in the near future but will require extensive optimizations in two key areas: (1) the optimization of reaction preparation and composition to maximize long terms stability in adverse conditions and (2) the development of peripheral tools and packaging to facilitate ease of use over a wide user base. Moving forward, innovations in these two areas will be necessary to support any large-scale effort to bring biosensors from the lab to the field.

Optimizing reaction lyophilization procedures

The intended deployment sites for many point-of-use biosensing or biomanufacturing technologies are in the global south. Generally speaking, these regions tend to have warmer climates, which can complicate field deployment of cell-free biosensors. Indeed, the biosensors described in this manuscript had to be shipped and stored on ice to counteract heat damage from the ambient temperature in Nakuru county, Kenya. Furthermore, deployment in rural settings away from transportation infrastructure will require improvements in long term reaction stability to

enable continuous use. Therefore, after tuning individual reaction components to make our desired sensors, we must also ruggedize them by optimizing the process by which they are prepared for field use.

Although lyophilization is a long-established process for simplifying storage of pharmaceuticals or other compounds[187,188], there is still significant room for process optimization. Lyophilization works by taking a frozen product and putting it under vacuum; in these low-pressure conditions, water sublimates at ambient temperature, allowing for dehydration without heat damage to the lyophilized product. The exact ideal conditions for this process can vary, however, based on dimensions of the product being lyophilized, product composition, and water permeability of the lyophilized cake[189]. While previous ideal lyophilization conditions were determined through trial-and-error experimentation, there are new efforts to facilitate optimization through mathematical modeling of the lyophilization process[190,191]. Applying this framework to guide the lyophilization of cell-free reactions would help generate ideal conditions for their lyophilization, potentially improving shelf-life and minimizing loss of function.

Beyond optimizing the lyophilization process itself, there is substantial potential to increase reaction stability using additives called lyoprotectants. Generally speaking, these lyoprotectants work to either prevent product degradation during the lyophilization process or help slow degradation over long periods of shelf storage. Encouragingly, preliminary work adding lyoprotectants to cell-free reactions suggests that they can substantially enhance their thermostability, enabling storage at 50°C for up to a month[151]. Exploring the use of other promising additives including sugars[192,193], polysaccharides[194,195], or disordered tardigrade proteins[196,197] would further improve our ability to protect cell-free reactions, potential enabling up to years of long-term storage in even the harshest environments.

Developing packaging, usage guidelines, and peripheral devices

Previous studies on bringing biosensors into the field have relied on ad hoc packaging and device embodiments[23,158]. While this is acceptable for initial pilot tests, wider deployment will require optimizing these aspects of the sensors to maximize ease of use. This is particularly important to accommodate more diverse user bases, enabling any potential end user to operate a biosensor and generate actionable data. To be clear, many of the innovations necessary here are solidly outside the realm of pure synthetic biology; however, in acknowledgement of the interdisciplinary nature of the field and the need to contextualize scientific developments with roads to commercialization, it is helpful to offer a few broad strokes guidelines to guide progress moving forward.

The chief issues encountered by the biosensors used in this work relate largely to ease of use. Most notably, participants struggled with sample manipulation. For example, when rehydrating lyophilized reactions, participants repeatedly asked for rehydration volumes in “drops” of sample, which runs contrary to the precise volumes needed to generate accurate results. To remedy this, future device embodiments should by some means automate the addition of sample to a test, minimizing opportunity for user error. Furthermore, the issues encountered with subjective interpretations of ambiguous colorimetric results could be addressed using supplemental equipment as described previously in this section[185]. Finally, there is the potential to enhance the power of these sensors with microfluidics; performing complex liquid handling steps with minimal user input will be key in the development of low-cost water quality panels to provide rapid, comprehensive assessments of water safety. Further development of these technologies to support cell-free biosensors will build upon the strong foundation established by this and other works, setting the stage for the larger-scope visions in biosensing as a field to become a reality.

5.3 Closing perspective and final comments

Infrequent monitoring of a narrow range of contaminants has created significant gaps in our current understanding of water quality[12] and therefore water insecurity[160,198,199]. Synthetic biology has the potential to fill these gaps in knowledge by offering simple, field-deployable tools to report on individual water supplies or serve as pre-screening tools to be used with existing gold-standard methods to provide the large-scale, high-resolution data needed to track progress towards development goals. While there are existing field deployable tools, they are limited by the technical expertise, supplemental equipment, or dangerous chemical reagents required for their use. The potential for biosensors to decrease cost and improve ease-of-use for such diagnostics relative to current methods enables more frequent measurements across wider and more diverse regions, producing water quality data that are more comprehensive and specific than currently available.

There is significant promise for this to become a reality – current biosensor formats are accessible to an untrained user, and recent cost estimates suggest that their production can be scaled for global use. Using biosensors to generate spatiotemporal water quality data will enable more efficient resource allocation by showing exactly when and where interventions are necessary. Not only will such diagnostics provide important population-level information, but they have the potential to usher in the ability to simply and inexpensively assess water quality so that even untrained individuals can personally ensure the safety of their water. As such, advances in synthetic biology could facilitate global water quality monitoring by producing actionable contaminant data, guide the development of efficacious policies and programs, and inform choices about the water we consume.

References

(1) Gosling, S. N.; Arnell, N. W. A Global Assessment of the Impact of Climate Change on Water Scarcity. *Clim. Change* **2016**, *134* (3), 371–385.

(2) Kummu, M.; Guillaume, J. H. A.; de Moel, H.; Eisner, S.; Flörke, M.; Porkka, M.; Siebert, S.; Veldkamp, T. I. E.; Ward, P. J. The World's Road to Water Scarcity: Shortage and Stress in the 20th Century and Pathways towards Sustainability. *Sci. Rep.* **2016**, *6*, 38495.

(3) United Nations High-Level Panel on Water. Making Every Drop Count: An Agenda for Water Action https://reliefweb.int/report/world/making-every-drop-count-agenda-water-action-high-level-panel-water-outcome-document-14.

(4) United Nations Development Program. *Beyond Scarcity: Power, Poverty and the Global Water Crisis*; 2006.

(5) Honkonen, T. Water Security and Climate Change: The Need for Adaptive Governance. *Potchefstroom Electron. Law Journal/Potchefstroomse Elektron. Regsbl.* **2017**, *20* (1).

(6) World Economic Forum. The Global Risks Report 2019, 14th Edition https://www.weforum.org/reports/the-global-risks-report-2019.

(7) USAID. U.S. Government Global Water Strategy https://www.usaid.gov/what-we-do/water-and-sanitation/us-global-water-strategy.

(8) Wagstaff, A. The Millennium Development Goals for health: rising to the challenges http://documents.worldbank.org/curated/en/875031468329973611/The-millennium-development-goals-for-health-rising-to-the-challenges.

(9) Sachs, J. D. From Millennium Development Goals to Sustainable Development Goals. *Lancet* **2012**, *379* (9832), 2206–2211.

(10) World Health Organization; UNICEF. Water for life: making it happen https://www.who.int/water_sanitation_health/monitoring/jmp2005/en/.

(11) Bartram, J.; Brocklehurst, C.; Fisher, M. B.; Luyendijk, R.; Hossain, R.; Wardlaw, T.; Gordon, B. Global Monitoring of Water Supply and Sanitation: History, Methods and Future Challenges. *Int. J. Environ. Res. Public Health* **2014**, *11* (8), 8137–8165.

(12) Damania, R.; Desbureaux, S.; Rodella, A.-S.; Russ, J.; Zaveri, E. *Quality Unknown: The Invisible Water Crisis*; World Bank Publications, 2019.

(13) Stauber, C. The Sustainable Development Goals for Water: The Need to Consider Perception, Preference, and Safety. *Am. J. Trop. Med. Hyg.* **2017**, *97* (4), 985.

(14) UNICEF. SDG Global Indicators Related to Children https://data.unicef.org/resources/sdg-global-indicators-related-to-children/.

(15) World Health Organization. *Guidelines for Drinking-Water Quality, 4th Edition, Incorporating the 1st Addendum*; World Health Organization, 2018.

(16) Ellis, K.; Gowdy, C.; Jakomis, N.; Ryan, B.; Thom, C.; Biggs, C. A.; Speight, V. Understanding the Costs of Investigating Coliform and E. Coli Detections during Routine Drinking Water Quality Monitoring. *Urban Water J.* **2018**, *15* (2), 101–108.

(17) Fawell, J.; Bailey, K.; Chilton, J.; Dahi, E.; Magara, Y. *Fluoride in Drinking-Water*; IWA Publishing, 2006.

(18) Chelsea Technologies. UviLux. https://chelsea.co.uk/products/uvilux/.

(19) IDEXX. Coliform/E.coli water tests. https://www.idexx.com/en/water/products/?cy=y_category_252&cx=x_category_259&ts=all.

(20) Hach USA. Arsenic Low Range Test Kit. https://www.hach.com/arsenic-low-range-test-kit/product?id=7640217303.

(21) Salehi, A. S. M.; Shakalli Tang, M. J.; Smith, M. T.; Hunt, J. M.; Law, R. A.; Wood, D. W.; Bundy, B. C. Cell-Free Protein Synthesis Approach to Biosensing HTRβ-Specific Endocrine Disruptors. *Anal. Chem.* **2017**, *89* (6), 3395–3401.

(22) Alam, K. K.; Jung, J. K.; Verosloff, M. S.; Clauer, P. R.; Lee, J. W.; Capdevila, D. A.; Pastén,

P. A.; Giedroc, D. P.; Collins, J. J.; Lucks, J. B. Rapid, Low-Cost Detection of Water Contaminants Using Regulated In Vitro Transcription. *bioRxiv* **2019**. https://doi.org/10.1101/619296.

(23) Thavarajah, W.; Silverman, A. D.; Verosloff, M. S.; Kelley-Loughnane, N.; Jewett, M. C.; Lucks, J. B. Point-of-Use Detection of Environmental Fluoride via a Cell-Free Riboswitch-Based Biosensor. *ACS Synth. Biol.* **2019**, *9* (1), 10–18. https://doi.org/https://doi.org/10.1021/acssynbio.9b00347.

(24) Selifonova, O.; Burlage, R.; Barkay, T. Bioluminescent Sensors for Detection of Bioavailable Hg (II) in the Environment. *Appl. Environ. Microbiol.* **1993**, *59* (9), 3083–3090.

(25) Gräwe, A.; Dreyer, A.; Vornholt, T.; Barteczko, U.; Buchholz, L.; Drews, G.; Ho, U. L.; Jackowski, M. E.; Kracht, M.; Lüders, J. A Paper-Based, Cell-Free Biosensor System for the Detection of Heavy Metals and Date Rape Drugs. *PLoS One* **2019**, *14* (3), e0210940.

(26) Pellinen, T.; Huovinen, T.; Karp, M. A Cell-Free Biosensor for the Detection of Transcriptional Inducers Using Firefly Luciferase as a Reporter. *Anal. Biochem.* **2004**, *330* (1), 52–57.

(27) Rawson, D. M.; Willmer, A. J.; Turner, A. P. P. Whole-Cell Biosensors for Environmental Monitoring. *Biosensors* **1989**, *4* (5), 299–311.

(28) Stocker, J.; Balluch, D.; Gsell, M.; Harms, H.; Feliciano, J.; Daunert, S.; Malik, K. A.; Van der Meer, J. R. Development of a Set of Simple Bacterial Biosensors for Quantitative and Rapid Measurements of Arsenite and Arsenate in Potable Water. *Environ. Sci. Technol.* **2003**, *37* (20), 4743–4750.

(29) Prest, A. G.; Winson, M. K.; Hammond, J. R. M.; Stewart, G. The Construction and Application of a Lux-based Nitrate Biosensor. *Lett. Appl. Microbiol.* **1997**, *24* (5), 355–360.

(30) Virta, M.; Lampinen, J.; Karp, M. A Luminescence-Based Mercury Biosensor. *Anal. Chem.* **1995**, *67* (3), 667–669.

(31) Willardson, B. M.; Wilkins, J. F.; Rand, T. A.; Schupp, J. M.; Hill, K. K.; Keim, P.; Jackson, P. J. Development and Testing of a Bacterial Biosensor for Toluene-Based Environmental Contaminants. *Appl. Environ. Microbiol.* **1998**, *64* (3), 1006–1012.

(32) Tauriainen, S.; Karp, M.; Chang, W.; Virta, M. Luminescent Bacterial Sensor for Cadmium and Lead. *Biosens. Bioelectron.* **1998**, *13* (9), 931–938.

(33) Wen, K. Y.; Cameron, L.; Chappell, J.; Jensen, K.; Bell, D. J.; Kelwick, R.; Kopniczky, M.; Davies, J. C.; Filloux, A.; Freemont, P. S. A Cell-Free Biosensor for Detecting Quorum Sensing Molecules in P. Aeruginosa-Infected Respiratory Samples. *ACS Synth. Biol.* **2017**, *6* (12), 2293–2301.

(34) Takahashi, M. K.; Tan, X.; Dy, A. J.; Braff, D.; Akana, R. T.; Furuta, Y.; Donghia, N.; Ananthakrishnan, A.; Collins, J. J. A Low-Cost Paper-Based Synthetic Biology Platform for Analyzing Gut Microbiota and Host Biomarkers. *Nat. Commun.* **2018**, *9* (1), 3347. https://doi.org/10.1038/s41467-018-05864-4.

(35) Phillips, E. A.; Moehling, T. J.; Bhadra, S.; Ellington, A. D.; Linnes, J. C. Strand Displacement Probes Combined with Isothermal Nucleic Acid Amplification for Instrument-Free Detection from Complex Samples. *Anal. Chem.* **2018**, *90* (11), 6580–6586.

(36) Kawaguchi, T.; Chen, Y. P.; Norman, R. S.; Decho, A. W. Rapid Screening of Quorum-Sensing Signal N-Acyl Homoserine Lactones by an in Vitro Cell-Free Assay. *Appl. Environ. Microbiol.* **2008**, *74* (12), 3667–3671.

(37) Jiang, Y. S.; Riedel, T. E.; Popoola, J. A.; Morrow, B. R.; Cai, S.; Ellington, A. D.; Bhadra, S. Portable Platform for Rapid In-Field Identification of Human Fecal Pollution in Water. *Water Res.* **2018**, *131*, 186–195.

(38) Gootenberg, J. S.; Abudayyeh, O. O.; Lee, J. W.; Essletzbichler, P.; Dy, A. J.; Joung, J.; Verdine, V.; Donghia, N.; Daringer, N. M.; Freije, C. A. Nucleic Acid Detection with CRISPR-Cas13a/C2c2. *Science (80-.).* **2017**, *356* (6336), 438–442.

(39) Pardee, K.; Green, A. A.; Ferrante, T.; Cameron, D. E.; DaleyKeyser, A.; Yin, P.; Collins,

J. J. Paper-Based Synthetic Gene Networks. *Cell* **2014**, *159* (4), 940–954.
(40) Pardee, K.; Green, A. A.; Takahashi, M. K.; Braff, D.; Lambert, G.; Lee, J. W.; Ferrante, T.; Ma, D.; Donghia, N.; Fan, M. Rapid, Low-Cost Detection of Zika Virus Using Programmable Biomolecular Components. *Cell* **2016**, *165* (5), 1255–1266.
(41) Verosloff, M.; Chappell, J.; Perry, K. L.; Thompson, J. R.; Lucks, J. B. PLANT-Dx: A Molecular Diagnostic for Point-of-Use Detection of Plant Pathogens. *ACS Synth. Biol.* **2019**, *8* (4), 902–905.
(42) Ma, D.; Shen, L.; Wu, K.; Diehnelt, C. W.; Green, A. A. Low-Cost Detection of Norovirus Using Paper-Based Cell-Free Systems and Synbody-Based Viral Enrichment. *Synth. Biol.* **2018**, *3* (1), ysy018.
(43) Myhrvold, C.; Freije, C. A.; Gootenberg, J. S.; Abudayyeh, O. O.; Metsky, H. C.; Durbin, A. F.; Kellner, M. J.; Tan, A. L.; Paul, L. M.; Parham, L. A. Field-Deployable Viral Diagnostics Using CRISPR-Cas13. *Science (80-.).* **2018**, *360* (6387), 444–448.
(44) Spoelstra, W. K.; Jacques, J. M.; Nóbrega, F. L.; Haagsma, A. C.; Dogterom, M.; Idema, T.; Brouns, S. J. J.; Reese, L. CRISPR-Based DNA and RNA Detection with Liquid Phase Separation. *bioRxiv* **2018**, 471482.
(45) Romero, J. L. R.; Carver, G. D.; Johnson, P. A.; Perry, K. L.; Thompson, J. R. A Rapid, Sensitive and Inexpensive Method for Detection of Grapevine Red Blotch Virus without Tissue Extraction Using Loop-Mediated Isothermal Amplification. *Arch. Virol.* **2019**, *164* (5), 1453–1457.
(46) Thavarajah, W.; Verosloff, M. S.; Jung, J. K.; Alam, K. K.; Miller, J. D.; Jewett, M. C.; Young, S. L.; Lucks, J. B. A Primer on Emerging Field-Deployable Synthetic Biology Tools for Global Water Quality Monitoring. *npj Clean Water* **2020**, *3* (1), 1–10.
(47) Kaur, H.; Kumar, R.; Babu, J. N.; Mittal, S. Advances in Arsenic Biosensor Development–a Comprehensive Review. *Biosens. Bioelectron.* **2015**, *63*, 533–545.
(48) Bereza-Malcolm, L. T.; Mann, G.; Franks, A. E. Environmental Sensing of Heavy Metals through Whole Cell Microbial Biosensors: A Synthetic Biology Approach. *ACS Synth. Biol.* **2014**, *4* (5), 535–546.
(49) Wan, X.; Ho, T. Y. H.; Wang, B. Engineering Prokaryote Synthetic Biology Biosensors. *Handb. Cell Biosens.* **2019**, 1–37.
(50) Belkin, S.; Yagur-Kroll, S.; Kabessa, Y.; Korouma, V.; Septon, T.; Anati, Y.; Zohar-Perez, C.; Rabinovitz, Z.; Nussinovitch, A.; Agranat, A. J. Remote Detection of Buried Landmines Using a Bacterial Sensor. *Nat. Biotechnol.* **2017**, *35* (4), 308.
(51) Stirling, F.; Bitzan, L.; O'Keefe, S.; Redfield, E.; Oliver, J. W. K.; Way, J.; Silver, P. A. Rational Design of Evolutionarily Stable Microbial Kill Switches. *Mol. Cell* **2017**, *68* (4), 686–697.
(52) Silverman, A. D.; Karim, A. S.; Jewett, M. C. Cell-Free Gene Expression: An Expanded Repertoire of Applications. *Nat. Rev. Genet.* **2020**, *21*, 151–170. https://doi.org/10.1038/s41576-019-0186-3.
(53) Didovyk, A.; Tonooka, T.; Tsimring, L.; Hasty, J. Rapid and Scalable Preparation of Bacterial Lysates for Cell-Free Gene Expression. *ACS Synth. Biol.* **2017**, *6* (12), 2198–2208.
(54) Silverman, A. D.; Akova, U.; Alam, K. K.; Jewett, M. C.; Lucks, J. B. Design and Optimization of a Cell-Free Atrazine Biosensor. *ACS Synth. Biol.* **2020**. https://doi.org/10.1021/acssynbio.9b00388.
(55) Jumper, J.; Evans, R.; Pritzel, A.; Green, T.; Figurnov, M.; Ronneberger, O.; Tunyasuvunakool, K.; Bates, R.; Žídek, A.; Potapenko, A. Highly Accurate Protein Structure Prediction with AlphaFold. *Nature* **2021**, *596* (7873), 583–589.
(56) Mandal, M.; Breaker, R. R. Gene Regulation by Riboswitches. *Nat. Rev. Mol. cell Biol.* **2004**, *5* (6), 451.
(57) Tucker, B. J.; Breaker, R. R. Riboswitches as Versatile Gene Control Elements. *Curr. Opin.*

Struct. Biol. **2005**, *15* (3), 342–348.
(58) McCown, P. J.; Corbino, K. A.; Stav, S.; Sherlock, M. E.; Breaker, R. R. Riboswitch Diversity and Distribution. *RNA* **2017**, *23* (7), 995–1011.
(59) Ellington, A. D.; Szostak, J. W. In Vitro Selection of RNA Molecules That Bind Specific Ligands. *Nature* **1990**, *346* (6287), 818–822.
(60) Darmostuk, M.; Rimpelova, S.; Gbelcova, H.; Ruml, T. Current Approaches in SELEX: An Update to Aptamer Selection Technology. *Biotechnol. Adv.* **2015**, *33* (6), 1141–1161.
(61) Boussebayle, A.; Torka, D.; Ollivaud, S.; Braun, J.; Bofill-Bosch, C.; Dombrowski, M.; Groher, F.; Hamacher, K.; Suess, B. Next-Level Riboswitch Development—Implementation of Capture-SELEX Facilitates Identification of a New Synthetic Riboswitch. *Nucleic Acids Res.* **2019**, *47* (9), 4883–4895.
(62) Townshend, B.; Xiang, J. S.; Manzanarez, G.; Hayden, E. J.; Smolke, C. D. A Multiplexed, Automated Evolution Pipeline Enables Scalable Discovery and Characterization of Biosensors. *Nat. Commun.* **2021**, *12* (1), 1–15.
(63) Porter, E. B.; Polaski, J. T.; Morck, M. M.; Batey, R. T. Recurrent RNA Motifs as Scaffolds for Genetically Encodable Small-Molecule Biosensors. *Nat. Chem. Biol.* **2017**, *13*, 295.
(64) World Health Organization. *World Health Statistics 2016: Monitoring Health for the SDGs Sustainable Development Goals*; World Health Organization, 2016.
(65) Onda, K.; LoBuglio, J.; Bartram, J. Global Access to Safe Water: Accounting for Water Quality and the Resulting Impact on MDG Progress. *Int. J. Environ. Res. Public Health* **2012**, *9* (3), 880–894.
(66) Maheshwari, R. C. Fluoride in Drinking Water and Its Removal. *J. Hazard. Mater.* **2006**, *137* (1), 456–463.
(67) World Health Organization. Guidelines for Drinking-Water Quality. *WHO Chron.* **2011**, *38* (4), 104–108.
(68) Zhou, Y.; Zhang, J. F.; Yoon, J. Fluorescence and Colorimetric Chemosensors for Fluoride-Ion Detection. *Chem. Rev.* **2014**, *114* (10), 5511–5571.
(69) Baker, J. L.; Sudarsan, N.; Weinberg, Z.; Roth, A.; Stockbridge, R. B.; Breaker, R. R. Widespread Genetic Switches and Toxicity Resistance Proteins for Fluoride. *Science (80-.).* **2012**, *335* (6065), 233–235.
(70) Watters, K. E.; Strobel, E. J.; Angela, M. Y.; Lis, J. T.; Lucks, J. B. Cotranscriptional Folding of a Riboswitch at Nucleotide Resolution. *Nat. Struct. Mol. Biol.* **2016**, *23* (12), 1124.
(71) Doull, J.; Boekelheide, K.; Farishian, B. G.; Isaacson, R. L.; Klotz, J. B.; Kumar, J. V; Limeback, H.; Poole, C.; Puzas, J. E.; Reed, N. M. R. Fluoride in Drinking Water: A Scientific Review of EPA's Standards. *Natl. Acad. Washingt.* **2006**, 205–223.
(72) Zadeh, J. N.; Steenberg, C. D.; Bois, J. S.; Wolfe, B. R.; Pierce, M. B.; Khan, A. R.; Dirks, R. M.; Pierce, N. A. NUPACK: Analysis and Design of Nucleic Acid Systems. *J. Comput. Chem.* **2011**, *32* (1), 170–173.
(73) McNerney, M. P.; Zhang, Y.; Steppe, P.; Silverman, A. D.; Jewett, M. C.; Styczynski, M. P. Point-of-Care Biomarker Quantification Enabled by Sample-Specific Calibration. *Sci. Adv.* **2019**, *5* (9), eaax4473.
(74) Alam, K. K.; Tawiah, K. D.; Lichte, M. F.; Porciani, D.; Burke, D. H. A Fluorescent Split Aptamer for Visualizing RNA–RNA Assembly In Vivo. *ACS Synth. Biol.* **2017**, *6* (9), 1710–1721.
(75) Chappell, J.; Westbrook, A.; Verosloff, M.; Lucks, J. B. Computational Design of Small Transcription Activating RNAs for Versatile and Dynamic Gene Regulation. *Nat. Commun.* **2017**, *8* (1), 1051.
(76) Stark, J. C.; Huang, A.; Nguyen, P. Q.; Dubner, R. S.; Hsu, K. J.; Ferrante, T. C.; Anderson, M.; Kanapskyte, A.; Mucha, Q.; Packett, J. S.; et al. BioBits^{TM} Bright: A Fluorescent Synthetic Biology Education Kit. *Sci. Adv.* **2018**, *4* (8), eaat5107.
(77) Huang, A.; Nguyen, P. Q.; Stark, J. C.; Takahashi, M. K.; Donghia, N.; Ferrante, T.; Dy, A.

J.; Hsu, K. J.; Dubner, R. S.; Pardee, K.; et al. BioBits™ Explorer: A Modular Synthetic Biology Education Kit. *Sci. Adv.* **2018**, *4* (8), eaat5105.

(78) Haklay, M.; Weber, P. Openstreetmap: User-Generated Street Maps. *Ieee Pervas Comput* **2008**, *7* (4), 12–18.

(79) Rojas Zuniga, F.; Floor, G.; Malavassi, E.; Martinez Cruz, M.; Van Bergen, M. Fluorosis Dental En La Población Infantil En Las Cercanías Del Volcán Irazú, Costa Rica. *Congr. Latinoam. Estud. Química Paraguay* **2014**.

(80) Zhao, B.; Guffy, S. L.; Williams, B.; Zhang, Q. An Excited State Underlies Gene Regulation of a Transcriptional Riboswitch. *Nat. Chem. Biol.* **2017**, *13* (9), 968–974.

(81) Wickiser, J. K.; Winkler, W. C.; Breaker, R. R.; Crothers, D. M. The Speed of RNA Transcription and Metabolite Binding Kinetics Operate an FMN Riboswitch. *Mol. Cell* **2005**, *18* (1), 49–60.

(82) Karzbrun, E.; Shin, J.; Bar-Ziv, R. H.; Noireaux, V. Coarse-Grained Dynamics of Protein Synthesis in a Cell-Free System. *Phys. Rev. Lett.* **2011**, *106* (4), 48104.

(83) Ren, A.; Rajashankar, K. R.; Patel, D. J. Fluoride Ion Encapsulation by Mg 2+ Ions and Phosphates in a Fluoride Riboswitch. *Nature* **2012**, *486* (7401), 85.

(84) Moore, S. J.; MacDonald, J. T.; Wienecke, S.; Ishwarbhai, A.; Tsipa, A.; Aw, R.; Kylilis, N.; Bell, D. J.; McClymont, D. W.; Jensen, K.; et al. Rapid Acquisition and Model-Based Analysis of Cell-Free Transcription–Translation Reactions from Nonmodel Bacteria. *Proc. Natl. Acad. Sci.* **2018**, *115* (19).

(85) Greenlee, E. B.; Stav, S.; Atilho, R. M.; Brewer, K. I.; Harris, K. A.; Malkowski, S. N.; Mirihana Arachchilage, G.; Perkins, K. R.; Sherlock, M. E.; Breaker, R. R. Challenges of Ligand Identification for the Second Wave of Orphan Riboswitch Candidates. *RNA Biol.* **2018**, *15* (3), 377–390.

(86) Espah Borujeni, A.; Mishler, D. M.; Wang, J.; Huso, W.; Salis, H. M. Automated Physics-Based Design of Synthetic Riboswitches from Diverse RNA Aptamers. *Nucleic Acids Res.* **2015**, *44* (1), 1–13.

(87) Wu, M. J.; Andreasson, J. O. L.; Kladwang, W.; Greenleaf, W. J.; Das, R. Automated Design of Diverse Stand-Alone Riboswitches. *ACS Synth. Biol.* **2019**, *8* (8), 1838–1846.

(88) Frieda, K. L.; Block, S. M. Direct Observation of Cotranscriptional Folding in an Adenine Riboswitch. *Science (80-.).* **2012**, *338* (6105), 397–400.

(89) Drogalis, L. K.; Batey, R. T. Requirements for Efficient Ligand-Gated Co-Transcriptional Switching in Designed Variants of the B. Subtilis PbuE Adenine-Responsive Riboswitch in E. Coli. *PLoS One* **2020**, *15* (12), e0243155.

(90) Strobel, E. J.; Cheng, L.; Berman, K. E.; Carlson, P. D.; Lucks, J. B. A Ligand-Gated Strand Displacement Mechanism for ZTP Riboswitch Transcription Control. *Nat. Chem. Biol.* **2019**, *15* (11), 1067–1076.

(91) Silverman, A.; Kelley-Loughnane, N.; Lucks, J. B.; Jewett, M. C. Deconstructing Cell-Free Extract Preparation for in Vitro Activation of Transcriptional Genetic Circuitry. *ACS Synth. Biol.* **2018**, *8* (2), 403–414.

(92) Zhang, P.; Feng, H.; Yang, J.; Jiang, H.; Zhou, H.; Lu, Y. Detection of Inorganic Ions and Organic Molecules with Cell-Free Biosensing Systems. *J. Biotechnol.* **2019**, *300*, 78–86.

(93) Liu, X.; Silverman, A. D.; Alam, K. K.; Iverson, E.; Lucks, J. B.; Jewett, M. C.; Raman, S. Design of a Transcriptional Biosensor for the Portable, on-Demand Detection of Cyanuric Acid. *ACS Synth. Biol.* **2019**, *9* (1), 84–94.

(94) Voyvodic, P. L.; Pandi, A.; Koch, M.; Conejero, I.; Valjent, E.; Courtet, P.; Renard, E.; Faulon, J.-L.; Bonnet, J. Plug-and-Play Metabolic Transducers Expand the Chemical Detection Space of Cell-Free Biosensors. *Nat. Commun.* **2019**, *10* (1), 1–8.

(95) Gupta, S.; Sarkar, S.; Katranidis, A.; Bhattacharya, J. Development of a Cell-Free Optical Biosensor for Detection of a Broad Range of Mercury Contaminants in Water: A Plasmid DNA-Based Approach. *ACS Omega* **2019**, *4* (5), 9480–9487.

(96) Duyen, T. T. M.; Matsuura, H.; Ujiie, K.; Muraoka, M.; Harada, K.; Hirata, K. Paper-Based Colorimetric Biosensor for Antibiotics Inhibiting Bacterial Protein Synthesis. *J. Biosci. Bioeng.* **2017**, *123* (1), 96–100.
(97) Hunt, J. P.; Zhao, E. L.; Free, T. J.; Soltani, M.; Warr, C. A.; Benedict, A. B.; Takahashi, M. K.; Griffitts, J. S.; Pitt, W. G.; Bundy, B. C. Towards Detection of SARS-CoV-2 RNA in Human Saliva: A Paper-Based Cell-Free Toehold Switch Biosensor with a Visual Bioluminescent Output. *N. Biotechnol.* **2022**, *66*, 53–60.
(98) Hunt, J. P.; Barnett, R. J.; Robinson, H.; Soltani, M.; Nelson, J. A. D.; Bundy, B. C. Rapid Sensing of Clinically Relevant Glutamine Concentrations in Human Serum with Metabolically Engineered E. Coli-Based Cell-Free Protein Synthesis. *J. Biotechnol.* **2021**, *325*, 389–394.
(99) Boyd, M. A.; Kamat, N. P. Designing Artificial Cells towards a New Generation of Biosensors. *Trends Biotechnol.* **2021**, *39* (9), 927–939.
(100) Soltani, M.; Hunt, J. P.; Bundy, B. C. Rapid RNase Inhibitor Production to Enable Low-cost, On-demand Cell-free Protein Synthesis Biosensor Use in Human Body Fluids. *Biotechnol. Bioeng.* **2021**, *118* (10), 3973–3983.
(101) Adamala, K. P.; Martin-Alarcon, D. A.; Guthrie-Honea, K. R.; Boyden, E. S. Engineering Genetic Circuit Interactions within and between Synthetic Minimal Cells. *Nat. Chem.* **2017**, *9* (5), 431–439.
(102) Tan, C.; Saurabh, S.; Bruchez, M. P.; Schwartz, R.; LeDuc, P. Molecular Crowding Shapes Gene Expression in Synthetic Cellular Nanosystems. *Nat. Nanotechnol.* **2013**, *8* (8), 602–608.
(103) Nourian, Z.; Danelon, C. Linking Genotype and Phenotype in Protein Synthesizing Liposomes with External Supply of Resources. *ACS Synth. Biol.* **2013**, *2* (4), 186–193.
(104) Pereira de Souza, T.; Stano, P.; Luisi, P. L. The Minimal Size of Liposome-based Model Cells Brings about a Remarkably Enhanced Entrapment and Protein Synthesis. *ChemBioChem* **2009**, *10* (6), 1056–1063.
(105) Sakamoto, R.; Noireaux, V.; Maeda, Y. T. Anomalous Scaling of Gene Expression in Confined Cell-Free Reactions. *Sci. Rep.* **2018**, *8* (1), 1–8.
(106) Schaffter, S. W.; Schulman, R. Building in Vitro Transcriptional Regulatory Networks by Successively Integrating Multiple Functional Circuit Modules. *Nat. Chem.* **2019**, *11* (9), 829–838.
(107) Lentini, R.; Santero, S. P.; Chizzolini, F.; Cecchi, D.; Fontana, J.; Marchioretto, M.; Del Bianco, C.; Terrell, J. L.; Spencer, A. C.; Martini, L. Integrating Artificial with Natural Cells to Translate Chemical Messages That Direct E. Coli Behaviour. *Nat. Commun.* **2014**, *5* (1), 1–6.
(108) Martini, L.; Mansy, S. S. Cell-like Systems with Riboswitch Controlled Gene Expression. *Chem. Commun.* **2011**, *47* (38), 10734–10736.
(109) Dwidar, M.; Seike, Y.; Kobori, S.; Whitaker, C.; Matsuura, T.; Yokobayashi, Y. Programmable Artificial Cells Using Histamine-Responsive Synthetic Riboswitch. *J. Am. Chem. Soc.* **2019**, *141* (28), 11103–11114.
(110) Janas, T.; Janas, T.; Yarus, M. Specific RNA Binding to Ordered Phospholipid Bilayers. *Nucleic Acids Res.* **2006**, *34* (7), 2128–2136.
(111) Czerniak, T.; Saenz, J. P. Lipid Membranes Modulate the Activity of RNA through Sequence-Dependent Interactions. *Proc. Natl. Acad. Sci.* **2022**, *119* (4).
(112) World Health Organization. *Progress on Household Drinking Water, Sanitation and Hygiene 2000-2017: Special Focus on Inequalities*; World Health Organization, 2019.
(113) Fuge, R. Fluorine in the Environment, a Review of Its Sources and Geochemistry. *Appl. Geochemistry* **2019**, *100*, 393–406.
(114) McMahon, P. B.; Brown, C. J.; Johnson, T. D.; Belitz, K.; Lindsey, B. D. Fluoride Occurrence in United States Groundwater. *Sci. Total Environ.* **2020**, *732*, 139217.

(115) Barbier, O.; Arreola-Mendoza, L.; Del Razo, L. M. Molecular Mechanisms of Fluoride Toxicity. *Chem. Biol. Interact.* **2010**, *188* (2), 319–333.
(116) Pautot, S.; Frisken, B. J.; Weitz, D. A. Production of Unilamellar Vesicles Using an Inverted Emulsion. *Langmuir* **2003**, *19* (7), 2870–2879.
(117) Gonzales, D. T.; Yandrapalli, N.; Robinson, T.; Zechner, C.; Tang, T. Y. D. Cell-Free Gene Expression Dynamics in Synthetic Cell Populations. *ACS Synth. Biol.* **2022**.
(118) Nishimura, K.; Matsuura, T.; Nishimura, K.; Sunami, T.; Suzuki, H.; Yomo, T. Cell-Free Protein Synthesis inside Giant Unilamellar Vesicles Analyzed by Flow Cytometry. *Langmuir* **2012**, *28* (22), 8426–8432.
(119) NIS Why. Nikon Offers Total Software Solution Covering Image Capture, Archiving, and Analysis. *Imaging 9100* (02), C9100-12.
(120) Nishimura, K.; Tsuru, S.; Suzuki, H.; Yomo, T. Stochasticity in Gene Expression in a Cell-Sized Compartment. *ACS Synth. Biol.* **2015**, *4* (5), 566–576.
(121) Nourian, Z.; Roelofsen, W.; Danelon, C. Triggered Gene Expression in Fed-vesicle Microreactors with a Multifunctional Membrane. *Angew. chemie* **2012**, *124* (13), 3168–3172.
(122) Saito, H.; Kato, Y.; Le Berre, M.; Yamada, A.; Inoue, T.; Yosikawa, K.; Baigl, D. Time-resolved Tracking of a Minimum Gene Expression System Reconstituted in Giant Liposomes. *ChemBioChem* **2009**, *10* (10), 1640–1643.
(123) Garenne, D.; Noireaux, V. Analysis of Cytoplasmic and Membrane Molecular Crowding in Genetically Programmed Synthetic Cells. *Biomacromolecules* **2020**, *21* (7), 2808–2817.
(124) Gutknecht, J.; Walter, A. Hydrofluoric and Nitric Acid Transport through Lipid Bilayer Membranes. *Biochim. Biophys. Acta (BBA)-Biomembranes* **1981**, *644* (1), 153–156.
(125) Discher, B. M.; Won, Y.-Y.; Ege, D. S.; Lee, J. C. M.; Bates, F. S.; Discher, D. E.; Hammer, D. A. Polymersomes: Tough Vesicles Made from Diblock Copolymers. *Science (80-.).* **1999**, *284* (5417), 1143–1146.
(126) Jacobs, M. L.; Boyd, M. A.; Kamat, N. P. Diblock Copolymers Enhance Folding of a Mechanosensitive Membrane Protein during Cell-Free Expression. *Proc. Natl. Acad. Sci.* **2019**, *116* (10), 4031–4036.
(127) Jespersen, H.; Andersen, J. H.; Ditzel, H. J.; Mouritsen, O. G. Lipids, Curvature Stress, and the Action of Lipid Prodrugs: Free Fatty Acids and Lysolipid Enhancement of Drug Transport across Liposomal Membranes. *Biochimie* **2012**, *94* (1), 2–10.
(128) Monnard, P.; Deamer, D. W. Membrane Self-assembly Processes: Steps toward the First Cellular Life. *Anat. Rec. An Off. Publ. Am. Assoc. Anat.* **2002**, *268* (3), 196–207.
(129) Kruyer, N. S.; Sugianto, W.; Tickman, B. I.; Alba Burbano, D.; Noireaux, V.; Carothers, J. M.; Peralta-Yahya, P. Membrane Augmented Cell-Free Systems: A New Frontier in Biotechnology. *ACS Synth. Biol.* **2021**, *10* (4), 670–681.
(130) Lazar, J. T.; Tabor, J. J. Bacterial Two-Component Systems as Sensors for Synthetic Biology Applications. *Curr. Opin. Syst. Biol.* **2021**, *28*, 100398.
(131) Hilburger, C. E.; Jacobs, M. L.; Lewis, K. R.; Peruzzi, J. A.; Kamat, N. P. Controlling Secretion in Artificial Cells with a Membrane and Gate. *ACS Synth. Biol.* **2019**, *8* (6), 1224–1230.
(132) Prüss-Ustün, A.; Wolf, J.; Bartram, J.; Clasen, T.; Cumming, O.; Freeman, M. C.; Gordon, B.; Hunter, P. R.; Medlicott, K.; Johnston, R. Burden of Disease from Inadequate Water, Sanitation and Hygiene for Selected Adverse Health Outcomes: An Updated Analysis with a Focus on Low-and Middle-Income Countries. *Int. J. Hyg. Environ. Health* **2019**, *222* (5), 765–777.
(133) World Health Organization. Progress on Household Drinking Water, Sanitation and Hygiene 2000-2020: Five Years into the SDGs. **2021**.
(134) United Nations. Sustainable Development Goal 6: Synthesis Report on Water and Sanitation. 2018.

(135) World Health Organization. WHO Global Water, Sanitation and Hygiene: Annual Report 2020. **2022**.
(136) Fewtrell, L.; Smith, S.; Kay, D.; Bartram, J. An Attempt to Estimate the Global Burden of Disease Due to Fluoride in Drinking Water. *J. Water Health* **2006**, *4* (4), 533–542.
(137) Amini, M.; Mueller, K. I. M.; Abbaspour, K. C.; Rosenberg, T.; Afyuni, M.; Møller, K. N.; Sarr, M.; Johnson, C. A. Statistical Modeling of Global Geogenic Fluoride Contamination in Groundwaters. *Environ. Sci. Technol.* **2008**, *42* (10), 3662–3668.
(138) Kimambo, V.; Bhattacharya, P.; Mtalo, F.; Mtamba, J.; Ahmad, A. Fluoride Occurrence in Groundwater Systems at Global Scale and Status of Defluoridation–State of the Art. *Groundw. Sustain. Dev.* **2019**, *9*, 100223.
(139) Kanduti, D.; Sterbenk, P.; Artnik, B. Fluoride: A Review of Use and Effects on Health. *Mater. Sociomed.* **2016**, *28* (2), 133.
(140) Riggs, B. L.; Hodgson, S. F.; O'fallon, W. M.; Chao, E. Y. S.; Wahner, H. W.; Muhs, J. M.; Cedel, S. L.; Melon III, L. J. Effect of Fluoride Treatment on the Fracture Rate in Postmenopausal Women with Osteoporosis. *N. Engl. J. Med.* **1990**, *322* (12), 802–809.
(141) Pollick, H. The Role of Fluoride in the Prevention of Tooth Decay. *Pediatr. Clin.* **2018**, *65* (5), 923–940.
(142) DenBesten, P.; Li, W. Chronic Fluoride Toxicity: Dental Fluorosis. *Fluoride oral Environ.* **2011**, *22*, 81–96.
(143) Srivastava, S.; Flora, S. J. S. Fluoride in Drinking Water and Skeletal Fluorosis: A Review of the Global Impact. *Curr. Environ. Heal. reports* **2020**, *7* (2), 140–146.
(144) Cox, G. J.; Nathans, J. W. A Study of the Taste of Fluoridated Water. *J. Am. Water Works Assoc.* **1952**, *44* (10), 940–942.
(145) Gevera, P.; Mouri, H.; Maronga, G. Occurrence of Fluorosis in a Population Living in a High-Fluoride Groundwater Area: Nakuru Area in the Central Kenyan Rift Valley. *Environ. Geochem. Health* **2019**, *41* (2), 829–840.
(146) Gevera, P.; Mouri, H. Natural Occurrence of Potentially Harmful Fluoride Contamination in Groundwater: An Example from Nakuru County, the Kenyan Rift Valley. *Environ. earth Sci.* **2018**, *77* (10), 1–19.
(147) Hosmer Jr, D. W.; Lemeshow, S.; Sturdivant, R. X. *Applied Logistic Regression*; John Wiley & Sons, 2013; Vol. 398.
(148) Choubisa, S. L. Fluoride Distribution in Drinking Groundwater in Rajasthan, India. *Curr. Sci.* **2018**, 1851–1857.
(149) Raza, M.; Hussain, F.; Lee, J.-Y.; Shakoor, M. B.; Kwon, K. D. Groundwater Status in Pakistan: A Review of Contamination, Health Risks, and Potential Needs. *Crit. Rev. Environ. Sci. Technol.* **2017**, *47* (18), 1713–1762.
(150) Nickson, R.; McArthur, J.; Burgess, W.; Ahmed, K. M.; Ravenscroft, P.; Rahmanñ, M. Arsenic Poisoning of Bangladesh Groundwater. *Nature* **1998**, *395* (6700), 338.
(151) Wilding, K. M.; Zhao, E. L.; Earl, C. C.; Bundy, B. C. Thermostable Lyoprotectant-Enhanced Cell-Free Protein Synthesis for on-Demand Endotoxin-Free Therapeutic Production. *N. Biotechnol.* **2019**, *53*, 73–80.
(152) Sharpes, C. E.; McManus, J. B.; Blum, S. M.; Mgboji, G. E.; Lux, M. W. Assessment of Colorimetric Reporter Enzymes in the Pure System. *ACS Synth. Biol.* **2021**, *10* (11), 3205–3208.
(153) Sajid, M.; Kawde, A.-N.; Daud, M. Designs, Formats and Applications of Lateral Flow Assay: A Literature Review. *J. Saudi Chem. Soc.* **2015**, *19* (6), 689–705.
(154) Borremans, B.; Hobman, J. L.; Provoost, A.; Brown, N. L.; van Der Lelie, D. Cloning and Functional Analysis of the Pbr Lead Resistance Determinant of Ralstonia Metallidurans CH34. *J. Bacteriol.* **2001**, *183* (19), 5651–5658.
(155) Liu, T.; Ramesh, A.; Ma, Z.; Ward, S. K.; Zhang, L.; George, G. N.; Talaat, A. M.; Sacchettini, J. C.; Giedroc, D. P. CsoR Is a Novel Mycobacterium Tuberculosis Copper-

Sensing Transcriptional Regulator. *Nat. Chem. Biol.* **2007**, *3* (1), 60–68.
(156) Aichi, M.; Omata, T. Involvement of NtcB, a LysR Family Transcription Factor, in Nitrite Activation of the Nitrate Assimilation Operon in the Cyanobacterium Synechococcus Sp. Strain PCC 7942. *J. Bacteriol.* **1997**, *179* (15), 4671–4675.
(157) Wu, J.; Rosen, B. P. The ArsR Protein Is a Trans-acting Regulatory Protein. *Mol. Microbiol.* **1991**, *5* (6), 1331–1336.
(158) Jung, J. K.; Alam, K. K.; Verosloff, M. S.; Capdevila, D. A.; Desmau, M.; Clauer, P. R.; Lee, J. W.; Nguyen, P. Q.; Pastén, P. A.; Matiasek, S. J. Cell-Free Biosensors for Rapid Detection of Water Contaminants. *Nat. Biotechnol.* **2020**, 1–9.
(159) Promoters/Catalog/Anderson. *iGEM Registry of Standard Biological Parts*.
(160) Young, S. L.; Boateng, G. O.; Jamaluddine, Z.; Miller, J. D.; Frongillo, E. A.; Neilands, T. B.; Collins, S. M.; Wutich, A.; Jepson, W. E.; Stoler, J. The Household Water InSecurity Experiences (HWISE) Scale: Development and Validation of a Household Water Insecurity Measure for Low-Income and Middle-Income Countries. *BMJ Glob. Heal.* **2019**, *4* (5), e001750.
(161) Brunette, W.; Sudar, S.; Sundt, M.; Larson, C.; Beorse, J.; Anderson, R. Open Data Kit 2.0: A Services-Based Application Framework for Disconnected Data Management. In *Proceedings of the 15th Annual International Conference on Mobile Systems, Applications, and Services*; 2017; pp 440–452.
(162) Seed, P. DIAGT: Stata Module to Report Summary Statistics for Diagnostic Tests Compared to True Disease Status. **2010**.
(163) Taylor, N. D.; Garruss, A. S.; Moretti, R.; Chan, S.; Arbing, M. A.; Cascio, D.; Rogers, J. K.; Isaacs, F. J.; Kosuri, S.; Baker, D. Engineering an Allosteric Transcription Factor to Respond to New Ligands. *Nat. Methods* **2016**, *13* (2), 177–183.
(164) d'Oelsnitz, S.; Kim, W.; Burkholder, N.; Javanmardi, K.; Thyer, R.; Zhang, Y.; Alper, H.; Ellington, A. Using Structurally Fungible Biosensors to Evolve Improved Alkaloid Biosyntheses. **2021**.
(165) Guedez, A.; Sherman, M.; Ryu, Y. Dual Genetic Selection of the Theophylline Riboswitch with Altered Aptamer Specificity for Caffeine. *Biochem. Biophys. Res. Commun.* **2021**, *579*, 105–109.
(166) Jung, J. K.; Archuleta, C. M.; Alam, K. K.; Lucks, J. B. Programming Cell-Free Biosensors with DNA Strand Displacement Circuits. *Nat. Chem. Biol.* **2022**, *18* (4), 385–393.
(167) Kaur, H. Recent Developments in Cell-SELEX Technology for Aptamer Selection. *Biochim. Biophys. Acta (BBA)-General Subj.* **2018**, *1862* (10), 2323–2329.
(168) Kohlberger, M.; Gadermaier, G. SELEX: Critical Factors and Optimization Strategies for Successful Aptamer Selection. *Biotechnol. Appl. Biochem.* **2021**.
(169) Wu, Y. X.; Kwon, Y. J. Aptamers: The "Evolution" of SELEX. *Methods* **2016**, *106*, 21–28.
(170) Lyu, C.; Khan, I. M.; Wang, Z. Capture-SELEX for Aptamer Selection: A Short Review. *Talanta* **2021**, *229*, 122274.
(171) Kaiser, C.; Schneider, J.; Groher, F.; Suess, B.; Wachtveitl, J. What Defines a Synthetic Riboswitch?–Conformational Dynamics of Ciprofloxacin Aptamers with Similar Binding Affinities but Varying Regulatory Potentials. *Nucleic Acids Res.* **2021**, *49* (7), 3661–3671.
(172) Hötzel, J.; Suess, B. Structural Changes in Aptamers Are Essential for Synthetic Riboswitch Engineering. *J. Mol. Biol.* **2022**, 167631.
(173) Etzel, M.; Mörl, M. Synthetic Riboswitches: From Plug and Pray toward Plug and Play. *Biochemistry* **2017**, *56* (9), 1181–1198. https://doi.org/10.1021/acs.biochem.6b01218.
(174) Wachsmuth, M.; Domin, G.; Lorenz, R.; Serfling, R.; Findeiß, S.; Stadler, P. F.; Mörl, M. Design Criteria for Synthetic Riboswitches Acting on Transcription. *RNA Biol.* **2015**, *12* (2), 221–231.
(175) Berens, C.; Suess, B. Riboswitch Engineering—Making the All-Important Second and Third Steps. *Curr. Opin. Biotechnol.* **2015**, *31*, 10–15.

(176) Schmidt, C. M.; Smolke, C. D. RNA Switches for Synthetic Biology. *Cold Spring Harb. Perspect. Biol.* **2019**, *11* (1).
(177) Gorman, S. D.; D'Amico, R. N.; Winston, D. S.; Boehr, D. D. Engineering Allostery into Proteins. *Protein Allostery Drug Discov.* **2019**, 359–384.
(178) Groseclose, T. M.; Rondon, R. E.; Hersey, A. N.; Milner, P. T.; Kim, D.; Zhang, F.; Realff, M. J.; Wilson, C. J. Biomolecular Systems Engineering: Unlocking the Potential of Engineered Allostery via the Lactose Repressor Topology. *Annu. Rev. Biophys.* **2021**, *50*, 303–321.
(179) Mathony, J.; Niopek, D. Enlightening Allostery: Designing Switchable Proteins by Photoreceptor Fusion. *Adv. Biol.* **2021**, *5* (5), 2000181.
(180) Herde, Z. D.; Short, A. E.; Kay, V. E.; Huang, B. D.; Realff, M. J.; Wilson, C. J. Engineering Allosteric Communication. *Curr. Opin. Struct. Biol.* **2020**, *63*, 115–122.
(181) Skolnick, J.; Gao, M.; Zhou, H.; Singh, S. AlphaFold 2: Why It Works and Its Implications for Understanding the Relationships of Protein Sequence, Structure, and Function. *J. Chem. Inf. Model.* **2021**, *61* (10), 4827–4831.
(182) Kryshtafovych, A.; Schwede, T.; Topf, M.; Fidelis, K.; Moult, J. Critical Assessment of Methods of Protein Structure Prediction (CASP)—Round XIII. *Proteins Struct. Funct. Bioinforma.* **2019**, *87* (12), 1011–1020.
(183) AlQuraishi, M. Machine Learning in Protein Structure Prediction. *Curr. Opin. Chem. Biol.* **2021**, *65*, 1–8.
(184) Kuhlman, B.; Bradley, P. Advances in Protein Structure Prediction and Design. *Nat. Rev. Mol. Cell Biol.* **2019**, *20* (11), 681–697.
(185) Karlikow, M.; da Silva, S. J. R.; Guo, Y.; Cicek, S.; Krokovsky, L.; Homme, P.; Xiong, Y.; Xu, T.; Calderón-Peláez, M.-A.; Camacho-Ortega, S. Field Validation of the Performance of Paper-Based Tests for the Detection of the Zika and Chikungunya Viruses in Serum Samples. *Nat. Biomed. Eng.* **2022**, *6* (3), 246–256.
(186) Amalfitano, E.; Pardee, K. Logic Invades Cell-Free Biosensing. *Nat. Chem. Biol.* **2022**, *18* (4), 356–358.
(187) Williams, N. A.; Polli, G. P. The Lyophilization of Pharmaceuticals: A Literature Review. *PDA J. Pharm. Sci. Technol.* **1984**, *38* (2), 48–60.
(188) Gaidhani, K. A.; Harwalkar, M.; Bhambere, D.; Nirgude, P. S. Lyophilization/Freeze Drying–a Review. *World J. Pharm. Res.* **2015**, *4* (8), 516–543.
(189) Kawasaki, H.; Shimanouchi, T.; Kimura, Y. Recent Development of Optimization of Lyophilization Process. *J. Chem.* **2019**, *2019*.
(190) Zhou, D.; Shang, S.; Tharp, T.; Jameel, F.; Sinha, K.; Nere, N. K. Leveraging Lyophilization Modeling for Reliable Development, Scale-up and Technology Transfer. *AAPS PharmSciTech* **2019**, *20* (7), 1–12.
(191) Tchessalov, S.; Latshaw II, D.; Nulu, S.; Bentley, M.; Tharp, T.; Ewan, S.; Chen, X. Application of First Principles Primary Drying Model to Lyophilization Process Design and Transfer: Case Studies from the Industry. *J. Pharm. Sci.* **2021**, *110* (2), 968–981.
(192) Sundaramurthi, P.; Suryanarayanan, R. Trehalose Crystallization during Freeze-Drying: Implications on Lyoprotection. *J. Phys. Chem. Lett.* **2010**, *1* (2), 510–514.
(193) Basholli-Salihu, M.; Mueller, M.; Salar-Behzadi, S.; Unger, F. M.; Viernstein, H. Effect of Lyoprotectants on β-Glucosidase Activity and Viability of Bifidobacterium Infantis after Freeze-Drying and Storage in Milk and Low PH Juices. *LWT-Food Sci. Technol.* **2014**, *57* (1), 276–282.
(194) Nugraheni, R. W.; Setyawan, D.; Yusuf, H. Physical Characteristics of Liposomal Formulation Dispersed in HPMC Matrix and Freeze-Dried Using Maltodextrin and Mannitol as Lyoprotectant. *Pharm. Sci.* **2017**, *23* (4), 285–292.
(195) Hinrichs, W. L. J.; Sanders, N. N.; De Smedt, S. C.; Demeester, J.; Frijlink, H. W. Inulin Is a Promising Cryo-and Lyoprotectant for PEGylated Lipoplexes. *J. Control. Release* **2005**,

103 (2), 465–479.
(196) Schill, R. O.; Mali, B.; Dandekar, T.; Schnölzer, M.; Reuter, D.; Frohme, M. Molecular Mechanisms of Tolerance in Tardigrades: New Perspectives for Preservation and Stabilization of Biological Material. *Biotechnol. Adv.* **2009**, *27* (4), 348–352.
(197) Piszkiewicz, S. Tardigrade Disordered Proteins as Potential Excipients for Biologics. The University of North Carolina at Chapel Hill 2019.
(198) Jepson, W. E.; Wutich, A.; Colllins, S. M.; Boateng, G. O.; Young, S. L. Progress in Household Water Insecurity Metrics: A Cross-disciplinary Approach. *Wiley Interdiscip. Rev. Water* **2017**, *4* (3), e1214.
(199) Wutich, A.; Budds, J.; Eichelberger, L.; Geere, J.; Harris, L. M.; Horney, J. A.; Jepson, W.; Norman, E.; O'Reilly, K.; Pearson, A. L. Advancing Methods for Research on Household Water Insecurity: Studying Entitlements and Capabilities, Socio-Cultural Dynamics, and Political Processes, Institutions and Governance. *Water Secur.* **2017**, *2*, 1–10.
(200) Nudler, E.; Mironov, A. S. The Riboswitch Control of Bacterial Metabolism. *Trends Biochem. Sci.* **2004**, *29* (1), 11–17.
(201) Wayment-Steele, H.; Wu, M.; Gotrik, M.; Das, R. Evaluating Riboswitch Optimality. *Methods Enzymol.* **2019**, *623*, 417–450.
(202) Dambach, M.; Sandoval, M.; Updegrove, T. B.; Anantharaman, V.; Aravind, L.; Waters, L. S.; Storz, G. The Ubiquitous YybP-YkoY Riboswitch Is a Manganese-Responsive Regulatory Element. *Mol. Cell* **2015**, *57* (6), 1099–1109.
(203) Price, I. R.; Gaballa, A.; Ding, F.; Helmann, J. D.; Ke, A. Mn2+-Sensing Mechanisms of YybP-YkoY Orphan Riboswitches. *Mol. Cell* **2015**, *57* (6), 1110–1123.
(204) Ramesh, A.; Winkler, W. C. Magnesium-Sensing Riboswitches in Bacteria. *RNA Biol.* **2010**, *7* (1), 77–83.
(205) Furukawa, K.; Ramesh, A.; Zhou, Z.; Weinberg, Z.; Vallery, T.; Winkler, W. C.; Breaker, R. R. Bacterial Riboswitches Cooperatively Bind Ni2+ or Co2+ Ions and Control Expression of Heavy Metal Transporters. *Mol. Cell* **2015**, *57* (6), 1088–1098.
(206) Bouchard, M. F.; Sauvé, S.; Barbeau, B.; Legrand, M.; Brodeur, M.-È.; Bouffard, T.; Limoges, E.; Bellinger, D. C.; Mergler, D. Intellectual Impairment in School-Age Children Exposed to Manganese from Drinking Water. *Environ. Health Perspect.* **2010**, *119* (1), 138–143.
(207) Oulhote, Y.; Mergler, D.; Barbeau, B.; Bellinger, D. C.; Bouffard, T.; Brodeur, M.-È.; Saint-Amour, D.; Legrand, M.; Sauvé, S.; Bouchard, M. F. Neurobehavioral Function in School-Age Children Exposed to Manganese in Drinking Water. *Environ. Health Perspect.* **2014**, *122* (12), 1343–1350.
(208) Wilson, R. C.; Smith, A. M.; Fuchs, R. T.; Kleckner, I. R.; Henkin, T. M.; Foster, M. P. Tuning Riboswitch Regulation through Conformational Selection. *J. Mol. Biol.* **2011**, *405* (4), 926–938.
(209) Drogalis, L. K.; Batey, R. T. Requirements for Efficient Cotranscriptional Regulatory Switching in Designed Variants of the Bacillus Subtilis PbuE Adenine-Responsive Riboswitch. *bioRxiv* **2018**. https://doi.org/10.1101/372573.
(210) Meyer, M. M.; Hammond, M. C.; Salinas, Y.; Roth, A.; Sudarsan, N.; Breaker, R. R. Challenges of Ligand Identification for Riboswitch Candidates. *RNA Biol.* **2011**, *8* (1), 5–10.
(211) Stoddard, C. D.; Widmann, J.; Trausch, J. J.; Marcano-Velázquez, J. G.; Knight, R.; Batey, R. T. Nucleotides Adjacent to the Ligand-Binding Pocket Are Linked to Activity Tuning in the Purine Riboswitch. *J. Mol. Biol.* **2013**, *425* (10), 1596–1611.
(212) Weigand, J. E.; Gottstein-Schmidtke, S. R.; Demolli, S.; Groher, F.; Duchardt-Ferner, E.; Wöhnert, J.; Suess, B. Sequence Elements Distal to the Ligand Binding Pocket Modulate the Efficiency of a Synthetic Riboswitch. *ChemBioChem* **2014**, *15* (11), 1627–1637.
(213) Lynch, S. A.; Gallivan, J. P. A Flow Cytometry-Based Screen for Synthetic Riboswitches.

Nucleic Acids Res. **2008**, *37* (1), 184–192.
(214) Ceres, P.; Trausch, J. J.; Batey, R. T. Engineering Modular 'ON'RNA Switches Using Biological Components. *Nucleic Acids Res.* **2013**, *41* (22), 10449–10461.
(215) Gilbert, S. D.; Reyes, F. E.; Edwards, A. L.; Batey, R. T. Adaptive Ligand Binding by the Purine Riboswitch in the Recognition of Guanine and Adenine Analogs. *Structure* **2009**, *17* (6), 857–868.
(216) Strobel, E. J.; Angela, M. Y.; Lucks, J. B. High-Throughput Determination of RNA Structures. *Nat. Rev. Genet.* **2018**, *19* (10), 615–634.
(217) Darty, K.; Denise, A.; Ponty, Y. VARNA: Interactive Drawing and Editing of the RNA Secondary Structure. *Bioinformatics* **2009**, *25* (15), 1974.
(218) COVID-19 Coronavirus Pandemic https://www.worldometers.info/coronavirus/.
(219) Lau, H.; Khosrawipour, T.; Kocbach, P.; Ichii, H.; Bania, J.; Khosrawipour, V. Evaluating the Massive Underreporting and Undertesting of COVID-19 Cases in Multiple Global Epicenters. *Pulmonology* **2021**, *27* (2), 110–115.
(220) Esbin, M. N.; Whitney, O. N.; Chong, S.; Maurer, A.; Darzacq, X.; Tjian, R. Overcoming the Bottleneck to Widespread Testing: A Rapid Review of Nucleic Acid Testing Approaches for COVID-19 Detection. *Rna* **2020**, *26* (7), 771–783.
(221) Peeling, R. W.; Olliaro, P. L.; Boeras, D. I.; Fongwen, N. Scaling up COVID-19 Rapid Antigen Tests: Promises and Challenges. *Lancet Infect. Dis.* **2021**, *21* (9), e290–e295.
(222) Vandenberg, O.; Martiny, D.; Rochas, O.; van Belkum, A.; Kozlakidis, Z. Considerations for Diagnostic COVID-19 Tests. *Nat. Rev. Microbiol.* **2021**, *19* (3), 171–183.
(223) Zhang, F.; Abudayyeh, O. O.; Gootenberg, J. S. A protocol for detection of COVID-19 using CRISPR diagnostics https://www.broadinstitute.org/files/publications/special/COVID-19 detection (updated).pdf.
(224) Broughton, J. P.; Deng, X.; Yu, G.; Fasching, C. L.; Servellita, V.; Singh, J.; Miao, X.; Streithorst, J. A.; Granados, A.; Sotomayor-Gonzalez, A.; et al. CRISPR–Cas12-Based Detection of SARS-CoV-2. *Nat. Biotechnol.* **2020**, *38* (7), 870–874. https://doi.org/10.1038/s41587-020-0513-4.
(225) Gabrielle, M. E.; Schukkink, R. A. F.; van Gemen, B. Nucleic Acid Sequence-Based Amplification (NASBA) for the Identification of Mycobacteria. *Microbiology* **1993**, *139* (10), 2423–2429.
(226) Green, A. A.; Silver, P. A.; Collins, J. J.; Yin, P. Toehold Switches: De-Novo-Designed Regulators of Gene Expression. *Cell* **2014**, *159* (4), 925–939. https://doi.org/https://doi.org/10.1016/j.cell.2014.10.002.
(227) Chappell, J.; Takahashi, M. K.; Lucks, J. B. Creating Small Transcription Activating RNAs. *Nat. Chem. Biol.* **2015**, *11* (3), 214–220.
(228) Jinek, M.; Chylinski, K.; Fonfara, I.; Hauer, M.; Doudna, J. A.; Charpentier, E. A Programmable Dual-RNA–Guided DNA Endonuclease in Adaptive Bacterial Immunity. *Science (80-.).* **2012**, *337* (6096), 816–821.
(229) Ackerman, C. M.; Myhrvold, C.; Thakku, S. G.; Freije, C. A.; Metsky, H. C.; Yang, D. K.; Simon, H. Y.; Boehm, C. K.; Kosoko-Thoroddsen, T.-S. F.; Kehe, J. Massively Multiplexed Nucleic Acid Detection with Cas13. *Nature* **2020**, 1–6.
(230) Fu, Y.; Foden, J. A.; Khayter, C.; Maeder, M. L.; Reyon, D.; Joung, J. K.; Sander, J. D. High-Frequency off-Target Mutagenesis Induced by CRISPR-Cas Nucleases in Human Cells. *Nat. Biotechnol.* **2013**, *31* (9), 822–826.
(231) Cho, S. W.; Kim, S.; Kim, Y.; Kweon, J.; Kim, H. S.; Bae, S.; Kim, J.-S. Analysis of Off-Target Effects of CRISPR/Cas-Derived RNA-Guided Endonucleases and Nickases. *Genome Res.* **2014**, *24* (1), 132–141.
(232) Anderson, K. R.; Haeussler, M.; Watanabe, C.; Janakiraman, V.; Lund, J.; Modrusan, Z.; Stinson, J.; Bei, Q.; Buechler, A.; Yu, C. CRISPR Off-Target Analysis in Genetically Engineered Rats and Mice. *Nat. Methods* **2018**, *15* (7), 512–514.

(233) Thyme, S. B.; Akhmetova, L.; Montague, T. G.; Valen, E.; Schier, A. F. Internal Guide RNA Interactions Interfere with Cas9-Mediated Cleavage. *Nat. Commun.* **2016**, *7* (1), 1–7.
(234) Dang, Y.; Jia, G.; Choi, J.; Ma, H.; Anaya, E.; Ye, C.; Shankar, P.; Wu, H. Optimizing SgRNA Structure to Improve CRISPR-Cas9 Knockout Efficiency. *Genome Biol.* **2015**, *16* (1), 1–10.
(235) Kocak, D. D.; Josephs, E. A.; Bhandarkar, V.; Adkar, S. S.; Kwon, J. B.; Gersbach, C. A. Increasing the Specificity of CRISPR Systems with Engineered RNA Secondary Structures. *Nat. Biotechnol.* **2019**, *37* (6), 657–666.
(236) Hendel, A.; Bak, R. O.; Clark, J. T.; Kennedy, A. B.; Ryan, D. E.; Roy, S.; Steinfeld, I.; Lunstad, B. D.; Kaiser, R. J.; Wilkens, A. B. Chemically Modified Guide RNAs Enhance CRISPR-Cas Genome Editing in Human Primary Cells. *Nat. Biotechnol.* **2015**, *33* (9), nbt-3290.
(237) Ryan, D. E.; Taussig, D.; Steinfeld, I.; Phadnis, S. M.; Lunstad, B. D.; Singh, M.; Vuong, X.; Okochi, K. D.; McCaffrey, R.; Olesiak, M. Improving CRISPR–Cas Specificity with Chemical Modifications in Single-Guide RNAs. *Nucleic Acids Res.* **2018**, *46* (2), 792–803.
(238) Yin, H.; Song, C.-Q.; Suresh, S.; Wu, Q.; Walsh, S.; Rhym, L. H.; Mintzer, E.; Bolukbasi, M. F.; Zhu, L. J.; Kauffman, K. Structure-Guided Chemical Modification of Guide RNA Enables Potent Non-Viral in Vivo Genome Editing. *Nat. Biotechnol.* **2017**, *35* (12), 1179–1187.
(239) Chen, J. S.; Ma, E.; Harrington, L. B.; Da Costa, M.; Tian, X.; Palefsky, J. M.; Doudna, J. A. CRISPR-Cas12a Target Binding Unleashes Indiscriminate Single-Stranded DNase Activity. *Science (80-.).* **2018**, *360* (6387), 436–439.
(240) Kim, H.; Lee, W.; Oh, Y.; Kang, S.-H.; Hur, J. K.; Lee, H.; Song, W.; Lim, K.-S.; Park, Y.-H.; Song, B.-S. Enhancement of Target Specificity of CRISPR–Cas12a by Using a Chimeric DNA–RNA Guide. *Nucleic Acids Res.* **2020**, *48* (15), 8601–8616.
(241) Liu, L.; Li, X.; Ma, J.; Li, Z.; You, L.; Wang, J.; Wang, M.; Zhang, X.; Wang, Y. The Molecular Architecture for RNA-Guided RNA Cleavage by Cas13a. *Cell* **2017**, *170* (4), 714–726.
(242) Vester, B.; Wengel, J. LNA (Locked Nucleic Acid): High-Affinity Targeting of Complementary RNA and DNA. *Biochemistry* **2004**, *43* (42), 13233–13241.
(243) Anzalone, A. V; Randolph, P. B.; Davis, J. R.; Sousa, A. A.; Koblan, L. W.; Levy, J. M.; Chen, P. J.; Wilson, C.; Newby, G. A.; Raguram, A. Search-and-Replace Genome Editing without Double-Strand Breaks or Donor DNA. *Nature* **2019**, *576* (7785), 149–157.

Appendix A - Strategies for Riboswitch Engineering and Evolution

A.1 Introduction

Over the course of this work, I have demonstrated the *crcB* fluoride riboswitch's potential as a diagnostic tool. However, this potential is currently not generalizable to riboswitches as a category of sensors. While many classes of riboswitch have been characterized since their relatively recent discovery, most of these riboswitches respond to cellular metabolites of low diagnostic interest[58]. Many natural riboswitches also have low dynamic ranges and high background expression – because they are often used in metabolic regulation[200], they do not possess the switch-like activity ideal for biosensing. Instead of switching from a tightly regulated OFF state to a strongly activated ON state, they instead switch between leaky repression and weak activation[201]. This intended purpose also means that few known riboswitches naturally respond to compounds other than those involved in metabolism, though riboswitches have been identified for fluoride[69], manganese[202,203], magnesium[204], nickel[205], and cobalt[205].

This state of affairs outlines a list of needs for riboswitch-based biosensing moving forward. Most pressingly, we need a strategy to detect non-native ligands using riboswitches. There is currently a single digit library of diagnostically relevant targets with characterized cognate riboswitches, which do not necessarily have the dynamic range and activation necessary for robust sensing. Moving forward, we require a set of strategies to both adapt existing switches for implementation in a biosensor and develop synthetic switches for emerging targets.

In this appendix, I outline my preliminary efforts to address these needs. I begin with work I conducted to improve dynamic range for a manganese-sensing riboswitch, exploring both rational and selection-based strategies. Afterwards, I discuss the field of synthetic riboswitch engineering in general, followed by a more focused look at a synthetic dopamine-sensing riboswitch. Finally, I outline a strategy to sort a library of transcriptional riboswitch variants in a cell-free reaction, offering an alternative to conventional FACS methods.

A.2 Preliminary rational engineering strategies for a manganese-sensing riboswitch

Of the available diagnostically relevant ligands, manganese presents the most compelling target – although it is an essential nutrient, manganese is neurotoxic when consumed at high levels over extended periods of time[206,207]. For this reason, I chose to use a manganese-sensing riboswitch to develop a manganese biosensor. There are two well-characterized manganese-sensing switches: the translational *mntP* switch from *E. coli*[202], and the transcriptional *yoaB* switch from *L. lactis*[203]. For its origin in *E. coli,* I first attempted to apply my previous strategies with the fluoride sensor to the *mntP* switch, using it to regulate the expression of sfGFP under Anderson promoter J23119. Unlike the *crcB* fluoride riboswitch, however, *mntP* showed limited switching in cell-free extract. Thus, to use this switch in an engineered biosensor, we require a means to improve its dynamic range while maintaining strong activation.

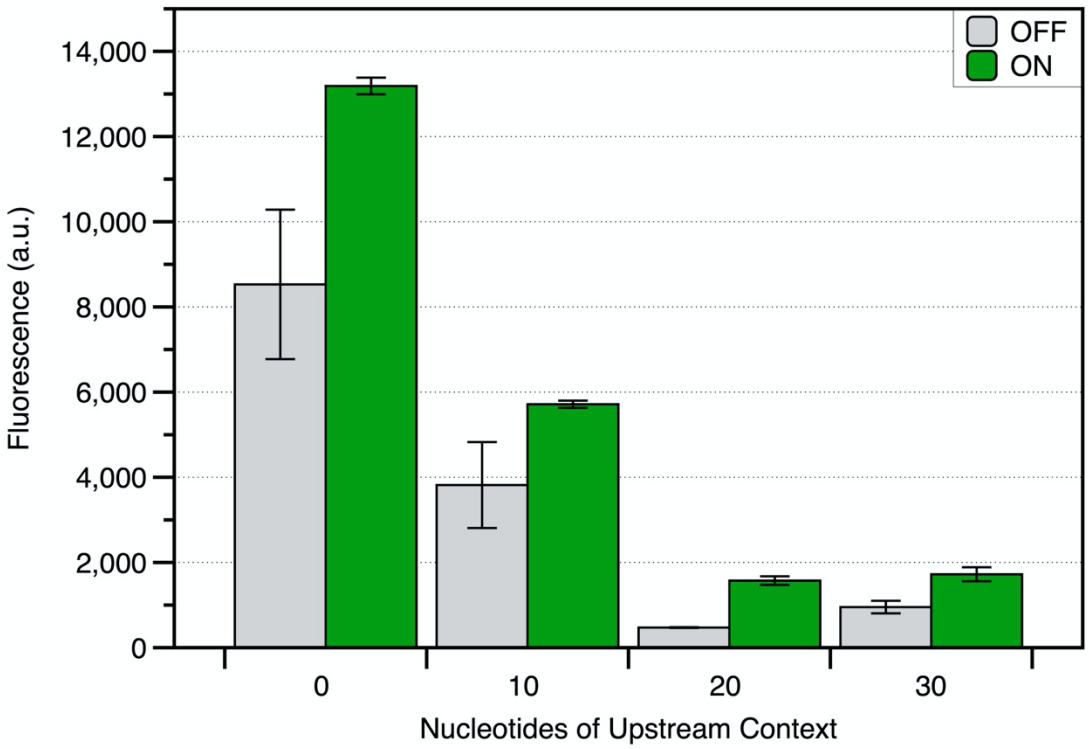

Figure A-1. Activation for wild type *mntP* manganese riboswitch and variants with added nucleotides of upstream context.
ON condition uses 1 mM $MnCl_2$, OFF condition uses purified water. Error bars are standard deviation from three technical replicates.

Previous work analyzing the effect of upstream nucleotide context on an S-adenosyl methionine (SAM) binding riboswitch suggests that regions not directly involved with ligand binding or gene expression may still affect riboswitch activity by stabilizing intermediary structures[208]. For example, with the SAM riboswitch, the formation of a helix upstream of the riboswitch sequence stabilizes the ligand unbound ON structure, increasing signal and dynamic range. To see if a similar interaction could improve function for the *mntP* riboswitch, I tested the wild type switch alongside variants with 10, 20, or 30 nucleotides of the switch's native context appended to the 5' end (**Figure A-1**). When testing activation, I noticed that the 10 and 30 nucleotide variants significantly decreased signal strength without affecting dynamic range. A similar decrease in signal strength was also observed in the 20-nucleotide variant, but interestingly, dynamic range increased from approximately 1.5 to 3 (**Figure A-1**).

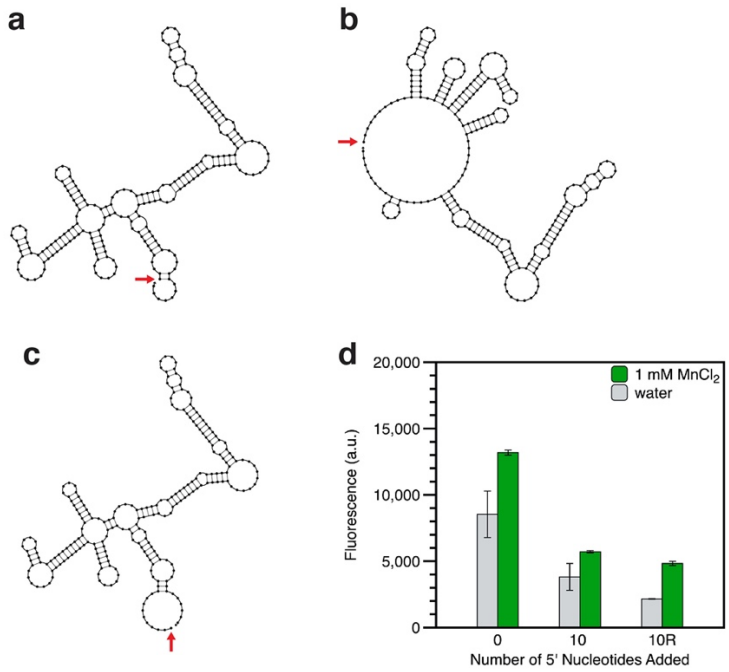

Figure A-2. Added upstream context to wild type mntP and resulting change in gene expression. **(a)** No added nucleotides of upstream context. **(b)** 20 base pairs of the *mntP* riboswitch's native context added upstream. **(c)** 10 base pairs computationally predicted to be unstructured added upstream. 5' end of each transcript is marked with a red arrow. Structures designed and generated using NUPACK[72]. **(d)** Gene expression in the presence and absence of manganese with 0, 10 native, or 10 arbitrary nucleotides predicted to be unstructured.

Analyzing the structure of this 20-nucleotide variant, I noticed that it was distinct from the wild type and other variants in that the 5' end of the transcript was predicted to be completely unstructured. From this, I hypothesized that unstructured 5' sequence preferentially suppresses a sensor's OFF state, possibly by increasing transcript susceptibility to nucleases. To further interrogate this phenomenon, I next designed a 10 nucleotide 5' sequence predicted to be completely unstructured using NUPACK[72] (**Figure A-2c**). As predicted, this sequence also increased dynamic range (**Figure A-2d**), reinforcing our hypothesis. Thus, while this change alone does not provide sufficient functional improvement to use the *mntP* switch in a biosensor, it provides a simple strategy to affect riboswitch dynamic range and suggests that even relatively simple engineering strategies can have a significant effect on riboswitch function.

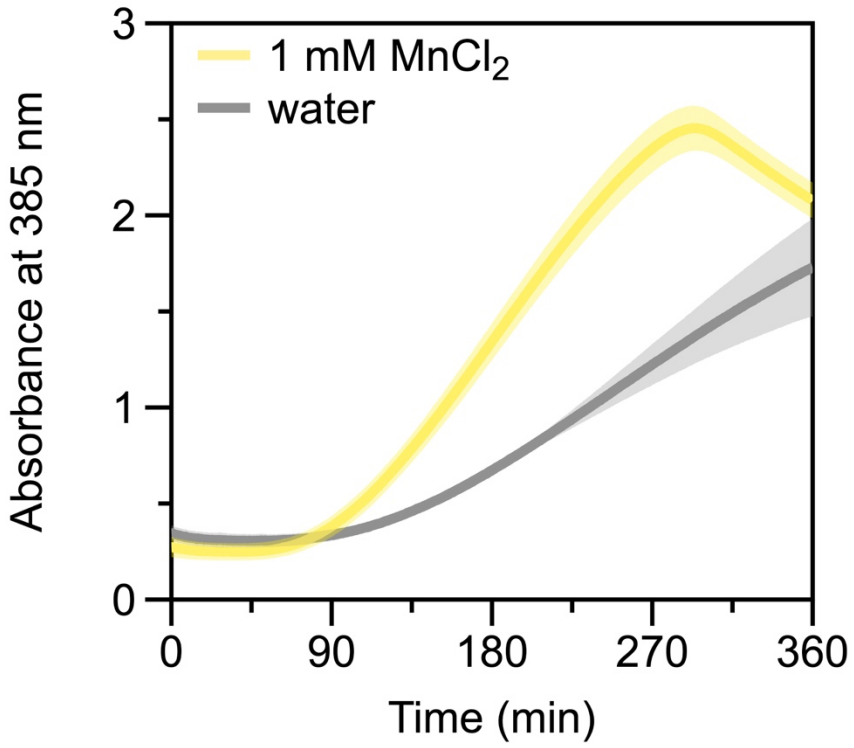

Figure A-3. Kinetic traces for mntP riboswitch with 20 nucleotides of upstream context regulating production of catechol dioxygenase.
Error shading is standard deviation from three technical replicates.

Having made a small improvement to the switch's dynamic range, I next attempted to use the simple reporter and template concentration optimizations applied with the fluoride riboswitch.

I hypothesized that I could reduce template concentration to eliminate leak, then exchange sfGFP for catechol dioxygenase as the reporter to take advantage of the latter's implicit amplification step via substrate turnover. Unfortunately, these strategies did not bring sufficient improvement to use the *mntP* switch for cell-free sensing. While I did observe differences in activation time between the induced and uninduced conditions, the difference was small, and activation was slow even at high inducer concentrations. Ultimately, this inadequate performance suggests that riboswitches must reach a certain minimum threshold before these optimizations are useful.

A.3 Ribosome binding site mutant library design for a manganese-sensing riboswitch

In the absence of a natural upstream sequence improving function for the *mntP* switch, I next tried to engineer the switch itself for improved function. Previous work by the Batey group indicates that riboswitch engineering can be approached semi-rationally by selecting regions important for riboswitch function and randomizing them, screening for desired mutants[209]. This is a particularly prudent approach given that riboswitches bind their ligands cotranscriptionally; while it is possible to computationally predict the minimum free energy structure for a riboswitch[72], computationally predicting how RNA will bind a ligand as it is being transcribed is currently beyond our grasp.

We began applying this strategy by mutating the RBS in the translational *mntP* switch. In its OFF state, the *RBS* is occluded by folding upon itself into a hairpin; manganese binding prevents the formation of this hairpin, freeing the RBS and enabling translation[202]. Because the RBS sequence does not have any long-range interactions within the riboswitch, it is a promising target for mutagenesis due to the relatively low probability that mutations to the RBS will completely disrupt the switching progress. Furthermore, the RBS sequence deviates from the consensus *E. coli* sequence, presenting the possibility that a stronger RBS sequence that is still capable of folding into a hairpin could ameliorate the observed problems with low expression.

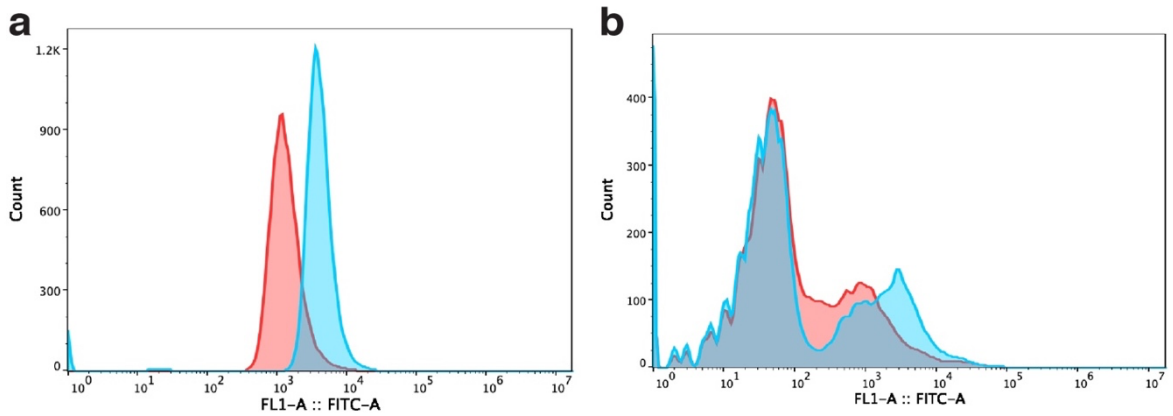

Figure A-4. Characterization of wild type mntP riboswitch and mutant RBS library.
(a) Wild type and **(b)** mutant populations were characterized in the presence (blue) and absence (red) of 4 mM $MnCl_2$.

I created a library by randomizing a 7-nucleotide region upstream of the start codon in the wild-type *mntP* switch. The library was assembled via inverse PCR using randomized primers, transformed into TG1 *E. coli* and characterized via flow cytometry. As expected, a significant portion of the mutant population was broken OFF both in the presence and absence of manganese. However, a distinct population of the mutants were shown to shift after induction (**Figure A-4b**), with some mutants in this pool even outperforming the wild type switch. The presence of these functional mutants supports the validity of saturation mutagenesis as a possible riboswitch evolution strategy.

A.4 Aptamer mutant library design for a manganese sensing riboswitch

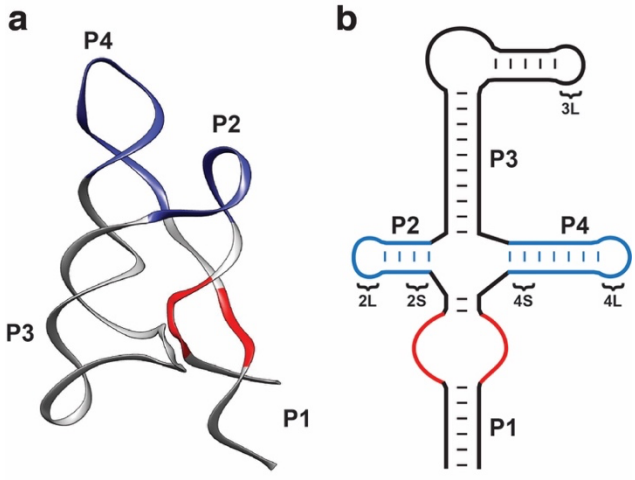

Figure A-5. The yybP-ykoY manganese binding aptamer.
P2 and P4 helices are marked in blue and ligand binding pocket is marked in red for **(a)** crystal structure (PDB: 4Y1I) and **(b)** schematic representation. Regions denoted with S and L marked on the P2, P3, and P4 helices denote mutation targets on the helix stem and loop, respectively.

In searching for additional mutation targets to tune the riboswitch's function, I also looked to its aptamer region. The yybP-ykoY manganese-binding aptamer is largely conserved between all manganese-sensing riboswitches, with a highly conserved ligand-binding pocket and four less conserved helices[210]. The relative lack of conservation of these helices[210], combined with crystallography data indicating that these regions are not directly involved in the ligand binding process[203], suggest that they would be suitable targets for mutant library design. Previous work in tuning riboswitch function supports this hypothesis – mutational studies on SAM[211] and synthetic neomycin[212] riboswitches show that mutating regions distal to the binding pocket can tune riboswitch switching.

This analysis would begin by determining the role of the yybP-ykoY aptamer's P2 and P4 helices in ligand binding and resulting riboswitch activation – conservation analysis shows that the helices are structurally conserved but have significant sequence variation between species[210]. Confirming that the sequences are necessary for riboswitch function despite this lack of sequence conservation would then suggest that variation in their sequences can be used to tune riboswitch

function. This could be done by generating four separate aptamer libraries in total – one each for both the stem and the loop of both helices (2S, 2L, 4S, and 4L in **Figure A-5**).

A.5 FACS strategies to parse a riboswitch mutant library

Moving forward, these libraries could be sorted using fluorescence-activated cell sorting (FACS), which has been previously used to generate synthetic theophylline-sensing riboswitches[213]. This would involve sorting the library both in the presence and absence of manganese. In the presence of manganese, gates would be designed to isolate the mutants with the highest fluorescent signal. In the absence of manganese, gates would instead be designed to isolate mutants with levels of leak similar to those seen for the wild type switch. These pools would then be sequenced and analyzed to identify sequences that are present in the induced pool but absent in the uninduced pool; the sequences isolated from this analysis should consist of bistable mutants and strongly activating mutants that are simply not represented in the other pool due to undersampling, though the latter should not be disproportionally present given the sampling size 50,000 cells per run – approximately three times the theoretical maximum library size.

In the event of problems with undersampling, the library size could be further reduced by beginning the Shine-Dalgarno sequence with the consensus “AGGAGG” sequence and randomizing the following 5-nucleotide sequence upstream of the start codon, decreasing library size by a factor of 16 at the cost of biasing the library towards strongly activating mutants that are broken ON. Additionally, NUPACK[72] could be used to analyze sequences shown to permit gene expression in the presence of manganese; screening for regions that are predicted to fold in order to occlude the RBS in a hairpin in the absence of manganese would allow for the exclusion of sequences likely to be broken ON.

As an alternative to these troubleshooting methods, the library size could also be increased by mutating the entirety of the RBS then running a two-step process consisting of a positive and negative selection. First, the library would be run in the presence of manganese,

sorting for the most highly activating mutants. These mutants would then be sorted again in the absence of manganese to remove sequences that are broken ON. Previous riboswitch sorting via FACS[213] suggests that the undersampling of a larger library does not necessarily preclude the harvesting of functional sequences, but this method does run the risk of selecting only for strong activation, rather than bistable sequences. As a result, it may exclude promising bistable sequences that do not perform as well as switches that are broken ON. Promising candidates from these sorting strategies would then have their function validated in cell-free extract.

A.6 Developing a cell-free riboswitch evolution strategy

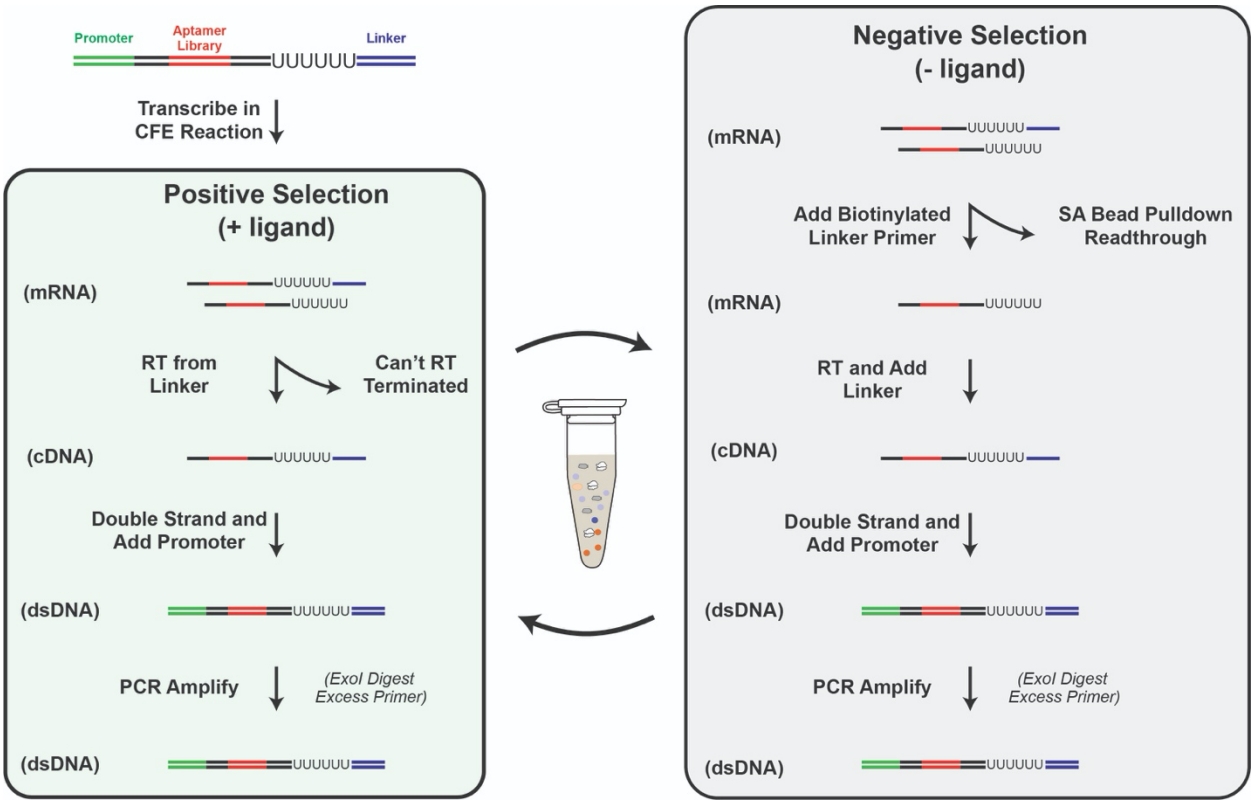

Figure A-6. Scheme for cell-free selection of riboswitch variants.

As an alternative to selecting riboswitch variants *in vivo* and porting promising variants into a cell-free system, I also propose the direct selection of riboswitch variants from a cell-free reaction (**Figure A-6**). This strategy would allow for the selection of riboswitches in their intended

context, which could mitigate biases specific to the selection context used. Furthermore, because riboswitches can display substantially different dynamic ranges *in vitro*, *in vivo*, and in a cell-free reaction[23,70], this is particularly important for generating switches that function as predicted after the selection process.

This strategy is built around iterations of positive and negative selections for a library of transcriptional riboswitch mutants based on the presence or absence of a linker downstream of the switch's poly-U tract. For a positive selection to identify variants that permit gene expression in the presence of the inducing ligand, successful sequences can be identified by the presence of the linker. By reverse transcribing off the linker sequence and reintroducing the promoter sequence with a double stranding primer, we can then generate a library of all variants that permitted readthrough past the riboswitch sequence. This library can then be amplified by PCR for subsequent rounds of selection.

For a negative selection, we are instead running the reaction in the absence of the inducing ligand and selecting for the absence of the linker sequence. In this case, we must remove the full-length sequences from the reaction before reverse transcribing the remaining sequences. I propose their removal using a biotinylated primer binding to the downstream linker sequence, along with streptavidin beads. This would allow for the specific removal of riboswitch variants containing the linker sequence, while leaving the terminated sequences lacking the linker in the reaction. By reverse transcribing from the sequences with a primer containing the linker sequence and double stranding with a primer containing the promoter sequence, we can once again create a library ready for amplification by PCR. Iterating with successive rounds of positive and negative selections should therefore yield a library of bistable mutants capable of inducing gene expression in the presence of the target ligand. This library can then be analyzed by next generation sequencing.

Figure A-7. Construct architecture for riboswitch selection scheme.

Because this strategy does not necessarily require cell growth or next generation sequencing between individual selection rounds, it has the advantage of being fast and inexpensive, allowing multiple rounds of selection to be carried out in a single day. Unfortunately, this comes with the disadvantage of sequence constraints in the template (**Figure A-7**); the need to bind to a known sequence to regenerate the promoter and linker sequences limits the mutable region of the riboswitch to a small tract in the middle of the sequence. While this may be acceptable for certain libraries, particularly aptamer libraries that would already be in that area, this limitation does reveal the need for an alternative method to select variants from more diverse sequence libraries.

This could be accomplished by performing next generation sequencing after each selection round. As opposed to analyzing sequences at the end of the selection process, this strategy would allow for the identification of terminated or antiterminated sequences based on read length. Because this would not require the presence of specific sequence features to enable subsequent rounds of selection, this carries the benefit of expanding the library of selectable sequences at increased financial and labor cost. Riboswitch variants could then be carried over to the next round of selection based on their representation after sequencing. Collectively, this broad direction of strategies or variants thereof would enable the selection of riboswitch variants with improved dynamic range in a cell-free reaction, driving forward the engineering of biosensors actuated by RNA.

A.7 An overview of synthetic riboswitch engineering

Moving beyond this work with existing natural switches, unlocking the full potential of riboswitch engineering will require strategies to build synthetic switches to detect non-native

ligands. In the literature, the phrase “synthetic riboswitch” carries a broad range of meanings. Most frequently, it is used to refer to riboswitch mutants in general, *e.g.*, changing a single nucleotide in a riboswitch’s aptamer creates a synthetic riboswitch, because the resulting construct does not occur in nature. To disambiguate: in this subsection, I am referring specifically to the wholesale removal of a riboswitch’s aptamer for replacement with a different aptamer to create an entirely new switch with a different cognate target. While we have not yet reached the “plug and play” ideal for this process, the last few years of work have taken very promising first steps towards detecting arbitrary ligands with synthetic riboswitches.

The first step in generating a synthetic riboswitch is finding a bistable expression platform capable of rearranging itself in response to ligand binding. This overarching goal has already been partially realized – work by the Batey group has yielded a “decoupled” *pbuE* riboswitch, wherein the expression platform has been modified to accept foreign aptamers[214]. It is currently hypothesized that this decoupling works because the aptamer binding to its ligand affects a kinetic mechanism contributing to terminator nucleation[209]. The terminating structure is thermodynamically favored and will eventually be formed regardless of ligand binding; however, binding of a ligand to the aptamer delays the nucleation of the terminating hairpin for long enough to prevent its formation until after RNA polymerase proceeds past it[209]. Because of this, ligand binding enables the expression of downstream genes. The creation of this system is a substantial step forward for synthetic riboswitch engineering; the existence of a modular expression platform means that only the aptamer sequences need to be selected for when engineering a new switch.

Generating a synthetic riboswitch also requires the generation of an aptamer capable of binding to the ligand of interest. While previous studies have shown that the ligand specificity of a riboswitch’s aptamer can be changed by mutagenesis of the binding pocket[215], this is limited to changing specificity to other related compounds. For example, a purine binding riboswitch can be mutated to bind to other purine analogues that it does not natively act on. Detecting targets lacking

a natural riboswitch sensing a similar compound, however, will require the generation of novel aptamers to be fused to a modular expression platform.

While not necessarily a solved problem, the field of aptamer generation is fairly well tread; systematic evolution of ligands by exponential enrichment (SELEX) has been used for almost three decades to generate novel aptamers[60]. A breadth of different SELEX variants for different target applications have been developed in the past decades, but they all follow the same general selection strategy. Briefly, a randomly generated oligo pool is washed over the target of interest, with unbound oligos being removed from the pool. The binding sequences are then eluted and amplified, and the progress is repeated. Iteration upon this process yields tightly binding aptamers against ligands of interest.

This type of aptamer selection strategy has immense potential for synthetic riboswitch engineering; the pairing of a SELEX-derived aptamer with a modular expression platform could enable rapid construction of riboswitches against targets of interest. Unfortunately, there are still several outstanding challenges prohibiting the “plug and play” assembly of riboswitches from individual components. The fusion of a SELEX-derived aptamer to an expression platform creates a suboptimal interaction between the two, frequently resulting in switches that are broken either ON or OFF. This is partially due to intrinsic features of SELEX as a selection method – by repeatedly selecting for tightly binding sequences, the final candidate pool consists only of sequences that bind to their targets with low K_D, which not necessarily facilitate function in a riboswitch. Recent work has yielded a method called RNA Capture-SELEX which enriches for binding sequences that are also capable of conformational rearrangement based on the presence or absence of their target ligand[61]. Additionally, the use of preexisting riboswitch aptamer sequences as scaffolds for selection and evolution has shown promise for isolating sequences that are compatible with riboswitch fusion[63].

Even with these advances, there is still substantial work to be done in optimizing the interaction between a selected aptamer and a decoupled expression platform. Although regions

of the aptamer and expression platform can be individually mutated, it is often difficult to infer how these mutations will affect the interaction between the two. Furthermore, it is difficult to design these interactions; RNA folding pathways are often complex and difficult to characterize[216], and as a result, it is time and labor intensive to get the information needed for rational engineering efforts. Because of this, reaching the full potential of chimeric riboswitches will require novel methods to tune aptamer-expression platform interactions.

A.8 Detecting dopamine with a synthetic riboswitch

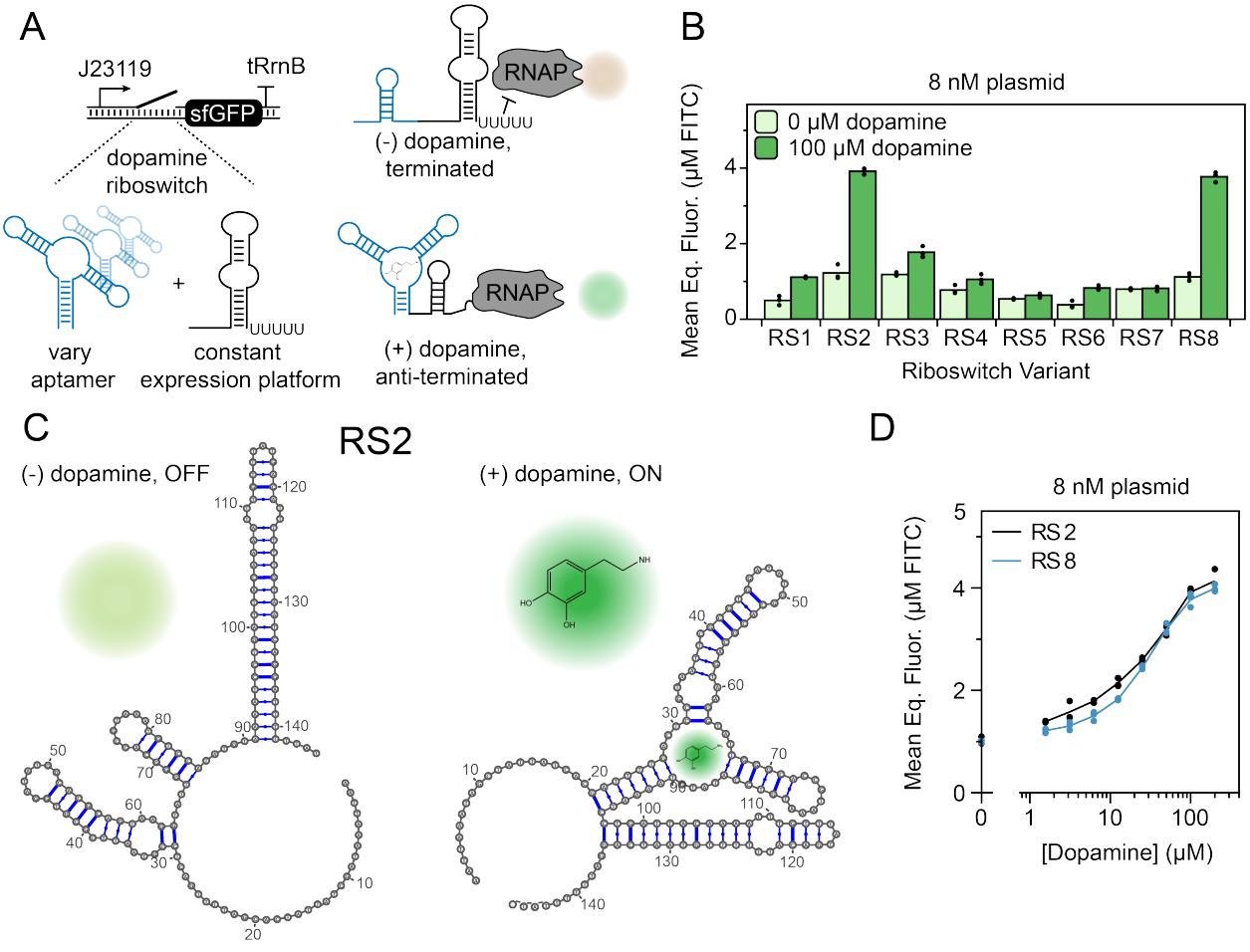

Figure A-8. Dopamine riboswitch structure and characterization.
(a) Design and construction of dopamine riboswitches and deployment in a cell-free gene expression (CFE) platform. **(b)** ON/OFF for a panel of riboswitch variants. 8 nM of purified plasmid DNA corresponding to each designed riboswitch variant was added to a CFE reaction at a final concentration of 0 μM (OFF) or 100 μM (ON) dopamine. Reported endpoint values are the mean (bars) of three technical replicates (displayed as individual data points) after 4 hours at 30 °C, background-subtracted by a no-DNA blank. **(c)**

Schematic representation of RS2 riboswitch folds modeled from the full-length RNA sequence using Mfold and folding constraints. Without dopamine, the expression platform is predicted to fold into an intrinsic terminator. Dopamine binding to the aptamer is predicted to prevent the formation of the terminator, thus enabling expression of the downstream gene. Secondary structures were rendered using VARNA[217]. **(d)** Dopamine dose-response for riboswitch variants RS2 and RS8. Reported endpoint values are the mean of three technical replicates (displayed as individual data points) after 4 hours at 30 °C, background-subtracted by a no-DNA blank, with 8 nM of the indicated plasmid supplied along with dopamine at the range of indicated concentrations. Figure and caption adapted from "Engineering a Synthetic Dopamine-Responsive Riboswitch for *In Vitro* Biosensing," submitted to ACS Synthetic Biology in 2022. I am sixth author on this work.

Previous efforts have yielded the DGR-II dopamine aptamer, derived from a scaffold based on the native *pbuE* aptamer sequence[63]. We first sought to verify that the decoupled *pbuE* expression platform would function with a foreign aptamer by testing a DGR-II/*pbuE* fusions developed by our collaborators in the Chavez group at the Air Force Research Laboratory, which is intended to function as a dopamine-sensing riboswitch. The switch is a transcriptional ON switch, activating gene expression in the presence of dopamine. Cross-validating their previous work, we first tested these switches in cell-free extract, cloning them into an expression cassette consisting of the switch expressed under Anderson promoter J23119 and regulating the expression of sfGFP (**Figure A-6a)**. While we did notice appreciable leaky activation for many of the variants, variants RS2 and RS8 robustly activated in the presence of dopamine (**Figure A-6b**). These switches were also shown to be partially specific to dopamine, responding the structurally similar norepinephrine but not the structurally dissimilar serotonin.

While this is a promising step forward for the field, there remain unaddressed issues that would substantially inform our knowledge of riboswitch engineering. First, it is unclear why some aptamer variants can form functional switches after fusion with an expression platform, while others do not. The ability to computationally identify bistable switches would significantly expedite the development cycle, limiting experimental testing to confirmation, rather than screening. Furthermore, the selection for these aptamers was done in the nucleotide context of decoupled *pbuE* expression platform, which would likely limit their use in other future decoupled expression platforms. Moving forward, resolving these concerns and developing a clear set of design

principles would bring us closer to rapid design of switches against arbitrary targets, massively enhancing the potential of riboswitches as a biosensing tool.

A.9 Conclusions

Given the breadth of these threads from my PhD, it would perhaps be the most helpful if I discussed, with the benefit of hindsight, which of these avenues I believe would be the most productive for future research. Personally, I would enjoy seeing the cell-free selection scheme pursued further. In my hands, it had a brief but promising life before being crushed by the early stages of the pandemic, but I believe that it had a strong foundation to build upon for the creation of a robust selection strategy. Moving forward with it, however, I would recommend simply running next generation sequencing after every selection round and transcribing barcoded sequences; the original strategy may have, in retrospect, weighted cleverness over efficacy. Additionally, I would recommend the optimization of the RNA extraction step to find the extraction time for maximum recovery of transcribed RNAs. Furthermore, I would disregard the methods described earlier in this appendix regarding the *in vivo* selection of a riboswitch library. The increased accessibility of next generation sequencing to read barcoded sequences has somewhat obviated the benefits of FACS for this particular type of selection scheme.

Building on that selection, it would be a very interesting, if challenging, undertaking to use it to identify the rules governing the creation of synthetic riboswitches. While some initial attempts have been made[89,172], we are still far from being able to simply *de novo* design regulatory ligand binding RNAs. The ability to sort a massive library of synthetic transcriptional riboswitch variants *in vitro*, gather data on their termination and antitermination via next generation sequencing, then use machine learning identify rules for designing functional variants could be the trick to cracking this decades-long problem. Still, I acknowledge this is easier said than done. That said, if you, the reader, do end up using this strategy to revolutionize the field, I would like a place at the front of your Cell/Nature/Science paper's acknowledgements section.

Appendix B - Cas13a gRNA Engineering to Detect Difficult Targets

B.1 Introduction

The global impact of the COVID-19 pandemic needs little description[218], and has exposed substantial shortcomings in our civil infrastructure. One of the most important needs revealed in this last two years is the need for widely available, scalable diagnostic testing to inform public health measures. Throughout the pandemic, case numbers have been consistently underreported[219], leading to estimates extrapolated from test positivity rate, excess mortality, or post-surge seroprevalence testing. Unfortunately, this information cannot be used preventatively, and only guides retrospective analysis or triage of an already severe situation.

Accurate case counts and robust preventative screening require robust, widely available testing resources, which cannot be adequately supplied with existing technologies. The current gold standard for viral testing is an RT-qPCR test, which reverse transcribes then amplifies trace viral RNA from a patient sample to diagnose infection. Because of the work needed for sample preparation and reliance on expensive equipment, this technique is difficult to scale and susceptible to bottlenecking during case surges[220]. More recently, this testing strategy has been supplemented by widespread use of rapid antigen tests, which use a lateral flow assay to detect viral proteins from a patient sample. While these tests can be run in minutes, rather than hours, and used onsite, their low sensitivity leads to frequent false negatives and failure to diagnose asymptomatic patients[221,222]. The ideal diagnostic technology would combine the strengths of these two tools, offering rapid, accurate results on demand for the untrained user.

The last eight years have seen substantial synthetic biology efforts to develop such a technology. From Ebola to Zika, Dengue to COVID-19, research has strived meet public health challenges with new technologies to ease testing and safeguard public health. In this appendix, I outline some of those efforts before focusing on CRISPR-Cas strategies and my own research on addressing one of the limitations of Cas13a-based sensors.

B.2. Synthetic biology tools for viral diagnostics

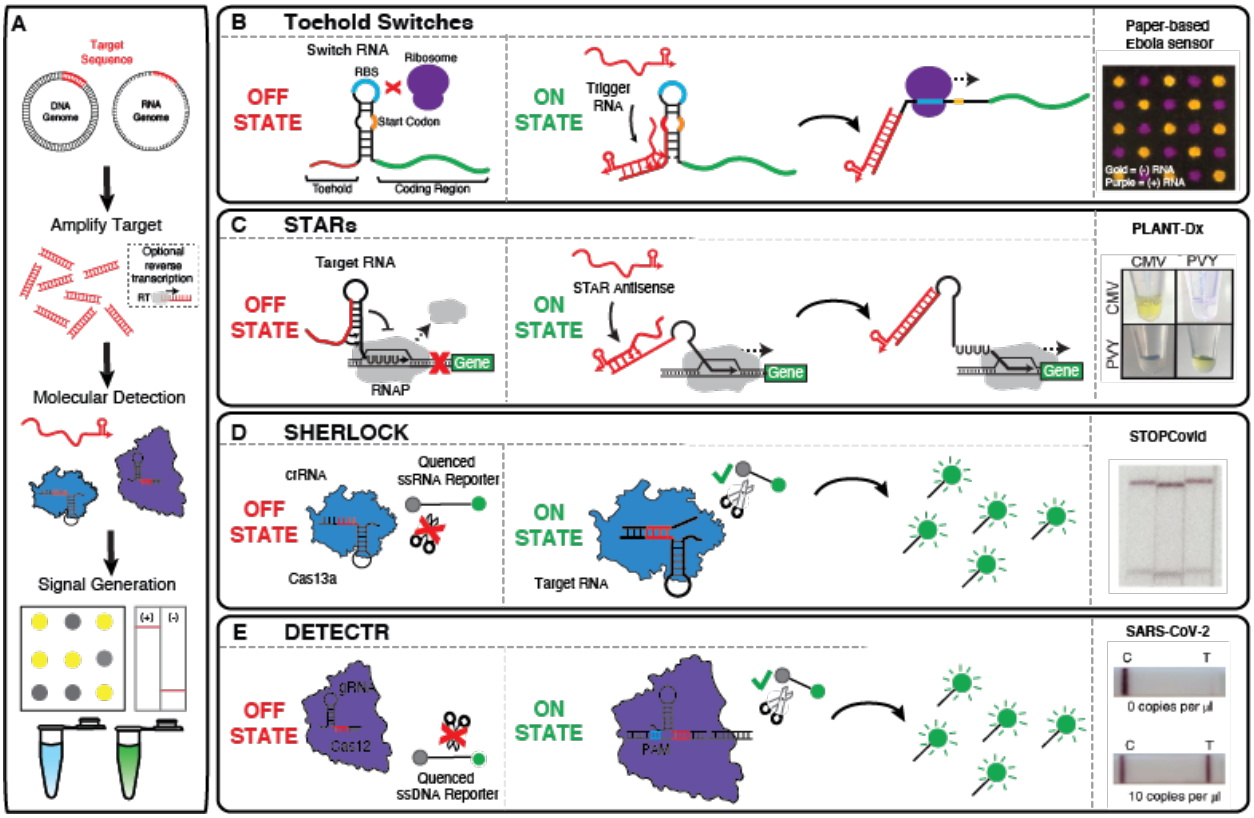

Figure B-1. Summary of RNA-based pathogen biosensors.
(a) General overview of RNA-based molecular diagnostics for pathogens. **(b)** Toehold switches control translation to modulate signal generation. They have been integrated into a paper-based sensor for Ebola detection. Image from Pardee *et. al.*[39] with permission. **(c)** STARs leverage transcriptional regulation to detect pathogenic nucleic acids. They have been used in a colorimetric assay to detect plant viruses. Image from Verosloff *et. al.*[41] with permission. **(d)** SHERLOCK and **(e)** DETECTR leverage collateral cleavage activity of Cas proteins to detect viral RNA. Images from Zhang *et. al.*[223] and Broughton *et. al.*[224] respectively, with permissions. SHERLOCK and DETECTR have been used to detect SARS-CoV-2.

Engineered RNA systems offer a flexible starting point for designing diagnostic systems that identify specific pathogen genomic signatures by detecting specific sequences in the pathogenic genome (**Figure B-1a**). These systems all utilize the same broad strategy of designing an RNA to bind to a target pathogen DNA or RNA sequence, accomplished by simply changing the engineered RNAs sequence. Diagnostic detection methods can then be made by building off this binding interaction to generate a detectable signal, typically in the form of fluorescence or a color change. If needed, pathogen target sequences can be amplified before detection to enhance the analytical sensitivity of the diagnostic scheme[225].

Some engineered RNAs can detect specific sequences by directly leveraging the programmability of RNA primary sequence and secondary structure. In both the toehold switch[226] and small transcription activating RNA (STAR)[227] mechanisms, specific RNA-RNA interactions drive a change in RNA structure leading to the activation and detectable expression of a reporter gene. Toehold switches consist of a hairpin structure that has been designed to sequester a ribosome binding site and start codon that govern the translation of a downstream reporter gene. Additionally, this hairpin also includes a 'toehold' sequence that is complementary to the desired diagnostic target. When the target nucleic acid sequence is present in a cell-free gene expression reaction, its binding to the toehold switch initiates an RNA structure rearrangement that unfurls the hairpin, exposing the ribosome binding site to initiate translation of the downstream reporter gene (**Figure B-1b**). The STAR mechanism is designed to work in a similar fashion, however with target binding preventing formation of a terminating hairpin which enables transcription of the downstream reporter gene (**Figure B-1c**).

Both toehold switches and STARs have been recently implemented in viral diagnostics. The first application for toehold switches came near the beginning of the recent West African Ebola epidemic, where lyophilized cell-free reactions containing Ebola-specific toehold switches were demonstrated to detect nanomolar concentrations of viral RNA via coupling to an isothermal amplification step[39]. The subsequent South America Zika virus epidemic saw the expansion of this work, streamlining the sensor development and testing pipeline to generate engineered toehold switches that functioned as viral sensors within a week of identifying a target sequence[40]. Importantly, these sensors could detect viral RNA in infected plasma samples and distinguish between Zika and the clinically and genetically similar Dengue virus. Beyond these epidemic virus applications, toeholds have also been used for the strain-specific screening of gut flora from stool samples[34], while STARs have be applied to the detection of plant viruses[41].

Beyond these synthetic RNA structures, existing RNA-based detection mechanisms have also been repurposed for pathogen diagnostics. In particular, the discovery of CRISPR-Cas

systems has enabled the detection of viral sequences by leveraging the Cas proteins' sequence-dependent nuclease activity. In nature, CRISPR-Cas systems serve as a bacterial immune system, cleaving recognized viral sequences to prevent reinfection. They function via a Cas (**C**RISPR **as**sociated) protein bound to a guide RNA (gRNA) that can hybridize to a target nucleic acid sequence for recognition. In this RNA-protein complex, the Cas protein facilitates the hybridization of the gRNA to its intended target through canonical base pairing interactions, enabling specificity down to single nucleotide resolution[228]. The flexibility of these systems makes them high-value targets for engineering; there is a range of natural CRISPR-Cas systems available that are broadly divided into six types based on their structure, editing mechanism, and nucleic acid target.

One Cas protein used for pathogen sensing is the type VI Cas protein Cas13a, which detects RNA and acts as an indiscriminate ribonuclease after detection. This indiscriminate ribonuclease activity can form the basis for a diagnostic reaction using an RNA-linked fluorophore-quencher pair – if the Cas13a-gRNA complex recognizes its target, it can then cleave the fluorophore-quencher pair and generate a detectable signal (**Figure B-1d**). When combined with strategies to amplify the pathogen genome targets, this technique allows sensitive detection of a range of pathogens. This was first demonstrated with SHERLOCK (**S**pecific **H**igh sensitivity **E**nzymatic **R**eporter Un**LOCK**ing)[38], which was reported to detect attomolar levels of genetic material. Complemented with a sample processing protocol to eliminate nucleases from body fluids[43], this method can be used to detect viral RNA directly from body fluids at titers as low as 1 copy per microliter. This system can also be massively multiplexed through the use of carefully designed gRNA sequences and automated liquid handling methods, with simultaneous detection demonstrated for a panel of 169 unique pathogen targets[229].

B.3 Engineered guides for Cas9

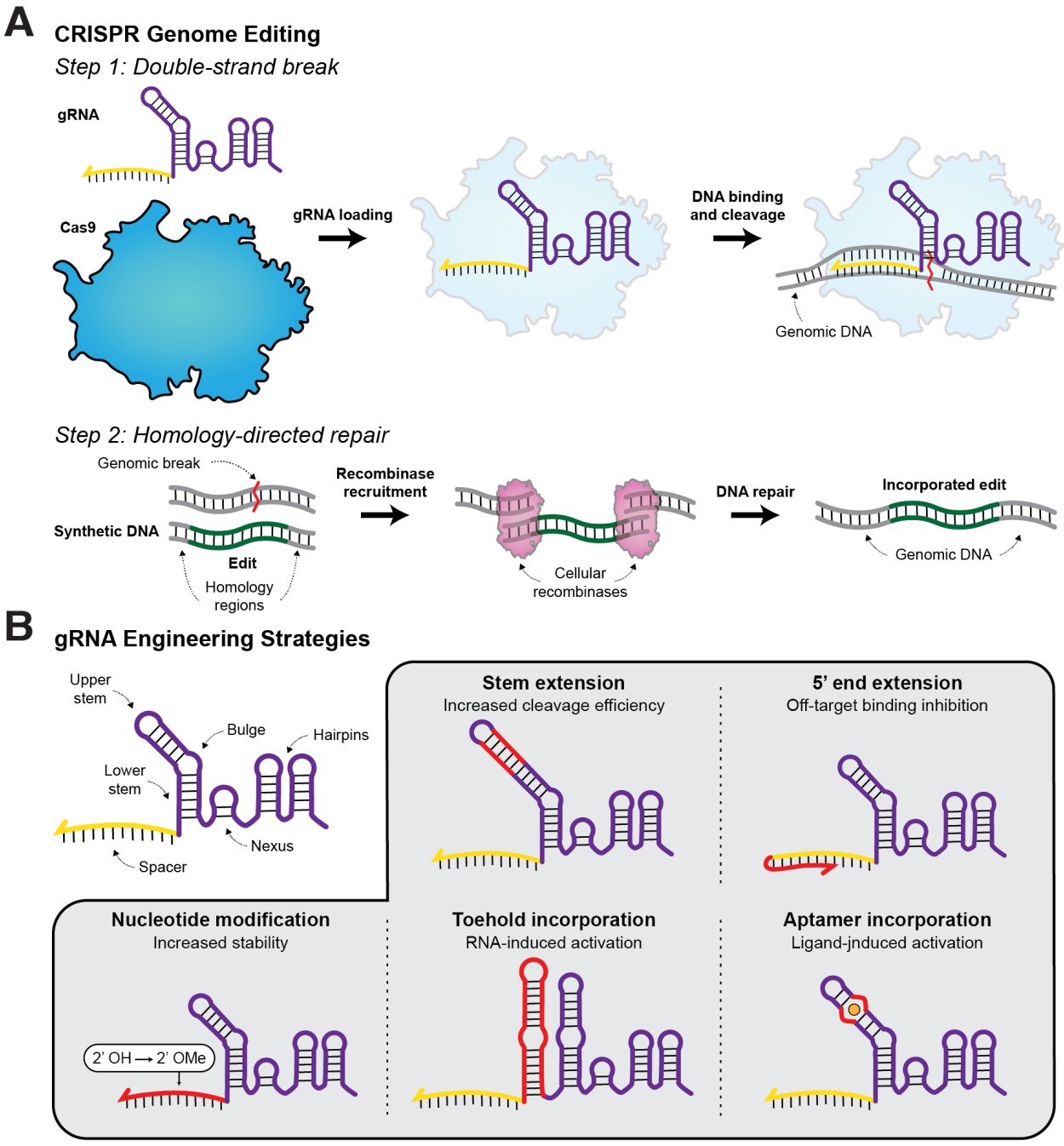

Figure B-2. Enhancement of Cas9 editing rate and specificity via gRNA engineering.
(a) Schematic of Cas9 editing mechanism. Cas9 mediates the sequence specific binding of its gRNA spacer sequence to a corresponding site on the target DNA. Recognition initiates site-specific DNA cleavage. Externally supplied synthetic DNA containing homology regions to the desired editing site as well as introduced sequence changes is then utilized by cellular recombination machinery repair the break, adding the desired donor sequence to the DNA. **(b)** Example gRNA modifications (bolded) and functions. Engineering the gRNA with additional sequences and chemical modifications can increase cleavage efficiency and gRNA stability, reduce off-target editing, and confer novel functions.

While there is currently a lack of robust literature on chemically modified guides for Cas13a, we can begin to formulate strategies by looking at efforts to chemically modify guides for other Cas proteins. Cas proteins are touted to function at single nucleotide resolutions, Cas9 has well-documented off-target activity and can remain highly active in human cell lines even with small mismatches between the target and gRNA[230–232]. A recent study in mice has demonstrated the full effect of this activity by identifying multiple off-target editing sites distributed throughout the genome[232]. Fortunately, these off-target effects can be mitigated by careful selection of target sites, along with engineering the gRNA for increased fidelity[231].

These RNA engineering strategies are effective because the structure of a gRNA plays a key role in determining its editing activity, and structural modifications can tune its editing behavior. For example, previous work showed that strong base pairing in the gRNA's stem regions, nexus, and hairpins decreases editing activity[233], while the extension of gRNA's upper stem significantly increases it by disrupting a thymine-rich sequence of nucleotides[234]. Designed structures can also be used to increase specificity – the addition of a hairpin to the gRNA spacer sequence reduces off-target activity by disfavoring off-target binding[235]. This occurs because the hairpin must be displaced by the target DNA sequence to enable gRNA binding and cleavage, which is more thermodynamically favorable for an entirely complementary sequence than a partially mismatched one.

Moving beyond what is possible with nature's biological tools offers a means to further tune CIRPSR-Cas systems – chemically synthesizing gRNAs enables the modification of their nucleotides with functional groups that can improve editing rate and specificity. For example, 2'-O-methylation and related RNA modifications increase gRNA stability, resulting in a corresponding increase in editing rate[236]. Similar modifications have also been used to reduce off-target cleavage without sacrificing on-target activity[237]. Notably, while modifying portions of the gRNA that directly interface with Cas9 has been shown to reduce its activity, the remainder of the gRNA sequence tolerates heavy modification[238].

B.4 A DNA-RNA "hybrid" guide for Cas12a

More directly relevant to engineering Cas13a is the ssDNA-targeting Cas12a. By changing the Cas protein used to the type V Cas protein Cas12a, a similar scheme can be used to detect DNA targets. Cas12a acts as an indiscriminate single stranded DNAse after binding its single stranded DNA target, which can be used to cleave a ssDNA-linked fluorophore-quencher pair upon detection (**Figure B-1e**). This was demonstrated with DETECTR (**D**NA **E**ndonuclease **T**argeted **C**RISPR **T**rans **R**eporter), which was used to detect low levels of human papillomavirus from patient samples[239].

Recent efforts have demonstrated the ability to tune the cleavage activity of Cas12a via modification of the nucleotides in its spacer[240]. This is done by replacing the RNA nucleotides in Cas12a's spacer sequence with DNA nucleotides; because the DNA-RNA heteroduplex has a thermodynamically stronger bond than a DNA-DNA duplex, this substitution reduces the binding affinity between the spacer and target sequence. This substitution therefore destabilizes mismatched sequences that would otherwise be capable of initiating cleavage, preventing it and reducing off-target activity.

B.5 Tuning spacer-target binding affinity for Cas13a with DNA-RNA hybrid gRNA

My first efforts sought to extrapolate this logic to Cas13a. However, because Cas13a binds ssRNA, rather than ssDNA, the logic is reversed; replacing nucleotides in the spacer with DNA would increase, rather than decrease, binding affinity to the target sequence. We would therefore expect to see a decrease in Cas13a's limit of detection, or an increase in its ability to attack otherwise difficult structured sequences. The former would benefit existing isothermal amplification-based diagnostic technologies by reducing detection threshold and therefore reducing time to detection, while the latter would facilitate sensor design by enabling the detection of a wider range of targets.

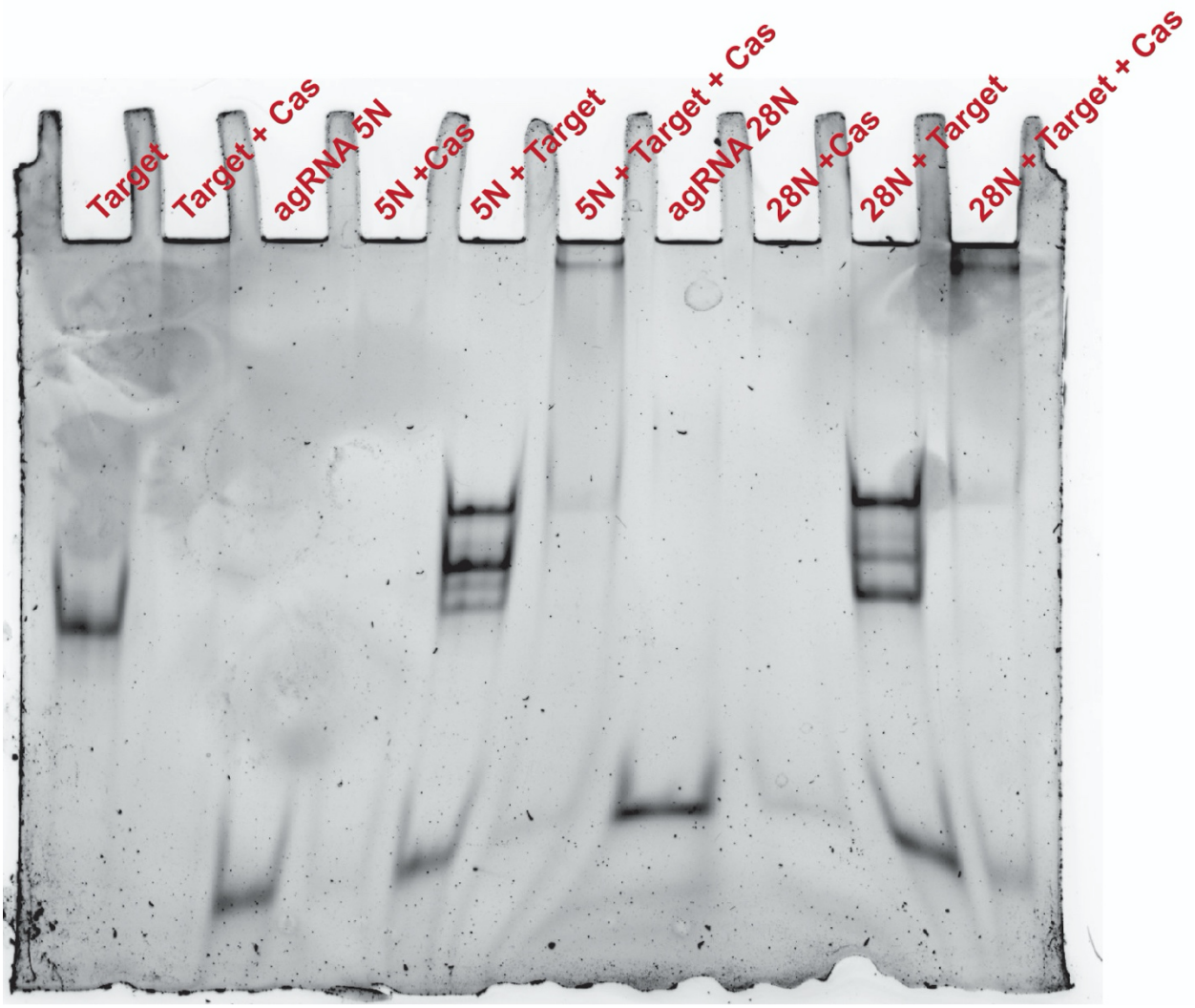

Figure B-3. Electrophoretic motility shift assay (EMSA) for DNA-RNA guides and targets bound to dCas13 Lbu.
"5N" indicates that the five nucleotides on the 3' end of the gRNA have been replaced with DNA, while "28N" indicates that all 28 nucleotides of the spacer have been replaced with DNA.

I first attempted to confirm that Cas13a was still capable of binding to the DNA-RNA hybrid guide RNAs. To do so, I performed an electrophoretic motility shift assay (EMSA) using two hybrid guides – one with 5 nucleotides of the spacer replaced with DNA, and the other with all 28. Encouragingly, both variants showed that they were capable of both (1) binding to their cognate target and (2) enabling the formation of a Cas13a-target-gRNA complex. Less encouragingly, however, the variant with 28 nucleotides replaced with DNA showed no cleavage activity in a collateral cleavage reaction with the target sequence. Contrasting this, however, the variant with 5 nucleotides replaced retained its ability to activate Cas13a's collateral cleavage.

Figure B-4. Breakpoints of regions to substitute gRNA nucleotides with DNA.
The following gRNAs were designed, with ranges indicating regions of nucleotides substituted with DNA: (1) 1-4, (2) 1-8, (3) 9-15, (4) 25-28, (5) 21-28, (6) 17-28.

To further interrogate this phenomenon, I created additional variants with selected regions modified to incorporate DNA instead of RNA. These regions were walked out systematically from the 5’ and 3’ ends, along with one in the middle “seed” region, shown to be important for Cas13a’s conformational rearrangement before cleavage[241]. While all of these variants remained able to cleave target structured and unstructured RNA sequences, they were all less effective than the unmodified guide in cleaving structured sequences. Similarly, no modified guide exhibited a lower limit of detection than the unmodified guide.

B.6 Tuning spacer-target binding affinity with chemically modified gRNA

Building on my previous attempt, I opted to swap the DNA nucleotides in Cas13a’s guide with chemically modified nucleotides. This builds on my previous hypothesis; if the goal is to make the interaction between the guide and the spacer as thermodynamically favorable as possible, then the nucleotides introduced don’t necessarily need to be DNA. Instead, I could simply try to use chemically modified nucleotides to maximize binding favorability. This was done using methylated RNA nucleotides, which have a higher binding affinity for RNA than unmethylated nucleotides. I also made similar guides using conformationally locked nucleic acids[242] (LNAs), hypothesizing that their improved binding due to constrained structure would also increase the binding affinity of the guide to its target. Additionally, I attempted to mitigate the negative effect that modifying nucleotides would have on cleavage activity to limiting modifications to nucleotides shown not to contact Cas13a[241]. Unfortunately, however, I saw a continuation of the previously

observed trend, where none of these modified guides were capable of outperforming the unmodified guide.

This suggests that while gRNA binding affinity with its cognate target is an important contributor to cleavage activity, it is not the only important contributor. In the work done with Cas12a[239], the reduced cleavage activity was a feature, not a bug; even if overall cleavage decreased, as long as cleavage was more specific in general then the modifications would be an improvement over the unmodified guide. Regardless, we have still gained useful information here; over the course of this study, I have better characterized the relationship between gRNA modifications and cleavage activity for Cas13a and shown that Cas13a can bind gRNAs with even heavily modified spacers. This information may be of use moving forward as we further build diagnostic and therapeutic systems utilizing Cas13a.

B.7 Conclusions

My candid opinion is that while the promise of engineering guides for Cas proteins is an exciting and potentially very fruitful field of study, this project direction may not be the most productive one in terms of potential to improve CRISPR-Cas diagnostics. From my preliminary data, I suspect that the modifications to the guide are by default decreasing cleavage activity, outweighing the benefits of increased binding affinity. As an alternative, I would recommend protein engineering. We already have a solid foundational understanding of the structure and mechanism of action for Cas13a[241]; building on this by modifying the Cas protein to improve its activity or imbue it with new functions could vastly improve its capabilities as a diagnostic tool. Of particular interest in this regard would be the engineering of Cas13a fusion proteins. The development of prime editing has already shown that fusing Cas and other proteins can enable novel functions[243]; extrapolating this logic to Cas13a by fusing a helicase to unravel structured targets could be the road to enhancing Cas13a's ability to attack them.

Appendix C - Supplemental Information

C.1 SI for "Development of a Cell-Free, Riboswitch-Based Fluoride Biosensor"

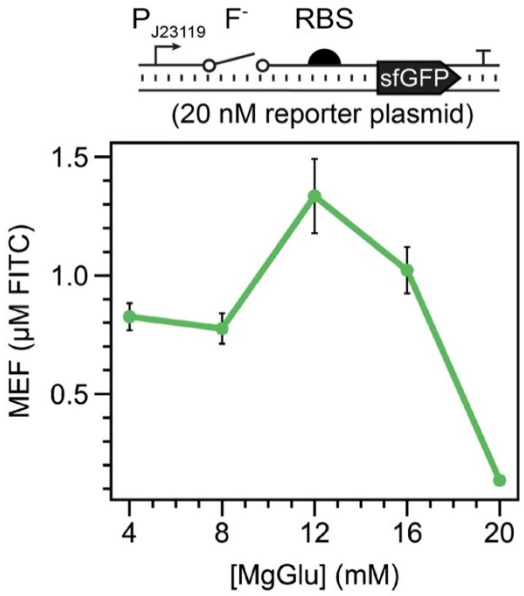

Supplemental Figure 1. Fluoride riboswitch magnesium optimization.
Reactions were supplied with 1 mM NaF and varying magnesium glutamate as indicated. Data shown are endpoint measurements from an eight-hour experiment. Error bars represent one standard deviation from three technical replicates. This experiment indicated that a magnesium glutamate concentration of 12 mM gave optimal fluorescence, though we note that optimal magnesium concentration can vary between extracts

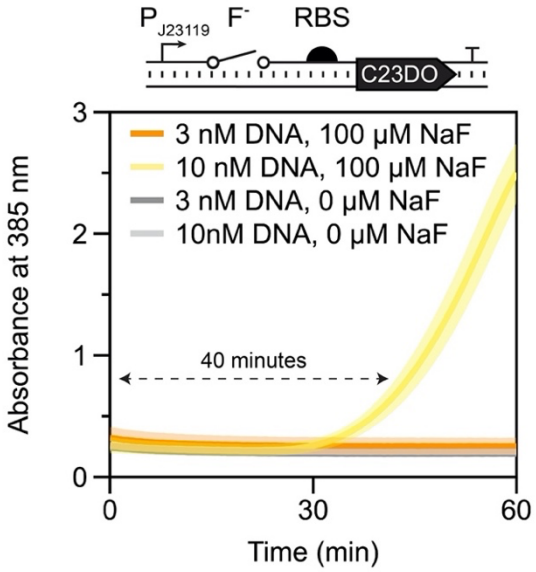

Supplemental Figure 2. Kinetic traces for reaction conditions depicted in Figure 2-3B.
This experiment was run at 37°C to best mirror experimental conditions for reactions run in PCR tubes. Visible activation is seen in 40 minutes for the condition with 10 nM biosensor DNA and 100 μM NaF, corroborating the results depicted in Figure 3B. Trajectories represent average and error shading represents one standard deviation from three technical replicates.

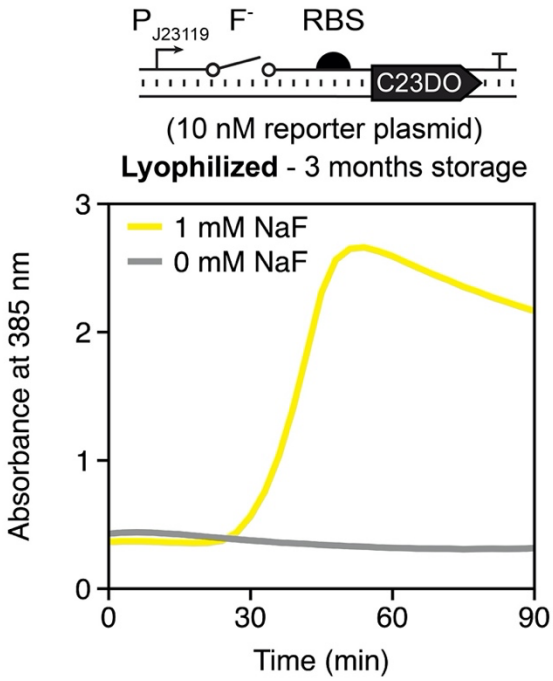

Supplemental Figure 3. Lyophilized reactions remain viable after three months of storage in desiccant.
Reactions were stored in darkness under ambient conditions before rehydration with 20μL of water with or without 1mM NaF. Trajectories represent data from one experiment.

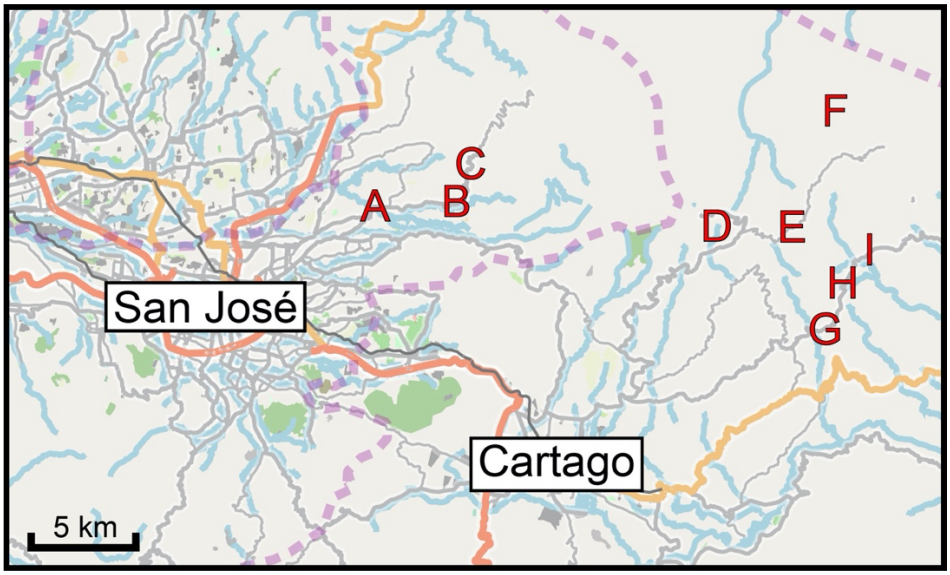

Supplemental Figure 4. Map of Costa Rican water sampling locations.
Sampling locations were determined from a previously published report about the presence of fluoride in water within this region[79]. Geographical data © OpenStreetMap contributors[78]. Each letter represents a unique source where 50 ml of water was sampled. Locations center around the Irazu volcano, a known source of fluoridated salts[79]. Data presented in Figure 4B is from locations B and E.

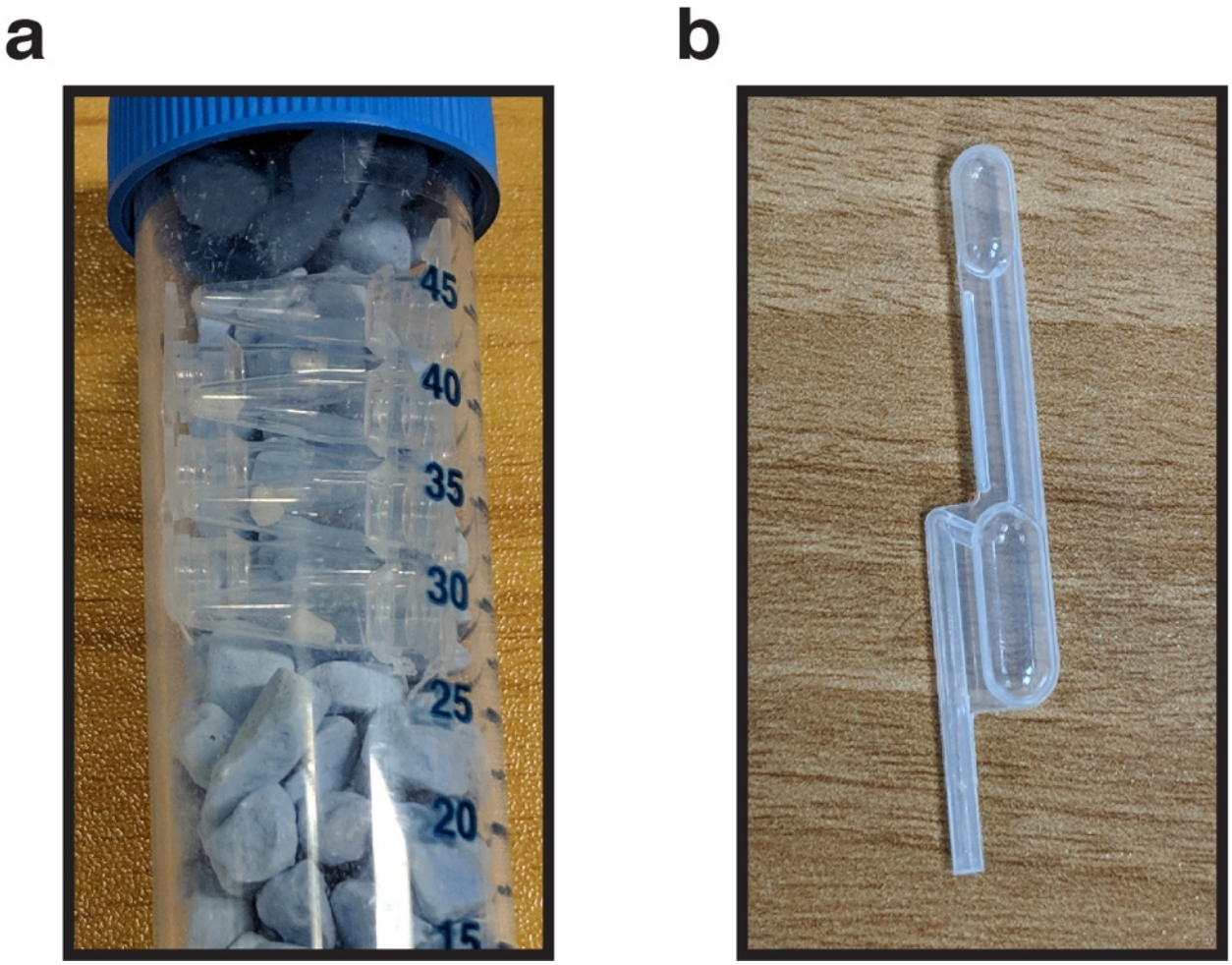

Supplemental Figure 5. Necessary field-testing equipment.
(a) Lyophilized reactions stored in a 50 mL conical tube filled with desiccant. Reactions can be individually removed from the strip for testing on demand. Because the reactions are not stored under nitrogen gas, the tube can be opened and resealed as many times as necessary. **(b)** 20 μL exact volume transfer pipette (Thomas Scientific, 1207F80). Pipettes measure approximately 5 cm lengthwise. By squeezing and releasing the bulb on top, 20 μL of fluid is transferred into the stem, with any excess entering the overflow reservoir. Squeezing the bulb again dispenses the water, which is added directly to the lyophilized reactions before incubation.

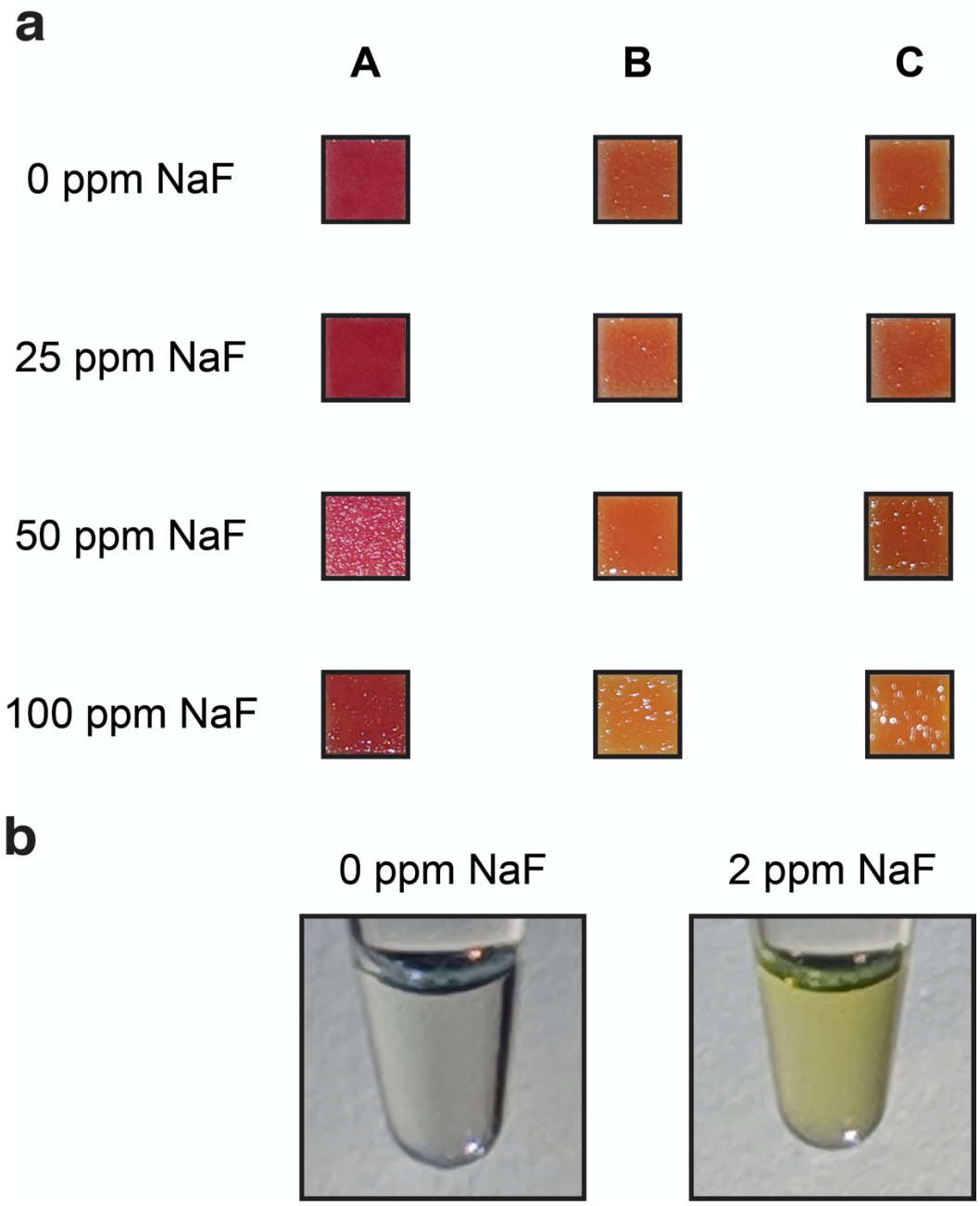

Supplemental Figure 6. The cell-free fluoride riboswitch biosensor is capable of higher-fidelity sensing than several currently available colorimetric assays.
(a) Color change from three anonymized commercially available test strips with a reported sensitivity range of 10-100+ ppm of fluoride. Strips were dipped in the indicated NaF concentration in Milli-Q water and held at room temperature for 30 seconds to wait for color change, as directed by supplied instructions. No readily apparent change was observed at any fluoride concentration. **(b)** Fluoride detection using a cell-free reaction containing 10 nM of the fluoride riboswitch regulated C23DO DNA template. The reaction was set up, incubated at 37°C for 1 hour, then mixed by pipetting before image capture. Despite the delayed activation due to time required for transcription and translation, clear activation can be seen at concentrations below 10 ppm.

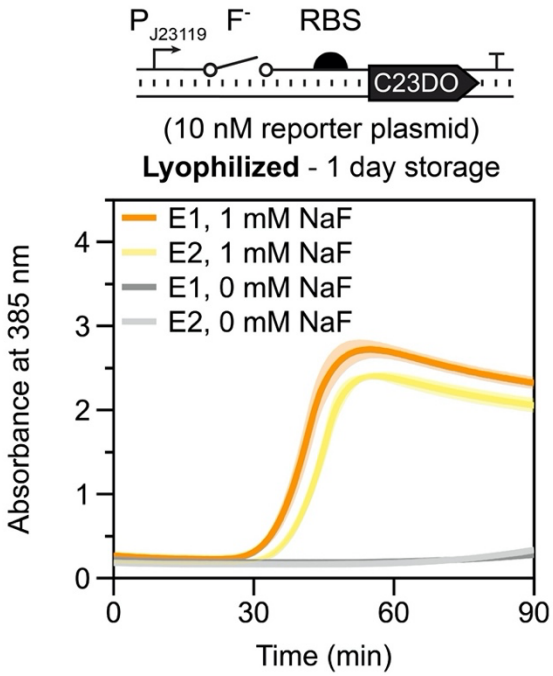

Supplemental Figure 7. Lyophilized reactions show little variability between batches of cell-free extract.
Cell-free reactions containing fluoride riboswitch-regulated C23DO were set up with different batches of cell-free extract (E1 and E2) and lyophilized overnight. The next morning, reactions were rehydrated and reaction progress, read out by absorbance at 385 nm, was monitored in a plate reader maintained at 30°C. The reactions reached maximal activation almost simultaneously in both conditions containing 1mM NaF (orange and yellow lines) and had negligible leak without added NaF (dark gray and light gray lines).

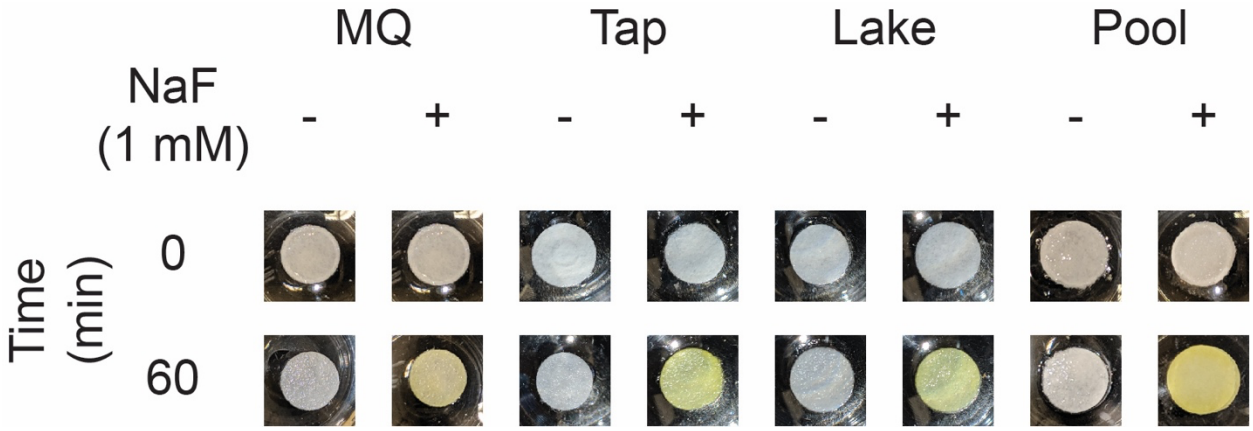

Supplemental Figure 8. Uncropped photos of lyophilized cell-free reactions on paper.
Reactions pictured here are the same as those pictured in Figure 4A. The slight pink color of some paper disks is the result of ambient lighting conditions and could not be observed by eye.

Name	Sequence 5' to 3'
pJBL3752: Anderson Promoter BBa_J23119_Spe1 / B.cereus Fluoride Riboswitch / RBS / Superfolder GFP coding sequence/ T1/TE terminator	ttgacagctagctcagtcctaggtataatactagttta**TAGGCGATGGAGTTCGCCATA** **AACGCTGCTTAGCTAATGACTCCTACCAGTATCACTACTGGTAGGA** **GTCTATTTTTTT**aggaggaaggatctatgagcaaaggagaagaacttttcactggagttgt cccaattcttgttgaattagatggtgatgttaatgggcacaaattttctgtccgtggagagggtgaagg tgatgctacaaacggaaaactcacccttaaatttatttgcactactggaaaactacctgttccgtggc caacacttgtcactactctgacctatggtgttcaatgcttttcccgttatccggatcacatgaaacggca tgacttttcaagagtgccatgcccgaaggttatgtacaggaacgcactatatctttcaaagatgacg ggacctacaagacgcgtgctgaagtcaagtttgaaggtgatacccttgttaatcgtatcgagttaaa gggtattgattttaaagaagatggaaacattcttggacacaaactcgagtacaactttaactcacac aatgtatacatcacggcagacaaacaaaagaatggaatcaaagctaacttcaaaattcgccaca acgttgaagatggttccgttcaactagcagaccattatcaacaaaatactccaattggcgatggccc tgtcctttaccagacaaccattacctgtcgacacaatctgtcctttcgaaagatcccaacgaaaagc gtgaccacatggtccttcttgagtttgtaactgctgctgggattacacatggcatggatgagctctaca aataaggatccaaactcgagtaaggatctccaggcatcaaataaaacgaaaggctcagtcgaa agactgggcctttcgttttatctgttgtttgtcggtgaacgctctctactagagtcacactggctcaccttc gggtgggcctttctgcgtttata
pJBL7025: Anderson Promoter BBa_J23119_Spe1 / B.cereus Fluoride Riboswitch / RBS / Catechol 2,3-dioxygenase coding sequence/ T1/TE terminator	ttgacagctagctcagtcctaggtataatactagttta**TAGGCGATGGAGTTCGCCATA** **AACGCTGCTTAGCTAATGACTCCTACCAGTATCACTACTGGTAGGA** **GTCTATTTTTTT**aggaggaaggatctatgaacaaaggtgtaatgcgaccgggccatgtgc agctgcgtgtactggacatgagcaaggccctggaacactacgtcgagttgctgggcctgatcgag atggaccgtgacgaccagggccgtgtctatctgaaggcttggaccgaagtggataagttttccctgg tgctacgcgaggctgacgagccgggcatggattttatgggtttcaaggttgtggatgaggatgctctc cggcaactggagcgggatctgatggcatatggctgtgccgttgagcagctacccgcaggtgaact gaacagttgtggccggcgcgtgcgcttccaggccccctccgggcatcacttcgagttgtatgcaga caaggaatatactggaaagtggggtttgaatgacgtcaatcccgaggcatggccgcgcgatctga aaggtatggcggctgtgcgtttcgaccacgccctcatgtatggcgacgaattgccggcgacctatg acctgttcaccaaggtgctcggtttctatctggccgaacaggtgctggacgaaaatggcacgcgcg tcgcccagtttctcagtctgtcgaccaaggcccacgacgtggccttcattcaccatccggaaaaag gccgcctccatcatgtgtccttccacctcgaaacctgggaagacttgcttcgcgccgccgacctgat ctccatgaccgacacatctatcgatatcggcccaacccgccacggcctcactcacggcaagacc atctacttcttcgacccgtccggtaaccgcaacgaagtgttctgcgggggagattacaactacccgg accacaaaccggtgacctggaccaccgaccagctgggcaaggcgatcttttaccacgaccgcat tctcaacgaacgattcatgaccgtgctgacctgataaggatccaaactcgagtaaggatctccagg catcaaataaaacgaaaggctcagtcgaaagactgggcctttcgttttatctgttgtttgtcggtgaac gctctctactagagtcacactggctcaccttcgggtgggcctttctgcgtttata

pJBL7026: Anderson Promoter BBa_J23119_Spe1 / B.cereus Fluoride Riboswitch / 3-Way Junction Dimeric Broccoli coding sequence / T1/TE terminator	ttgacagctagctcagtcctaggtataatactagttaTAGGCGATGGAGTTCGCCATAAACGCTGCTTAGCTAATGACTCCTACCAGTATCACTACTGGTAGGAGTCTATTTTTTTcccacatactctgatgatccgagacggtcgggtccagatattcgtatctgtcgagtagagtgtgggctcggatcattcatggcaagagacggtcgggtccagatattcgtatctgtcgagtagagtgtgggctcttgccatgtgtatgtgggccaggcatcaaataaaacgaaaggctcagtcgaaagactgggcctttcgttttatctgttgtttgtcggtgaacgctctctactagagtcacactggctcaccttcgggtgggcctttctgcgtttata

Supplemental Table 1. Sequences of constructs.
Constructs utilized the Anderson promoter BBa_J23119_Spe1 (blue), the *B. cereus crcB* fluoride riboswitch (red), a ribosome binding site (RBS) (pink), superfolder GFP (sfGFP) (green), catacholase 2,3 dioxygenase (C23DO) (yellow), three-way junction dimeric broccoli (3wjdb) (teal), and T1/TE terminator (grey).

Site	GPS Coordinates	Source	Measured [F^-] (ppm)	Activation	Negative Control	Positive Control
A	9°58'30"N 84°00'20"W	Indoor Faucet	0.2	No	Off	On
B	10°00'00"N 83°57'30"W	Muddy Ditch	0.3	No	Off	On
C	10°00'40"N 83°57'10"W	Indoor Faucet	0.2	No	Off	On
D	9°56'50"N 83°51'50"W	Outdoor Supply	1	Yes	Off	On
E	9°58'10"N 83°49'40"W	Muddy Ditch	1.2	Yes	Off	On
F	10°00'10"N 83°46'50"W	Outdoor Supply	0.5	No	Off	On
G	9°56'30"N 83°46'40"W	River	0.1	No	Off	On
H	9°57'10"N 83°46'20"W	River	0.3	No	Off	On
I	9°57'20"N 83°46'20"W	River	0.3	No	Off	On

Supplemental Table 2. GPS coordinates and documentation for water sampling sites depicted in Figure 2-4 and Supplemental Figure 4.
GPS coordinates are reported to the nearest ten-minute resolution and thus represent regions sampled rather than exact locations. Measured concentrations were determined with a fluoride sensing electrode as described in Materials and Methods. “Activation” refers to the production of a visually detectable yellow color after sensor rehydration (see Materials and Methods). Data presented in Figure 4B is from locations B and E. Permissions were received before sampling indoor faucets.

C.2 SI for "Encapsulating Cell-Free Biosensors to Mitigate Matrix Effects"

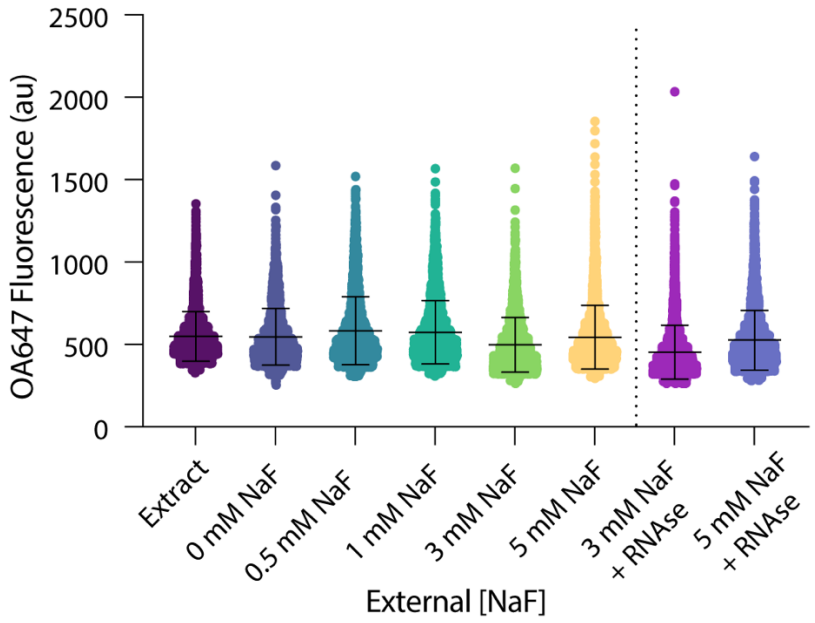

Supplemental Figure 9. OA647 retention in 2:1 cholesterol:POPC vesicles following encapsulation and protein expression.
Vesicle populations exposed to increasing fluoride in the external solution exhibit the retention of a volume marker, OA647, even when RNAse A is present externally. While average fluorescence varies slightly between populations, corresponding to differences in the size of analyzed vesicles between conditions, all samples exhibit similar fluorescence profiles consistent with the retention of protein-sized molecules within the vesicle interior.

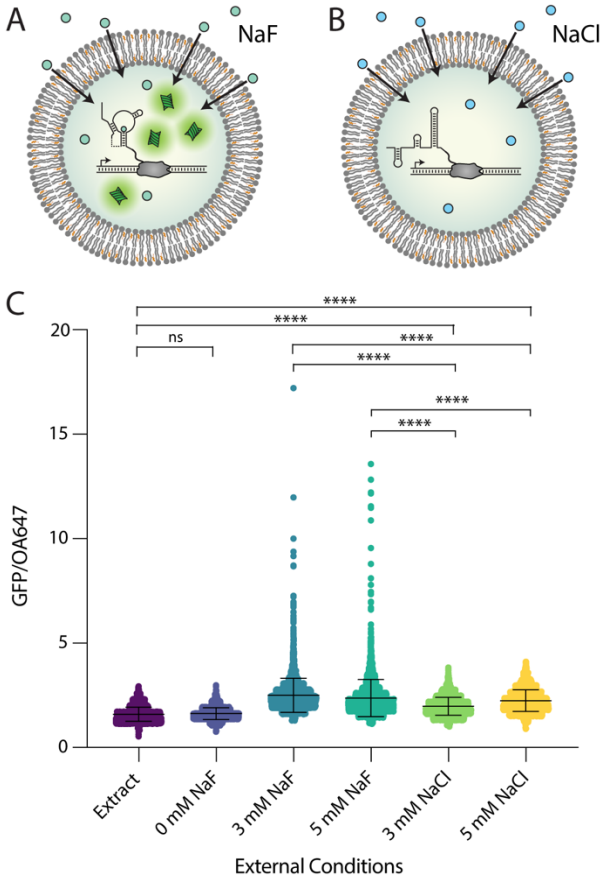

Supplemental Figure 10. An encapsulated riboswitch responds specifically to fluoride.
(a) Fluoride permeates the vesicle membrane to initiate the expression of a GFP reporter inside vesicles. **(b)** The external addition of NaCl does not result in robust GFP expression inside vesicles. **(c)** GPF/OA647 fluorescence in vesicles with either NaF or NaCl added to the external buffer. While a response is observed to increasing chloride, the magnitude is significantly less than the response to fluoride and there is no observed population shift towards highly active vesicles. Differences in expression between fluoride and chloride containing conditions were clearly distinguishable, indicating sufficient specificity to fluoride over chloride. **** $p \leq 0.0001$, nonsignificant (ns) $p > 0.1234$; p-values generated using a One-Way ANOVA and Tukey's Multiple Comparisons Test.

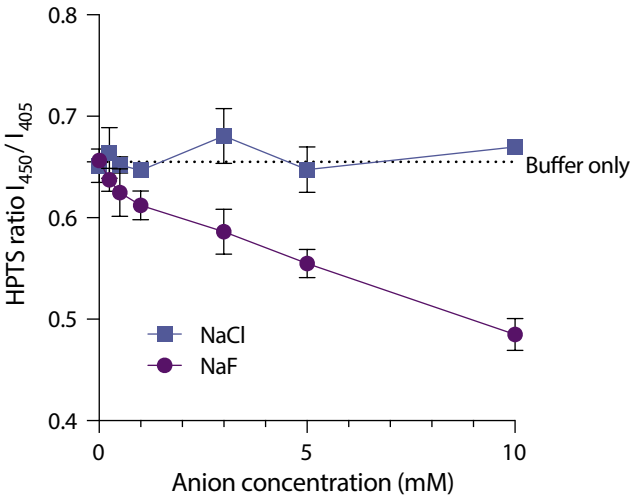

Supplemental Figure 11. pH decreases as increasing NaF is added externally to vesicles.
Lipid/cholesterol vesicles containing HPTS dye without cell-free expression systems show changes in fluorescence after addition of anions to the external solution, indicating a cross-membrane effect on pH caused by externally added NaF. Compared to NaCl and buffer only controls, the pH of the vesicle interior decreases in the presence of externally added NaF, as indicated by a decreasing fluorescence ratio of HPTS, a pH-sensitive dye. These results indicate that fluoride ions may permeate the membrane as HF, bringing H^+ ions with them as they pass through the membrane.

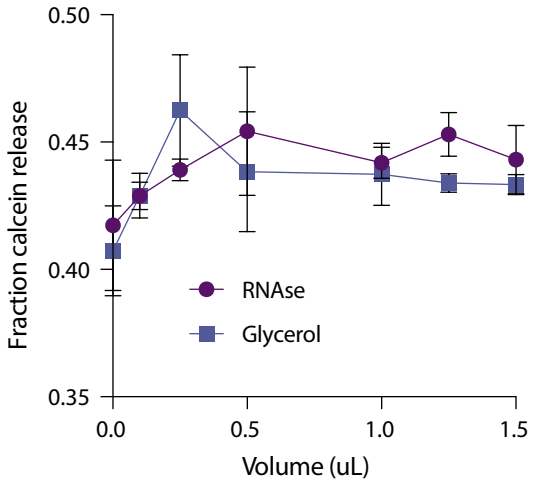

Supplemental Figure 12. Glycerol addition increases membrane permeability.
Lipid/cholesterol vesicles encapsulating calcein, a self-quenching fluorescent dye, show slightly increasing cargo leakage following glycerol addition to the surrounding buffer. In both the presence and absence of RNAse, addition of increasing volumes of 0.02% glycerol solutions (1.25 mL of which was added in vesicle studies) leads to slightly higher levels of calcein dye release from the vesicle interior, indicating increased membrane permeability to small molecules.

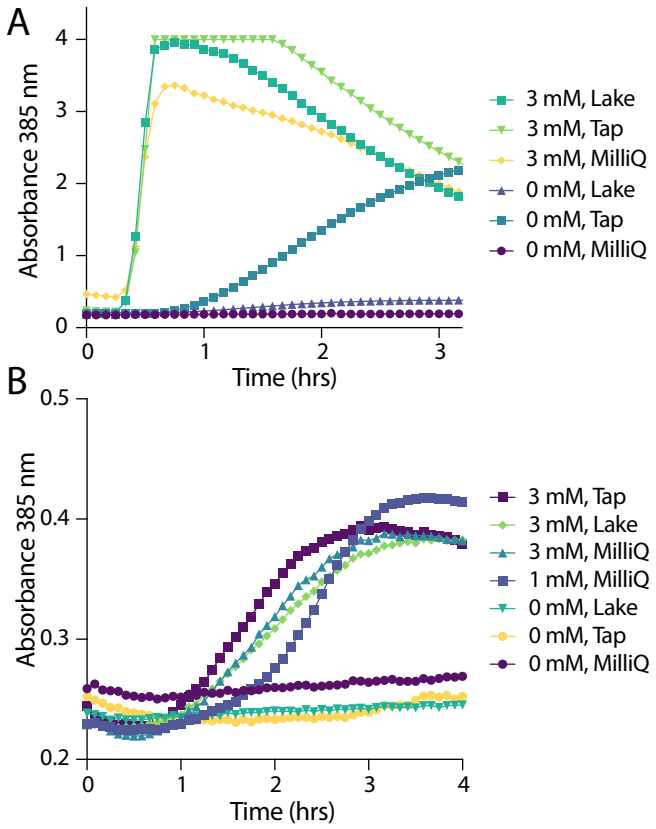

Supplemental Figure 13. Catecholase conversion in response to fluoride in bulk and inside of vesicles.
(a) Bulk reactions show slightly higher responses to 3 mM NaF supplemented in water samples taken from Lake and Tap water compared to laboratory-grade MilliQ water. Absorbance was also observed to increase in unsupplemented tap water, likely due to low levels of fluoride added to public drinking supply. **(b)** In vesicles, absorbance increases specifically in the presence of supplemented NaF. Quantification is difficult, with 1 mM NaF exhibiting a slightly delayed response compared to 3 mM NaF but a similar expression profile and maximum absorbance. Responses are similar between all 3 mM samples regardless of water source, with a slight increase in expression in unsupplemented tap water at later timepoints (consistent with bulk data). (n=1 example vesicle preparation shown here.

External NaF concentration	Mean Fluorescence GFP/OA647	SEM	Significantly different than 0 mM?	Skewness	Kurtosis
Extract	1.596	0.0054	ns	0.5225	0.8674
0 mM	1.625	0.0062		0.4007	0.4155
0.5 mM	2.250	0.0126	****	2.205	13.12
1 mM	2.388	0.0143	****	1.824	9.110
3 mM	2.500	0.0167	****	2.083	8.960
5 mM	2.372	0.0166	****	4.587	46.19

**** $p \leq 0.0001$, nonsignificant (ns) $p > 0.1234$; p-values generated using a One-Way ANOVA and Tukey's Multiple Comparisons Test.

Supplemental Table 3. GFP expression in response to externally added NaF in 2:1 cholesterol:POPC vesicles.
Descriptive statistics of GFP expression in populations of vesicles exposed to increasing amounts of externally added NaF. Statistical analysis was computed compared to 0 mM NaF conditions.

External NaF concentration	Mean GFP/OA647	SEM	Different than 0 mM?	Skewness	Kurtosis
POPC, 0 mM	2.904	0.01074		0.1471	-0.3680
POPC, 1 mM	3.968	0.02997	****	2.063	7.183
POPC, 3 mM	3.724	0.02570	****	2.433	9.854
POPC, 5 mM	3.190	0.01478	****	1.528	5.072
10% OA, 0 mM	1.997	0.004865		0.3135	0.1434
10% OA, 1 mM	2.850	0.02232	****	6.120	59.59
10% OA, 3 mM	2.839	0.03147	****	4.848	32.92
10% OA, 5 mM	2.909	0.03352	****	5.038	38.90
10% 1.8k, 0 mM	1.807	0.05333		0.6967	-0.2151
10% 1.8k, 1 mM	2.414	0.07304	**	5.698	39.98
10% 1.8k, 3 mM	2.353	0.04787	*	2.199	11.16
10% 1.8k, 5 mM	2.458	0.04654	**	3.247	19.66

**** $p \leq 0.0001$, ** $p \leq 0.0021$, * $p \leq 0.0332$, nonsignificant (ns) $p > 0.1234$; p-values generated using a One-Way ANOVA and Tukey's Multiple Comparisons Test.

Supplemental Table 4. GFP expression in response to externally added NaF in vesicles with varying membrane compositions.
Descriptive statistics of GFP expression in populations of vesicles with varying membrane compositions in response to increasing concentrations of externally added NaF. Statistical analysis was computed compared to 0 mM NaF conditions for each respective membrane composition.

External NaF concentration	Mean Fluorescence GFP/OA647	SEM	Significantly different than 0 mM?	Skewness	Kurtosis
Extract only	2.152	0.013	ns	0.9806	2.661
0 mM	2.213	0.013		0.9952	2.501
0.5 mM	3.071	0.026	****	2.236	9.502
1 mM	3.289	0.022	****	3.289	24.83
3 mM	2.930	0.023	****	3.746	34.26
5 mM	2.662	0.018	****	2.251	10.79

**** $p \leq 0.0001$, nonsignificant (ns) $p > 0.1234$; p-values generated using a One-Way ANOVA and Tukey's Multiple Comparisons Test.

Supplemental Table 5. GFP expression in response to externally added NaF in 2:1 cholesterol:POPC vesicles with RNAse A in the surrounding solution.
Descriptive statistics of GFP expression in populations of vesicles with RNAse present in the surrounding solution in response to increasing concentrations of externally added NaF. Statistical analysis was computed compared to 0 mM NaF conditions.

C3. SI for "Field-Deployment of a Cell-Free Biosensor in Nakuru County, Kenya"

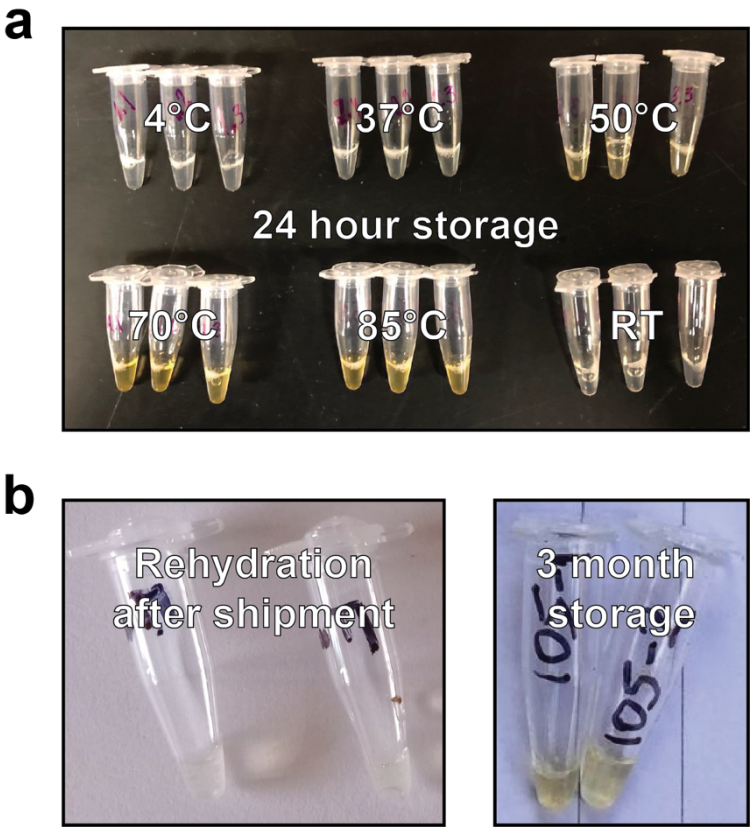

Supplemental Figure 14. Cell-free reactions degrade after storage at high temperatures.
a) Lyophilized reactions rehydrated with purified water after 24-hour storage at 4°C, 37°C, 50°C, 70°C, 85°C, and room temperature (RT, ~20°C). As temperatures increased, rehydration resulted in a yellow color likely due to component degradation and thus loss of function. This yellow color change confounds the interpretation of the intended yellow color change of the tests in the presence of fluoride causing false positives and test failure. (**b**) Tests from the first batch shipped to Kenya rehydrated immediately after arrival (left) and after three-month storage at ambient temperatures (right). Color change in the stored reactions resembles color change from 24-hour storage at high temperatures and was similarly reflective of loss of function.

Supplemental Figure 15. Fluoride testing field kit.
Pictured from left to right: foil pouch, vacuum bag, desiccant card, freeze-dried reactions in PCR tubes, and disposable micropipettes. Reactions and desiccant card are placed in the vacuum bag and sealed, then stored in the foil pouch to prevent photodegradation. Pipettes were packaged separately during testing but could also be stored in the foil pouch

Supplemental Figure 16. Geographic location of the study site.
Barut Ward, a subdivision of Nakuru County. Nakuru County is located in the Great Rift Valley, where geogenic fluoride is common. Geographical data © OpenStreetMap contributors.

Item	Vendor	Catalog Number	Cost per kit (USD)
CFE Reaction	N/A	N/A	$0.56[52]
Catechol	Alfa Aesar	A10164	$0
PCR Tubes	BrandTech Scientific	781332	$0.48
20 µL micropipette	Safe-Tec LLC	1020	$0.90
Dessicant	Uline	S-19581	$0.06
Vacuum bag	Amazon	B075KKWFYN	$0.09
Light-protectant bag	Uline	S-11661	$0.09
Total (per test kit)			$2.17
Total (per test)			**$0.72**
Photometer Reagents	Hanna Instruments	HI93739-03	$266
Total (per test)			**$0.89**

Supplemental Table 6. Cost breakdown of point-of-use fluoride biosensors compared to operating cost for a fluoride photometer.

Sample Number	Water Source	Fluoride (ppm)	Test Result
107-1	Rainwater Collection	0	True Negative
107-2	Mixed Rain/Borehole	5.4	True Positive
107-3	Borehole	6.5	True Positive
108-1	Rainwater Collection	0	True Negative
108-2	Borehole	6.5	True Positive
109-1	Borehole	5.7	True Positive
110-1	Borehole	6.6	True Positive
110-2	Borehole	4.9	True Positive
111-1	Borehole	5.8	True Positive
112-1	Borehole	5.6	True Positive
113-1	Rainwater Collection	0	True Negative
113-2	Mixed Rain/Borehole	7.9	True Positive
114-1	Borehole	6.2	True Positive
114-2	Borehole	5.5	True Positive
114-3	Mixed Rain/Borehole	5.3	True Positive
115-1	Borehole	6.1	True Positive
116-1	Borehole	6	True Positive
117-1	Mixed Rain/Borehole	3.9	True Positive
118-1	Protected Dug Well	8.8	True Positive
118-2	Borehole	5.8	True Positive
119-1	Rainwater Collection	0	False Positive

119-2	Protected Dug Well	7.4	True Positive
120-1	Borehole	5.7	True Positive
121-1	Borehole	5.8	True Positive
121-2	Rainwater Collection	1.1	False Positive
122-1	Borehole	6	True Positive
123-1	Protected Dug Well	7.7	True Positive
124-1	NAWASCO	5	True Positive
124-2	Protected Dug Well	15.8	True Positive
125-1	Protected Dug Well	18.7	True Positive
125-2	Borehole	15.8	True Positive
126-1	Rainwater Collection	0.4	True Negative
126-2	Protected Dug Well	17	True Positive
127-1	Borehole	5.1	True Positive
128-1	Borehole	5	True Positive
129-1	Borehole	5.4	True Positive
130-1	Rainwater Collection	0.4	True Negative
130-2	Borehole	7.2	True Positive
131-1	Protected Dug Well	8.8	True Positive
132-1	Rainwater Collection	0	False Positive
132-2	Protected Dug Well	10.8	True Positive
133-1	Rainwater Collection	0.5	True Negative
133-2	Protected Dug Well	8.8	True Positive
134-1	Rainwater Collection	0.8	True Negative
134-2	Protected Dug Well	8.7	True Positive
135-1	Surface Water	20	False Negative
135-2	Borehole	6	True Positive
136-1	Borehole	6.3	True Positive
137-1	Borehole	6.6	False Negative
137-2	Bagged Water	0.1	True Negative
138-1	Rainwater Collection	5.5	False Negative
138-2	Borehole	0.3	True Negative
139-1	Borehole	5.9	True Positive
139-2	Mixed Rain/Borehole	5.8	True Positive
140-1	Borehole	5.5	True Positive
141-1	Borehole	6.4	True Positive
142-1	Borehole	5.4	True Positive

Supplemental Table 7. Sources and test results for water tests used to determine point-of-use fluoride biosensor accuracy (n=57).

Variable Name	Label/Question	Response Codes	Notes
a11_date	1.1) Date of the Interview	month-date	
a12_hhvillID	1.2) Household - Village ID	Please refer to the next column for specification of the code breakdown	XX-YY (first two digits represent village identity and last two digits represent household identity)
a13_village	1.3) Village of respondent	1 Kelewet 2 Kigonor 3 Parkview 4 Kipsibol 99 other	
a13_village_99	1.3) If other, plese provide the name of the village		This is only in the case that the respondent's village was not in the list of the previous villages
a14_initials	1.4) Interviewer's Initials	DA- Diana Awuor KK-Karlmax Kiprotich	
a21_gender	2.1) Gender of Respondent	0 Male 1 Female 99 Other	The 99 extension is only applicable if the respondent does not identify as male nor female
a22_age	2.2) Age of Respondent	continuous	
a23_education	2.3) What is your level of education?	0 None 1 Some primary 2 Completed primary 3 Some secondary 4 Completed secondary 5 College/University 99 Other; specify	The 99 extension is only applicable if the respondent does not have the listed degrees of education
a24_primaryjob	2.4) Primary occupation in the last 12 months?	1 farming 2 livestock 3 farming & livestock 4 small business	96 extension is for other

		5 employee 6 unemployed 7 unable to work 8 student 99 Homekeeper 96 Other; specify	
a25_avg_hhincome	2.5) What is your average household income per week? (ksh)	Integer	
a31_totalppl	3.1) Number of total people in the household including you (respondent)	Integer	
a32_ppl2	3.2) Number of people in the household from ages 0-2	Integer	
a33_ppl5	3.3) Number of people in the household from ages 3-5	Integer	
a34_ppl15	3.4) Number of people in the household from ages 6-15	Integer	
a35_ppl15pl	3.5) Number of people in the household from ages 15+	Integer	
a36_didaddup	3.6) **For field team only** - Did you check that the reported number of people in 3.2-3.5 add up to the total number in 3.1?	1 Yes 0 No 97 Refused	
a41_hwise	4.1) In the last 4 weeks, how frequently did you or anyone in your households worry	**1** Never (0 times in the last 4 weeks) **2**	

	you would not have enough water for all of your household needs?	Rarely (1-2 times in the last 4 weeks) **3** Sometimes (3-10 times in the last 4 weeks) **4** Often (11-20 times in the last 4 weeks) **5** Always (More than 20 times in the last 4 weeks) **99** Don't Know **88** Not applicable/I don't have this	
a42_hwise	4.2) In the last 4 weeks, how frequently has your main water source been interrupted or limited (e.g. water pressure, less water than expected, river dried up)?	**See A41_hwise**	
a43_hwise	4.3) In the last 4 weeks, how frequently have problems with water meant that clothes could not be washed?	**See A41_hwise**	
a44_hwise	4.4) In the last 4 weeks, how frequently have or anyone had to change schedules of plans due to problems with your water sanitation? (Activities that may have been interrupted include	**See A41_hwise**	

	caring for others, doing household chores, agricultural work, income-generating activities, sleeping, etc)		
a45_hwise	4.5) In the last 4 weeks, how frequently have your children delayed or missed school in order to help provide for the household's water needs (fetching water)?	**See A41_hwise**	
a46_hwise	4.6) In the last 4 weeks, how frequently have you or anyone in your household had to change what was being eaten because there were problems with water (e.g., for washing foods, cooking, etc.)?	**See A41_hwise**	
a47_hwise	4.7) In the last 4 weeks, how frequently have you or anyone in your household had to go without washing hands after dirty activities (e.g., defecating or changing diapers, cleaning animal dung) because of problems with water?	**See A41_hwise**	
a48_hwise	4.8) In the last 4 weeks, how frequently have you or anyone in your household had to go without washing their body because of	**See A41_hwise**	

	problems with water (e.g., not enough water, dirty, unsafe)?		
a49_hwise	4.9) In the last 4 weeks, how frequently has your household water situation impacted the cultivation of your garden, crops, or fruit trees?	**See A41_hwise**	
a410_hwise	4.10) In the last 4 weeks, how frequently has your household water situation impacted your raising of animals and poultry?	**See A41_hwise**	
a411_hwise	4.11) In the last 4 weeks, how frequently have problems with water prevented you or anyone in your household from earning money (e.g. engaging in paid work, economic activities)?	**See A41_hwise**	
a412_hwise	4.12) In the last 4 weeks, how frequently has there not been as much water to drink as you would like for you or anyone in your household?	**See A41_hwise**	
a413_hwise	4.13) In the last 4 weeks, how frequently did you or anyone in your household feel angry about your water situation?	**See A41_hwise**	

a414_hwise	4.14) In the last 4 weeks, how frequently have you or anyone in your household gone to sleep thirsty because there wasn't any water to drink?	**See A41_hwise**	
a415_hwise	4.15) In the last 4 weeks, how frequently has there been no usable or drinkable water whatsoever in your household?	**See A41_hwise**	
a416_hwise	4.16) In the last 4 weeks, how frequently have problems with water caused you or anyone in your household to feel ashamed/excluded/stigmatized?	**See A41_hwise**	
a51_kab	5.1) I am now going to talk to you about your knowledge of fluoride and fluorosis. First, what is your understanding of [Fluoride]?	Open ended-Responses	
a52_kab	5.2) What is your understanding of [fluorosis]?	Open ended-Responses	
a53_kab	5.3) What are the effects of [Fluoride] exposure?	Open ended-Responses	
a54_kab	5.4) How can you prevent [fluorosis]?	Open ended-Responses	
a55_kab	5.5) How can you treat [fluorosis]?	Open ended-Responses	
a56_kab	5.6) How often do you worry about	Open ended-Responses	

	[fluorosis]?		
a57_kab	5.7) What were any precautions you have taken against [fluorosis]?	Open ended-Responses	
a58_kab	5.8) Do you know of anyone who has been harmed by [fluoride] in water?	1 Yes 0 No 97 Refused	If yes, a58_kab1 **Question:** Please tell me about the fluorosis—the person's age, gender, how it affected their life, and if they got any treatment. Do they know where the fluoride was coming from?
	5.9) Do you know of anybody else who has been harmed by fluoride in water?	1 Yes 0 No 97 Refused	If yes, a59_kab1 **Question:** Please tell me about the fluorosis—the person's age, gender, how it affected their life, and if they got any treatment. Do they know where the fluoride was coming from?
a60_waterinfo	6.0) Are you able to provide information about Water Sample #1?	1 Yes 0 No 97 Refused	
a61_source	6.1) What is the source of this water sample	1 Piped Water 2 Stand Pipe 3 Borehole/tube well 4 Protected dug well 5 Unprotected dug well 6 Protected Spring 7 Unprotected Spring 8 Rainwater	a61_source_14 "If someone else is responsible for your water, please specify" a61_source_1 extension is "If other, please specify your water source"

		Collection 9 Small Water Vendor 10 Tanker Truck 11 Bottled Water 12 Bagged / sachet water 13 Surface water (pond, river, lake) 14 Other person; specify 96 Other; specify	
a62_time	6.2) How long (in minutes) does it take to go to the water source, get water, and come back (including wait time)? If water souce is in household/compound, record 0		
a63_cookingdrink	6.3) Do you use water from this source for cooking and drinking?	1 Yes 0 No 97 Refused	
a64_worryf	6.4) Are you worried about contracting fluorosis from this sample of water?	1 Yes 0 No 97 Refused	
a65_thistreated	6.5) Has this specific sample of water been treated?	1 It hasn't 2 It has; specify 99 Don’t know	
a65_thistreated2	6.5 a) How has this sample of water been treated?	1 Do not treat it 2 Boiling 3 Filter 4 Chlorine Tablets 5 Distillation 6 bone char 99 Other	

a66_worryfl	6.6) Are you worried about contracting fluorosis from this sample of water?	1 yes 0 no	
a67_cost	6.7) What is the cost of water from this source (x per y)?	Open ended response	
a68_procuresample	6.8) Did you procure the water sample?	1 Yes, without a problem 2 Yes, but there was a problem (explain why) 3 No (explain why)	The 2 and 3 extensions allow the respondent to expand on the problem
a70_waterinfo	7.0) Are you able to provide information about Water Sample #2?	1 Yes 0 No 97 Refused	
a71_source	7.1) What is the source of this water sample	1 Piped Water 2 Stand Pipe 3 Borehole/tube well 4 Protected dug well 5 Unprotected dug well 6 Protected Spring 7 Unprotected Spring 8 Rainwater Collection 9 Small Water Vendor 10 Tanker Truck 11 Bottled Water 12 Bagged / sachet water 13 Surface water (pond, river, lake) 14 Other person; specify 96 Other; specify	14 extension is “If someone else is responsible for your water, please specify” 1 extension is “If other, please specify your water source”

a72_time	7.2) How long (in minutes) does it take to go to the water source, get water, and come back (including wait time)? If water source is in household/compound, record 0		
a73_cookingdrink	7.3) Do you use water from this source for cooking and drinking?	1 Yes 0 No 97 Refused	
a74_worryf	7.4) Are you worried about contracting fluorosis from this sample of water?	1 Yes 0 No 97 Refused	
a75_thistreated	7.5) Has this specific sample of water been treated?	1 It hasn't 2 It has; specify 99 Don’t know	
a75_thistreated2	7.5 a) How has this sample of water been treated?	1 Do not treat it 2 Boiling 3 Filter 4 Chlorine Tablets 5 Distillation 6 bone char 99 Other	
a76_worryfl	7.6) Are you worried about contracting fluorosis from this sample of water?	1 yes 0 no	
a77_cost	7.7) What is the cost of water from this source (x per y)?		
a78_procuresample	7.8) Did you procure the water sample?	1 Yes, without a problem 2 Yes, but there was a problem (explain why)	The 2 and 3 extensions allow the respondent to expand on the problem

		3 No (explain why)	
a80_waterinfo	8.0) Are you able to provide information about Water Sample #3?	1 Yes/0 No/ 97 Refused	
a81_source	8.1) What is the source of this water sample	1 Piped Water 2 Stand Pipe 3 Borehole/tube well 4 Protected dug well 5 Unprotected dug well 6 Protected Spring 7 Unprotected Spring 8 Rainwater Collection 9 Small Water Vendor 10 Tanker Truck 11 Bottled Water 12 Bagged / sachet water 13 Surface water (pond, river, lake) 14 Other person; specify 96 Other; specify	14 extension is “If someone else is responsible for your water, please specify” 1 extension is “If other, please specify your water source”
a82_time	8.2) How long (in minutes) does it take to go to the water source, get water, and come back (including wait time)? If water souce is in household/compound, record 0		
a83_cookingdrink	8.3) Do you use water from this source for cooking and drinking?	1 Yes 0 No 97 Refused	

a84_worryf	8.4) Are you worried about contracting fluorosis from this sample of water?	1 Yes 0 No 97 Refused	
a85_thistreated	8.5) Has this specific sample of water been treated?	1 It hasn't 2 It has; specify 99 Don't know	
a85_thistreated2	8.5 a) How has this sample of water been treated?	1 Do not treat it 2 Boiling 3 Filter 4 Chlorine Tablets 5 Distillation 6 bone char 99 Other	
a86_worryfl	8.6) Are you worried about contracting fluorosis from this sample of water?	1 Yes 0 No 97 Refused	
a87_cost	8.7) What is the cost of water from this source (x per y)?		
a88_procuresample	8.8) Did you procure the water sample?	1 Yes, without a problem 2 Yes, but there was a problem (explain why) 3 No (explain why)	The 2 and 3 extensions allow the respondent to expand on the problem
at0_test1	T1) Are you able to provide information about the conditions of Test 1?	1 Yes 0 No 97 Refused	
t11_observations	T1.1) For Field Staff only - Would you like to note any observations/comments about the test? Remember, if there is anything wrong with the test, please throw it out (absence of dessicant card. not		

	vaccuum sealed)		
t12_waterandtest	T1.2) At what time was water added to the test?	time	
t13_observpipette	T1.3) Do you have any observations about the pipetting technique of the respondent?		
at0_test2	T2) Are you able to provide information about the conditions of Test 2?	1 Yes 0 No 97 Refused	
t21_observation	T.2.1) For Field Staff only - Would you like to note any observations/comments about the test? Remember, if there is anything wrong with the test, please throw it out (absence of dessicant card. not vaccuum sealed)		
t22_waterandtest	T.2.2) At what time was water added to the test?		
t23_observpipette	T.2.3) Do you have any observations about the pipetting technique of the respondent?		
at0_test3	T3) Are you able to provide information about the conditions of Test 3?		
a88_observations	T.3.1) For Field Staff only - Would you like to note any observations/comments about the test? Remember, if there is anything wrong with		

	the test, please throw it our (absence of dessicant card. not vaccuum sealed)		
a89_waterandtest	T.3.2) At what time was water added to the test?		
a810_observpipette	T.3.3) Do you have any observations about the pipetting technique of the respondent?		
a90_results	9.0) Report test results for Sample #1?	1 Yes 0 No 97 Refused	
a901_ambienttemp	9.0.1) What is the ambient temperature (c)?		
a91_testid	9.1) Enter Test-ID for Sample 1		
a92_batchno	9.2) Batch # of testing kit	1 Batch No. 1 2 Batch No. 2	
a93_posctrlyellow	9.3) When did the positive control turn yellow?	6 0-1 hours 1 1-2 hours 2 2-3 hours 3 3-4 hours 4 4-5 hours 5 >5 hours 0 Never 99 Other; specify	
a95_samplyellow	9.4) When did the sample turn yellow?	6 0-1 hours 1 1-2 hours 2 2-3 hours 3 3-4 hours 4 4-5 hours 5 >5 hours 0 Never 99 Other; specify	
a96_particpantsee	9.5) Does the participant see yellow?	1 Yes 0 No 99 Other; specify	99 extension is for other

a97_agreewrespond	9.6) For Field Team ONLY - If they report that they see yellow, do you agree with the respondent's observation that the test is indeed yellow?	1 Yes 0 No 97 Refused	0 extension
a98_fluor	9.7) What fluoride concentration did the fluorimeter report (ppm)?		
a100_results	10.0) Report test results for Sample #2?	1 Yes 0 No 97 Refused	
a101_testid	10.1) Enter Test-ID for Sample 2		
a102_batchno	10.2) Batch # of testing kit	1 Batch No. 1 2 Batch No. 2	
a103_posctrlyellow	10.3) When did the positive control turn yellow?	6 0-1 hours 1 1-2 hours 2 2-3 hours 3 3-4 hours 4 4-5 hours 5 >5 hours 0 Never 99 Other; specify	
a105_samplyellow	10.4) When did the sample turn yellow?	6 0-1 hours 1 1-2 hours 2 2-3 hours 3 3-4 hours 4 4-5 hours 5 >5 hours 0 Never 99 Other; specify	
a106_particpantsee	9.5) Does the participant see yellow?	1 Yes 0 No 99 Other; specify	99 extension is for other
a107_agreewrespond	10.6) For Field Team ONLY - If they report that they see yellow, do you agree with the respondent's	1 Yes 0 No 97 Refused	

	observation that the test is indeed yellow?		
a108_fluor	10.7) What fluoride concentration did the fluorimeter report (ppm)?		
a110_results	11.0) Report test results for Sample #3?	1 Yes 0 No 97 Refused	
a111_testid	11.1) Enter Test-ID for Sample 3		
a112_batchno	11.2) Batch # of testing kit	1 Batch No. 1 2 Batch No. 2	
a113_posctrlyellow	11.3) When did the positive control turn yellow?	6 0-1 hours 1 1-2 hours 2 2-3 hours 3 3-4 hours 4 4-5 hours 5 >5 hours 0 Never 99 Other; specify	
a115_samplyellow	11.4) When did the sample turn yellow?	6 0-1 hours 1 1-2 hours 2 2-3 hours 3 3-4 hours 4 4-5 hours 5 >5 hours 0 Never 99 Other; specify	
a106_particpantsee	9.5) Does the participant see yellow?	1 Yes 0 No 99 Other; specify	99 extension is for other
a117_agreewrespond	11.6) For Field Team ONLY - If they report that they see yellow, do you agree with the respondent's observation that the test is indeed yellow?	1 Yes 0 No 97 Refused	0 extension - “If no, do you have any comments/observations?”
a118_fluor	11.7) What fluoride		

	concentration did the fluorimeter report (ppm)?		
a12_useexp	12.0) How was your experience of putting water samples into the test?		
a12_exptime	12.1) How was your experience with noticing when the color changed on the test?		
a12_useinterp	12.2) How was your experience of interpreting the test results?		
a12_improve	12.3) What could be improved about the tests?		
a12_whatyoulike	12.4) What did you like about the test?		
a12_implementhh	12.5) How likely are you to implement this test for your household's future water needs?	0 unlikely 1 most likely 3 definetely 4 unsure	
a12_tellusanything	12.6) Please ell us anything that you would like us to change about this test		
a12_interviewerinp	12.7) For field team only - any other observations, unique experiences, other things to remember about this interview?		

Supplemental Table 8. Fluoride biosensor user experience survey.
Questions up to and including a88 were asked before testing water samples. Questions beginning with a12 were asked after testing concluded.